



Analysis of synapse assembly in *Drosophila melanogaster*
Analyse des synaptischen Aufbaus der *Drosophila melanogaster*

Doctoral thesis for a doctoral degree
at the Graduate School of Life Sciences,
Julius-Maximilians-Universität Würzburg,
Section Biomedicine

submitted by

Wernher Fouquet

from

São Paulo

Würzburg **2008**

Submitted on:

Office stamp

Members of the *Promotionskomitee*:

Chairperson: Prof. Dr. Caroline Kisker

Primary Supervisor: Prof. Dr. Stephan J. Sigrist

Supervisor (Second): Prof. Dr Erich Buchner

Supervisor (Third): Dr. Asparouh Iliev

Date of Public Defence: 16.09.2009

Date of receipt of Certificates:

Acknowledgements

I would like to thank my instructor and supervisor Prof. Dr. Stephan Sigrist for giving me the opportunity to conduct these scientific studies in his research group. Over the years Stephan has been my major scientific mentor and thanks to him I had access to the most extraordinary equipment, which finally allowed me to perform my experiments. His diligent supervision and faithful friendship were decisive for the realization of this work. I would also like to thank both supervisors Prof. Dr. Erich Buchner and Dr. Asparouh Iliev for sharing their experience in discussions and supporting me on my project.

Thank you also to Dr. Marcus Dyba and to Dr. Jochen Sieber for sharing their expertise on both scientific and non-scientific discussions. For further collaborations, I would like to thank Prof. Dr. Stefan Hell, Dr. Robert Kellner, Dr. Katrin Willig, Dr. Birka Hein and all the crew from Leica Microsystems for support regarding the STED microscope. Thanks also to Dr. Manuela Schmidt, Dr. Birgit Greiner, Dr. Tobias Rasse, Harald Depner, Till Andlauer, and specially Dr. Carolin Wichmann, Dr. Robert Kittel, Frauke Christiansen-Engelhart, David Oswald and Sara Mertel for the nice working atmosphere, their contributions to this work, and constant support. I would also like to thank Andreas Schmid, Omid Khorramshahi, Tobias Schwarz and Dr. Gang Qin for work on receptors. In addition I thank Christine Quentin, Claudia Wirth and Franziska Zehe for the indispensable and excellent technical assistance, Eva Alberio for friendly and reliable coordination, and Frank Kötting and Gunther Tietsch for flawless technical constructions regarding the live imaging equipment.

Thanks to all ENI, ZEMM and MSZ members for contributing to the unique working atmosphere. Especially Felix Stark, Dr. Carlos Merino, Dr. Miranda Gonzalez, Heiko Röhse, Dr. Laura Stagi, Miriam Richter, Oliver Schade, Dr. Carola Sigrist, Christian Werner, Rui Tian and Karen Lui.

Thank you to my friends, particularly Raimund, Runk, Gustav, Ben, Peer and Hinrik, for supporting me in difficult times, while always giving me something to laugh about. I would like to thank my parents Jutta and Dietmar, which always encouraged me in my decisions and made them possible at the end. Thanks also to my family for their most affecting help. Finally, I thank Daniela, who accompanied me through wonderful times over the past years and supported me with almost self-sacrificing devotion.

Content

1 Summary	7
2 Introduction.....	10
2.1 Synapses.....	10
2.1.1 Relevance of synapses in neuronal communication	10
2.1.2 Molecular characterization of the presynaptic compartment in glutamatergic synapses	12
2.1.3 Mechanisms of synaptic vesicle exo- and endocytosis	16
2.1.4 Molecular characterization of the postsynaptic compartment in glutamatergic synapses	18
2.1.5 The formation of new synaptic terminals	19
2.2 Synaptic plasticity	24
2.2.1 Learning and memory is based on neuronal connectivity and synaptic modulation	24
2.2.2 Presynaptic contribution for synaptic modulation.....	25
2.2.3 Postsynaptic contribution for synaptic modulation	27
2.2.4 The role of synapse formation and retraction for LTP and LTD	28
2.3 The <i>Drosophila</i> NMJ as a model for glutamatergic synapses	30
2.3.1 Strengths of the fly as a model system.....	30
2.3.2 Development of the <i>Drosophila</i> NMJ	31
2.3.3 The structural organization of the <i>Drosophila</i> NMJ	33
2.3.4 Experience and activity-dependent synapse plasticity	35
2.4 Principles of stimulated emission depletion (STED)	36
2.5 Study objectives.....	38
3 Material and Methods	39
3.1 Molecular biology	39
3.1.1 Material	39
3.1.2 Cloning of fluorescently tagged proteins.....	40
3.1.2.1 Primer extension method.....	40
3.1.2.2 Gateway method	41
3.1.2.3 List of cloned vectors and transgenes	42
3.2 <i>Drosophila melanogaster</i>	43
3.2.1 Fly culturing.....	43
3.2.2 Transgenesis	43

3.2.3	The UAS/Gal4 system and drivers	44
3.2.4	Transgenic lines used in thesis	44
3.3	Immunohistochemistry	45
3.3.1	Material	45
3.3.2	Larval body wall preparation.....	45
3.3.3	Fixation and staining procedures.....	45
3.3.4	Atto-647N NHS-Ester antibody conjugation.....	47
3.4	Image Acquisition.....	47
3.4.1	Procedures for fixed samples imaging.....	47
3.4.2	Procedures for in-vivo imaging (time images / FRAPs).....	48
3.4.3	The LCS STED microscope and its acquisition settings	49
3.5	Image processing and analysis	50
3.5.1	Software.....	50
3.5.1.1	Confocal imaging.....	50
3.5.1.2	STED imaging	50
3.5.2	Image Quantifications.....	51
3.5.2.1	Defining the synapse number	51
3.5.2.2	Measuring the peak-to-peak distances	51
3.5.2.3	Defining the temporal sequence	51
3.5.2.4	Averaging of synapses	52
3.5.3	Statistical analysis.....	52
4	Results	53
4.1	Structural organization of the presynaptic active zone.....	53
4.1.1	The monoclonal antibody Nc82 labels Bruchpilot	53
4.1.2	AZ proteins localize at different distances from the AZ membrane	54
4.1.3	BRP extends vertical to AZ membrane.....	56
4.1.4	BRP localizes to the electron dense T-bar matrix	58
4.1.5	Proteomics identify <i>Drosophila</i> DSyd-1 via biochemical interaction to Bruchpilot.....	59
4.1.6	DLiprin- α and DSyd-1 are localized in 'quantal' clusters at the AZ edge.....	61
4.2	Observing synapse assembly <i>in vivo</i>	63
4.2.1	A temporal sequence of <i>in vivo</i> AZ assembly	63
4.2.2	BRP shows fast protein turn-over but no changes in its steady state signal.....	67

4.2.3 DLiprin- α dynamics at AZs are characterized by fast exchange and continuous remodeling	69
4.2.4 BRP accumulates late, in the AZ center, from diffuse pools	70
4.2.5 DLiprin- α and DSyd-1 co-fluctuate within an early, still reversible AZ assembly phase.....	71
4.3 Dissecting functional and structural roles of AZ proteins	72
4.3.1 <i>Brp</i> mutants lack T-bars and have a reduced vesicle release probability	72
4.3.2 DSyd-1 is important for efficient AZ formation	77
5 Discussion	83
5.1 The role of Bruchpilot at the active zone	84
5.1.1 Localization of Bruchpilot within the AZ	84
5.1.2 The function of T-bars	84
5.2 A sequential model of AZ formation	86
5.3 Discrete dynamic modules at the AZ edge	89
6 Appendix.....	91
6.1 Table of abbreviations.....	91
6.2 Table of Figures	93
6.4 Curriculum Vitae	106
6.5 Publications	108

1 Summary

The majority of rapid cell-to-cell communication mechanisms and information processing within the nervous system makes use of chemical synapses. Fast neurotransmission on these sites not only requires very close apposition of pre- and postsynaptic partners, but also depends on an effective structural arrangement of cellular components on both sides of the synaptic cleft. Synaptic vesicles fuse at active zones (AZs), characterized by an electron-dense protein mesh of insufficiently characterized composition and function. EM analysis of synapses identified electron dense structures thought (but not proven) to play an important role for vesicle release efficacy. The molecular organization of presynaptic AZs during Ca^{2+} influx-triggered neurotransmitter release is currently a focus of intense investigation.

Due to its appearance in electron micrographs, dense bodies at *Drosophila* synapses were named T-bars. Together with the lab of Erich Buchner, we recently showed that Bruchpilot (BRP) of the *Drosophila melanogaster*, homologous to the mammalian CAST/ERC family in its N-terminal half, is essential for the T-bar assembly at AZs and efficient neurotransmitter release respectively. The question, in which way BRP contributes to functional and structural organization of the AZ, was a major focus of this thesis.

First, stimulated emission depletion microscopy (STED), featuring significantly increased optical resolution, was used to achieve first insights into 'cytoarchitecture' of the AZ compartment. In addition, *in vivo* live imaging experiments following identified populations of synapses over extended periods were performed to address the trafficking of protein at forming synapses and thereby providing a temporal sequence for the AZ assembly process. Apart from BRP, two additional AZ proteins, DLiprin- α and DSyd-1, were included into the analysis, which were both shown to contribute to efficient AZ assembly.

Drosophila Syd-1 (DSyd-1) and *Drosophila* Liprin- α (DLiprin- α) clusters initiated AZ assembly, finally forming discrete 'quanta' at the AZ edge. ELKS-related Bruchpilot, in contrast, accumulated late from diffuse pools in the AZ

center, where it contributed to the electron dense specialization by adopting an extended conformation vertical to the AZ membrane. We show that D Syd-1 and DLiprin- α are important for efficient AZ formation.

The results of this thesis describe AZ assembly as a sequential protracted process, with matured AZs characterized by sub-compartments and likely quantal building blocks. This step-wise, in parts reversible path leading to mature AZ structure and function offers new control possibilities in the development and plasticity of synaptic circuits.

Zusammenfassung

Durch Ca^{2+} abhängige Neurotransmitterfreisetzung vermitteln chemische Synapsen die schnelle Informationsübertragung zwischen Nervenzellen. Voraussetzung hierfür sind gewisse zelluläre Eigenschaften, wie eine enge Korrelation zwischen der Prä- und Postsynapse und eine hoch spezialisierte Zusammensetzung von Proteinen. Synaptische Vesikel fusionieren mit der präsynaptischen aktiven Zone (AZ), welche sich aus einem dichten Netzwerk an vielfach noch unerforschter synaptischer Proteine zusammensetzt, das im Transmissionselektronenmikroskop elektronendicht erscheint. Des Weiteren sind ultrastrukturell elektronendichte präsynaptische Spezialisierungen erkennbar (dense bodies), die vermutlich (aber nicht nachweislich) bei der Freisetzung synaptischer Vesikel eine tragende Rolle spielen. Der molekulare Aufbau der AZ ist zurzeit ein weitverbreitetes Studienthema.

Die Synapsen der Fruchtfliege *Drosophila melanogaster* sind präsynaptisch gekennzeichnet durch eine elektronendichte Struktur, welche aufgrund ihrer charakteristischen Form auch als „T-bar“ bezeichnet wird. Durch die Kooperation mit dem Labor von Erich Buchner gelang es uns, das synaptische Protein Bruchpilot (BRP) zu identifizieren. BRP weist im N-terminalen Bereich Homologien zu der in Säuger gefundenen CAST/ERC Proteinfamilie auf, und ist essenziell für die Ausbildung der elektronendichten T-bars an den AZs und für eine effiziente Ausschüttung von Neurotransmitter. In wie weit BRP für die funktionelle und strukturelle

Organisation der AZ verantwortlich ist, sollte in der vorliegenden Arbeit erläutert werden.

Durch die neu entdeckte „stimulated emission depletion“ Mikroskopie (STED), ist es nun möglich, dank der erhöhten optischen Auflösung, neue Einsichten in die Architektur der AZ zu erlangen. Zusätzlich wurden mit Hilfe von in vivo Experimenten an lebenden Tieren Populationen von Synapsen über längere Zeiträume verfolgt, um so die Synapsenentstehung und den Proteintransport zu untersuchen. Auf diesem Weg sollte eine Abfolge der an der AZ Assemblierung beteiligten Proteine erstellt werden. Neben BRP wurden daher noch zwei weitere AZ Proteine berücksichtigt (DLiprin- α und DSyd-1), welche ebenfalls bei der Bildung neuer synaptischer Kontakten mitwirken.

Es konnte gezeigt werden, dass Proteincluster aus *Drosophila* Syd-1 (DSyd-1) und *Drosophila* Liprin- α (DLiprin- α) sehr früh während der Bildung neuer synaptischer Kontakte erscheinen und hierbei diskrete ‚Quanta‘ ausbilden, welche sich am Rand der AZ anlagerten. BRP hingegen erreichte die AZ zu einem späteren Zeitpunkt, wahrscheinlich aus diffusen Reservoirs und akkumulierte schließlich im Zentrum der AZ. Mit Hilfe der STED und konfokalen Mikroskopie konnte gezeigt werden, dass sich BRP in einer getreckten, vertikal zur Membran stehenden Orientierung in die elektronendichte Struktur, den T-bar, einfügt. Zudem sind DSyd-1 und DLiprin- α für eine effiziente Entstehung neuer AZs erforderlich.

Die in dieser Arbeit vorgestellten Ergebnisse deuten auf ein länger andauernden sequenziellen Assemblierungsprozess der AZ hin, in dem aus quantalen Baueinheiten Subkompartimente an ausgereiften AZs gebildet werden. Dieser gestaffelte, teils reversible Reifungsablauf der AZ eröffnet neue Möglichkeiten zur Kontrolle der Entwicklung und Plastizität neuronaler Netzwerke durch einen noch nicht beschriebenen Mechanismus.

2 Introduction

2.1 Synapses

2.1.1 Relevance of synapses in neuronal communication

The brain consists of an enormous assembly of cells that incessantly receives and processes information, analyzes and perceives it, in order makes decisions or to learn and store gathered information. In addition to reacting to stimuli, the central nervous system (CNS) can also take the initiative and start coordinated complex muscle contraction required for walking, swallowing and speaking. In order to control many aspects of behavior and thereby directly or indirectly the whole of the body, the nervous system engulfs an immense number of lines of communication comprised of nerve cells (neurons). Thus, neurons are the fundamental building blocks of the brain.

With the intuition to ensure fast information transduction between the neurons, required for the amount of information processed on a short interval, a specialized intercellular communication evolved in higher organisms. This asymmetric compartment at which one cell passes its information to the next is defined as a synapse. The human brain harbors a highly complex neuronal network consisting of 10^{10} to 10^{11} neurons which are interconnected with roughly 10^{15} synaptic contacts. Through synaptic interactions, a neuron takes account of specific electrical signals (e.g. action potentials) arising from many incoming neurons, thereby creating its own new message. This communication constitutes biological computation which results of signal transduction modulation and the establishment of new synaptic connections. One of the major research tasks is therefore to further understand the cellular mechanisms of synapse transmission and the meaning behind their signaling.

Despite the high grade of specialization and variety, all synapses apply to two basic transmission forms: electrical and chemical. At electrical synapses

the transmission is regulated by passive ion flow through tight gap junctions, necessary for extremely fast signal transduction, but with no modulation possibilities (Fig. 1a). Transmission at chemical synapses is mediated by paracrine intercellular communication, as rapid exocytose of neurotransmitter filled vesicles, which triggers an ion influx in the postsynaptic cell (Fig. 1b).

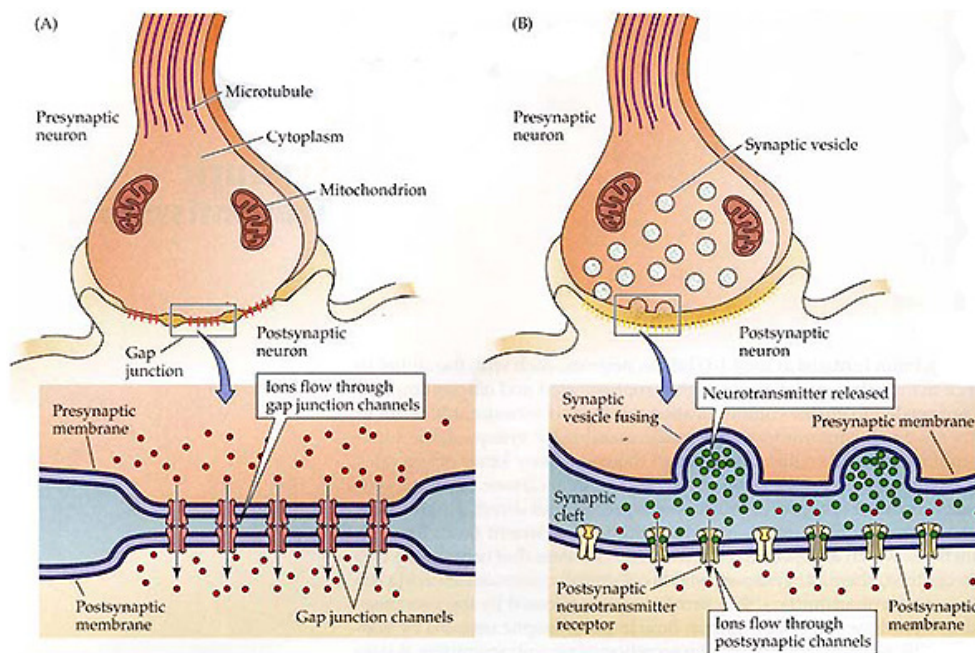


Fig. 1 The electrical and chemical synapse

a) Electrical synapse between two neurons. Gap junctions enable the passive direct ion flow from the presynaptic into the postsynaptic neuron. **b)** Chemical synapse. Synaptic vesicles filled with neurotransmitter fuse with the presynaptic plasma membrane and release the neurotransmitter into the synaptic cleft. The postsynaptic membrane harbors ion channels that bind the neurotransmitter, which results in conformational change that allows ion influx into the postsynaptic cell. (Adapted from Purves et al., 2001)

As an action potential propagating along the presynaptic axon reaches the chemical synapse, the Ca^{2+} concentration in the presynaptic terminal increases due to the opening of voltage gated Ca^{2+} -channels. The increased amount of Ca^{2+} in the terminal leads to the fusion of synaptic vesicles with the presynaptic membrane. Thereby, the neurotransmitter molecules are released from the vesicles into the synaptic cleft. Postsynaptic ion channels (receptors) specifically bind the neurotransmitter. The binding alters the receptor conformation and enables the influx of ions, which in turn initiates the signal propagation by changing the membrane potential of the postsynaptic cell.

Two types of transmission at chemical synapses can be discriminated: excitatory and inhibitory. Excitatory transmission often utilizes the neurotransmitters glutamate and acetylcholine, whereas classical inhibitory neurotransmitters are glycine or γ -aminobutyric acid (GABA). Neurotransmitters are generally categorized based on their chemical characteristics into four classes: amino acids (glutamate, aspartate, GABA, glycine, acetylcholine), peptides (e.g. vasopressin, somatostatin), monoamines (e.g. dopamine, serotonin) and other neurotransmitters (e.g. nitric oxide, CO).

The nature of the synaptic transmission (excitatory and inhibitory) plays an important role in signal transduction and biological computation, but is not the sole relevant factor responsible for synapse modulation. The establishment of new synaptic contacts and changes in the molecular organization of single synapses (synaptic plasticity) also make a sensible contribution to alterations in signaling as found in synapse potentiation and depression (see 2.2). Understanding the molecular architecture of synaptic contacts and the function of single synaptic proteins is therefore of crucial importance and a major subject of research in contemporary neuroscience.

2.1.2 Molecular characterization of the presynaptic compartment in glutamatergic synapses

The presynaptic terminal of a synapse consists of an aggregation of several specialized proteins necessary of the highly efficient exocytosis of synaptic vesicle into the synaptic cleft. Every single protein has its specific role, ranging from initiating the synapse assembly over scaffolding functions and vesicle recruitment/docking/release to endocytosis and vesicle recycling. The site where these proteins assemble and vesicle fusion takes place are denominated active zones (AZ) and the network of microfilaments and associated proteins that regulates the translocation of synaptic vesicles to the AZ and vesicle endocytosis is thereby named cytomatrix at the active zone (CAZ, Fig. 2, Zhai and Bellen 2004)

Numerous proteins have been identified in recent years to be part of the CAZ in mammals. Piccolo and Bassoon are large proteins (530 and 420 kDa)

found very early in synapse formation. The size of the proteins and the high amount of putative interaction regions (PDZ, zinc fingers, coiled-coil, proline-rich, C2 and SH3 domains) indicate a scaffolding function as many interactions with synaptic proteins could be demonstrated (Garner *et al.* 2000b). Similar functions have been implicated to RIM1 (Rab3 interacting protein) and CAST/ERC (Ziv and Garner 2004; Schoch and Gundelfinger 2006).

The protein CAST (CAZ-associated structural protein) is enriched in AZs, it interacts with prominent CAZ proteins (Ohtsuka *et al.* 2002; Takao-Rikitsu *et al.* 2004), and it may serve as a reliable AZ label (Hagiwara *et al.* 2005). The interaction partners include Bassoon (tom Dieck *et al.* 1998; Khimich *et al.* 2005), Piccolo (Fenster *et al.* 2000), Munc 13-1 (mammalian homologue of *C. elegans* Unc13 protein), an essential factor for the priming process of vesicles in the CNS (Augustin *et al.* 1999), and RIM1 (Rab3-interacting molecule-1) which provides a direct link between synaptic vesicles and the AZ (Wang *et al.* 2000; Betz *et al.* 2001).

Liprin- α was described as another key player found to be important for synapse formation in several model systems (Kaufmann *et al.* 2002; Dai *et al.* 2006; Olsen *et al.* 2006; Patel *et al.* 2006) and proven to directly interact with CAST, RIM1, LAR and MALS, thus, indirectly connected to Neurexin/Neurologin and voltage gated N-Type Ca^{2+} -channels (Olsen *et al.* 2006; Stryker and Johnson 2007). In *C. elegans* the Liprin- α homologue Syd-2 was found to genetically interact with Syd-1 and recruit several vital synaptic protein to the AZ (Dai *et al.* 2006; Patel *et al.* 2006).

Also crucial for the signal transduction are proteins associated to synaptic vesicle release cycle as v- and t-SNAREs (docking, priming and release, see 2.1.3) and Endophilin, Dynamin and Clathrin mediated endocytosis (Brodin *et al.* 2000) to only name a few (Fig. 2).

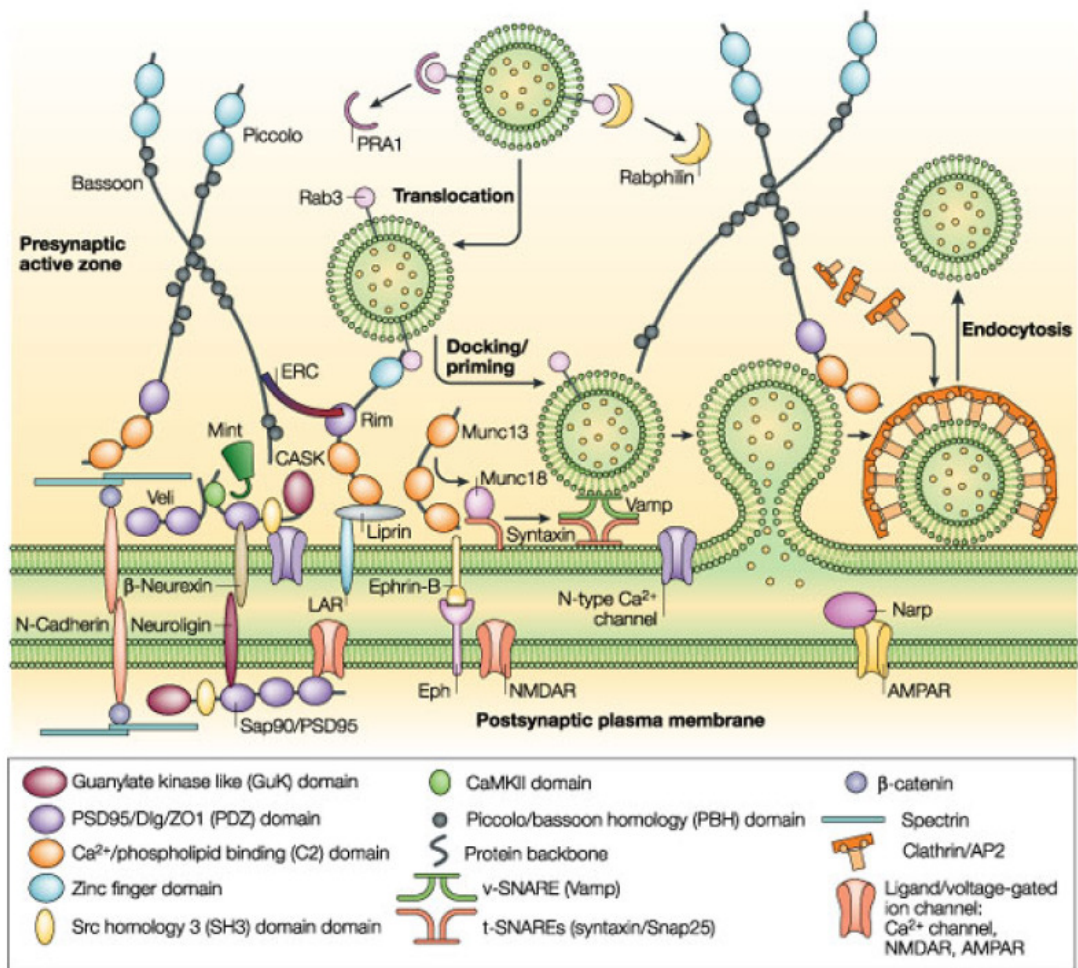


Fig. 2 Molecular components of the CAZ and the active zone

The CAZ and the AZ regulate the release of synaptic vesicles, which comprises vesicle translocation, docking and priming, membrane fusion and vesicle endocytosis. (Adapted from Ziv and Garner, 2004)

As described above many key players at the AZ have been characterized extensively regarding their genetic and biochemical interaction partners, domain structure and putative functions. However a deeper structural understanding of the architecture regarding the molecular composition at AZs is still lacking.

The description of AZs in electron-micrographs, even demonstrating several unique features, is in many ways conserved throughout the animal kingdom (Fig. 3). Some attributes as synaptic vesicles, a specialized AZ membrane and so called dense bodies are present in almost every organism.

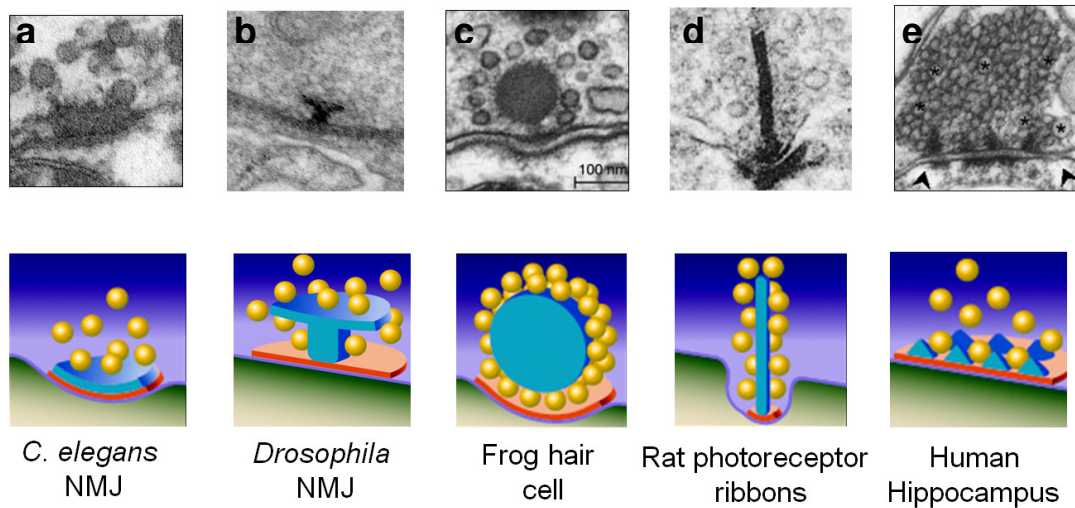


Fig. 3 Ultrastructure of the AZ

Schematic representations and electron micrographs of: **a)** neuromuscular junction (NMJ) terminal in *C. elegans*. **b)** T-bar at the *Drosophila* NMJ **c)** saccular hair cell in frog with a spherical dense projection dense bodies. **d)** triadic photoreceptor ribbon synapse in rat. **e)** excitatory synaptic terminal in human hippocampus (adaped from Zhai and Bellen, 2004). Red: specialized AZ membrane; Blue: dense projection; Yellow: synaptic vesicles (SVs)

Especially the dense bodies are thought to be important for vesicle tethering and release efficiency (von Gersdorff 2001). The extent of these electron-dense bodies varies greatly between synapse types, ranging from roughly 50 nm high pyramidally shaped particles in synapses of the mammalian central nervous system (Phillips *et al.* 2001), over approximately 70 nm long T-shaped protrusions (T-bars) at the *Drosophila* NMJ (Atwood *et al.* 1993), to the spherical synaptic ribbons found in vertebrate sensory synapses which extend 0.5 - 1 μm into the cytoplasm (Lenzi and von Gersdorff 2001). These structural differences most likely reflect the physiological demands set by the synaptic contact (Zhai and Bellen 2004). The composition of such dense bodies, though, remains largely unknown (Garner *et al.* 2000a). The resolution of conventional light microscopes is not high enough to reliably attribute the fluorescent label to distinct locations as small as the dense bodies. Many experiments have been done in order to immuno-label EM samples to gather additional information concerning the spatial protein distribution at AZ and, in many cases with success (RIBEYE, RIM1, Piccolo and Bassoon, tom Dieck *et al.* 2005). However, immuno-EM experiments are often challenging and latest developments in light microscopy (STED and

PALM, Klar *et al.* 2000; Heintzmann and Ficz 2007) could be a helpful addendum for answering these questions.

2.1.3 Mechanisms of synaptic vesicle exo- and endocytosis

The divalent cation calcium (Ca^{2+}) was found crucial for the transmission of nerve impulses, more than a century ago (Locke, 1894), even before the concept of chemical synaptic transmission was established (Loewi, 1921). Further work (Feng, 1940; Kuffler, 1942; Del Castillo and Stark, 1952) led to the calcium hypothesis which, combined with the quantal release hypothesis (Del Castillo and Katz, 1954), proposed that the release, or exocytosis, of neurotransmitter from synaptic vesicles is triggered by increased Ca^{2+} concentration in the presynaptic terminal (Katz and Miledi 1965). It was reported that the intrusion of an action potential (AP) into the terminal triggers the opening of voltage-gated Ca^{2+} -channels and that the exact amplitude and time course of the invading Ca^{2+} influx dictate the amplitude and time course of vesicle release (Barrett and Stevens 1972). The presynaptic Ca^{2+} signals describe highly localized (within tens of nanometers), transient microdomains in the direct vicinity of Ca^{2+} -channels (Llinas and Yarom 1981; Chad *et al.* 1984; Augustine and Neher 1992). Thus, the distance between Ca^{2+} -channels and the distance to the synaptic vesicles affects the characteristics of the synaptic release (Neher 1998).

As described above (2.1.1) the synaptic communication is very rapid, and synaptic sites display several *sine qua non* features that allow the presynaptic Ca^{2+} influx to be followed by a postsynaptic response on the sub-millisecond time scale. Both the tight alignment of pre- and postsynaptic membranes and the specialised presynaptic region of exocytosis, the AZ (Couteaux and Pecot-Dechavassine 1970; Landis *et al.* 1988), reflect the requirement for rapid signal transduction. As one of the swiftest biological cell processes, Ca^{2+} -triggered neurotransmitter release requires a molecular coupling of Ca^{2+} influx with vesicle fusion at the protein level (Rosenmund *et al.* 2003). The fusion of vesicles with the AZ membrane presumably follows binding of Ca^{2+} to the calcium sensing vesicle protein Synaptotagmin (Geppert *et al.* 1994; Koh and Bellen 2003), and is mediated by SNARE

(SNAP receptor) proteins, that include Synaptobrevin on synaptic vesicles and SNAP-25 and Syntaxin on the plasma membrane (Jahn *et al.* 2003; Sudhof 2004; Lang and Jahn 2008). To ensure rapid and efficient stimulus-secretion coupling, AZs display clusters of voltage-gated Ca^{2+} -channels close to vesicle docking sites. A study of the frog NMJ used electron tomography to reconstruct the three dimensional structure of the CAZ (Harlow *et al.* 2001). The spatial arrangement of Ca^{2+} -channels within AZ appears to be organized through interactions with AZ proteins that ultimately regulate release efficacy (Harlow *et al.* 2001; Cao *et al.* 2004).

Within the presynaptic terminal, vesicles participate in a cycle of exocytosis at the AZ and endocytosis at the adjacent periaxial zone, thereby enabling rapid and repeated use (Sudhof 2004). Of these vesicles, only a small fraction is docked to the synaptic membrane, while the rest reside in adjacent compartments. A number of attempts have been made to assign vesicles to distinct 'pools', reflecting particular functional properties. A prevalent model suggests the division into three distinct pools (Zucker and Regehr 2002; Rizzoli and Betz 2005): The readily releasable pool, comprised of vesicles docked to the AZ membrane and primed for release, the recycling pool of vesicles which maintain transmitter release during moderate physiological stimulation and the reserve pool, used as a storage of synaptic vesicles which participate in release only during strong and continuous stimulation deployed after the recycling pool has been depleted. The number of vesicles released at a synapse is determined by the number of primed vesicles and the release probability of the individual vesicles. Synapses comprised of vesicles with low release probability often display facilitation and augmentation whereas high release probability in synapses tend to exhibit depression (Zucker and Regehr 2002). In addition changes in the organization of the presynaptic AZ including the density, coupling and juxtaposition of Ca^{2+} -channels and synaptic vesicles are considered critical in this context (Atwood and Karunanithi 2002) and may also considerably vary the signal's strength and nature as observed in heterogeneous fusion kinetics upon Ca^{2+} influx observed by variable distances between Ca^{2+} -channels and vesicles (Neher 1998).

2.1.4 Molecular characterization of the postsynaptic compartment in glutamatergic synapses

Excitatory synapses in the vertebrate central nervous system (CNS) are predominately glutamatergic. Following synaptic vesicle release the neurotransmitter (glutamate) binds to glutamate-sensitive receptors, which can be categorized into two groups: metabotropic and ionotropic glutamate receptors. The tetrameric ionotropic glutamate receptor complexes are further subdivided into AMPA (alpha-amino-3-hydroxy-5-methyl-4-isoxazole-propionic acid), NMDA (N-methyl-D-aspartate) and kainate receptors. The glutamatergic transmission is supported by a specialized postsynaptic sub-cellular organization, called the postsynaptic density (PSD). The PSD is involved in clustering and anchoring of postsynaptic receptors and ion channels and contains a specialized sub-membranous cytoskeleton with a large number of proteins responsible for the organization of the PSD (Fig. 4, Kim and Sheng 2004). In contrast to the aggregation of presynaptic AZs assumedly involving the recruitment of preassembled transport vesicles (dense core vesicle or PTVs, see 2.1.5), the postsynaptic assembly seems to rely on gradual incorporation of component proteins (Bresler *et al.* 2004). Non-NMDA receptors may either be recruited into PSDs from a diffuse plasma membrane pool by lateral migration (presented in Borgdorff and Choquet 2002) or be incorporated via subunit specific constitutive or activity-dependent pathways (Bredt and Nicoll 2003), potentially using discrete number of slots available at the postsynaptic membrane (Barry and Ziff 2002). Moreover, postsynaptic glutamate receptor levels are regulated by a number of adaptor proteins, kinases and scaffolding molecules (McGee and Bredt 2003). Within the PSD, scaffolding proteins containing one or more PDZ domain are highly abundant (Fig. 4, Walikonis *et al.* 2000). Among them are PSD-95 (postsynaptic density protein 95) and SAP97 (synapse-associated protein 97), both membrane-associated guanylate kinases (MAGUKs), GRIP (glutamate receptor interacting protein), ABP (AMPA receptor binding protein) and PICK1 (protein interacting with C kinase), between others.

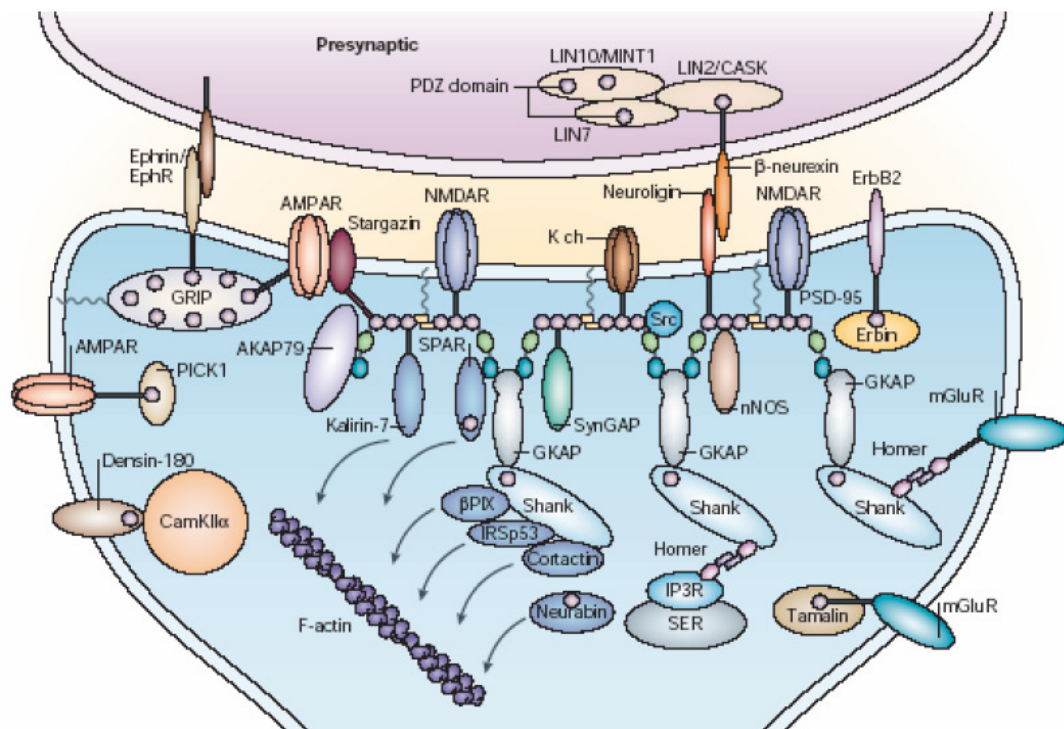


Fig. 4 Molecular components of the postsynaptic density (PSD)

Displayed are the main PDZ proteins involved in the organization of the PSD. PDZ domains are thereby demarked with small purple circles and the C-terminal cytoplasmic tails of transmembrane proteins by black lines. Abbreviations: AKAP79, A-kinase anchor protein 79; AMPAR, AMPA (α -amino-3-hydroxy-5-methyl-4-isoxazole propionic acid) receptor; β PIX, PAAK-interactive exchange factor; CaMKII α , α -subunit of Ca²⁺/calmodulin-dependent protein kinase II; GK, guanylate kinase-like domain; EphR, ephrin receptor; ErbB2, EGF-related peptide receptor; GKAP, guanylate kinase-associated protein; GRIP, glutamate-receptor-interacting protein; IP3R, IP3 receptor; IRSp53, insulin-receptor substrate p53; K ch, potassium channel; LIN7, lin7 homologue; LIN10, lin10 homologue; mGluR, metabotropic glutamate receptor; NMDAR, NMDA (*N*-methyl-D-aspartate) receptor; nNOS, neuronal nitric oxide synthase; PICK1, protein interacting with C kinase 1; PSD-95, postsynaptic density protein 95; SER, smooth endoplasmic reticulum; SH3, Src homology 3 domain; Shank, SH3 and ankyrin repeat-containing protein; SPAR, spine-associated RapGAP; SynGAP, synaptic Ras GTPase-activating protein. (Adapted from Kim and Sheng 2004)

2.1.5 The formation of new synaptic terminals

Excitatory synapses in the CNS are normally located on small lateral outgrowths of the postsynaptic dendrites, the so-called dendritic spines (Fig. 5). A major fraction of the cytoskeleton of the dendritic spines is formed by highly dynamic actin filaments, which capacitate the spines of rapid morphological changes (Tada and Sheng 2006). The acutely dynamic structural rearrangement and the establishment of new spines are meant to play an important role in synaptogenesis and synaptic plasticity (Yuste and Bonhoeffer 2001; Nikonenko *et al.* 2002; Matus 2005). Mature spines, which are increasingly stable in shape, are characterized both by an expanded

head and a narrow neck but they vary strongly in size and shape, from stubby, thin to mushroom-like formations (Fig. 5).

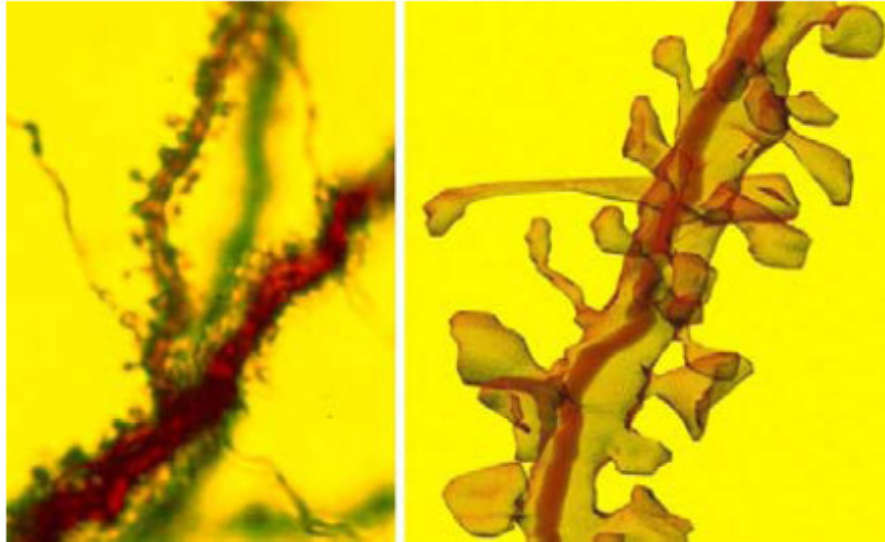


Fig. 5 Dendritic spines as a model for vertebrate synapse

Spiny dendrites from a hippocampal pyramidal neuron. **(a)** Light microscope image. **(b)** Reconstruction from serial electron micrographs. (Adapted from <http://synapses.mcg.edu/anatomy/dendrite/dendrite.stm>)

The development of dendritic spines commences with immature dendrites producing motile filopodia that probe the neuropil for presynaptic partners in order to establish new contacts (Fig. 6a). As soon as an initial contact of the presynaptic axon and the postsynaptic spine is created, structural proteins accumulate at the developing synaptic site (Fig. 6b). Hereon, spine maturation proceeds through the accumulation of synaptic vesicles and specialized proteins in the presynaptic terminal and the integration of glutamate receptors into the postsynaptic membrane (Fig. 6c and d).

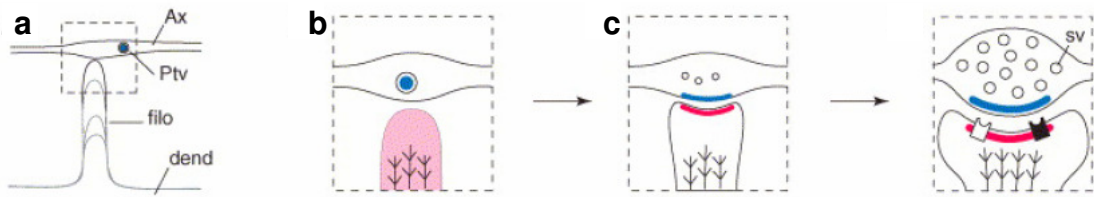


Fig. 6 Model for dendritic spine development

a) Growing postsynaptic dendritic filopodia (dend, filo) probing for its presynaptic partner (Ax). When the contact is established first synaptic precursor vesicles assemble at the target (PTV). **(b - c)** Specialized proteins are transported to the synapse, either diffuse (pink) or as discrete entities (blue). Synaptic vesicles begin to assemble at the active zone. **d)** Mature synapse with the development of presynaptic boutons and postsynaptic dendritic spines including the incorporation of glutamate receptors (NMDA, black; AMPA, white). (Modified from Matus, 2005)

While there is a basic understanding of the molecular organization of the AZ and the PSD, relatively little is known about the cellular processes by which AZs and PSDs are assembled (Ziv and Garner 2001; Goda and Davis 2003; McGee and Brecht 2003). Communication between pre- and postsynaptic sites during synapse formation are thereby thought to be a complex process involving a variety of cell surface receptors, their respective ligands and cell adhesion molecules (for review see Gundelfinger and tom Dieck 2000; Yamagata *et al.* 2003; Shen *et al.* 2004). Gathering insights into the spatial and temporal correlation between the pre- and postsynaptic site is one initial step towards understanding the interaction between these compartments.

Results obtained from *in vitro* experiments including retrospective immunohistochemistry suggest that presynaptic development precedes postsynaptic assembly. Newly assembled AZs can be functional within a period of 30-60 min after initial axo-dendritic contact (for review, see Ziv and Garner 2001). Thereby a preselected stoichiometric amount of proteins belonging to the CAZ are transported to nascent presynaptic sites via preformed precursor vesicles (Roos and Kelly 2000). The fusion of 1-4 of such vesicles with the presynaptic plasma membrane is supposedly sufficient to form an AZ (Zhai *et al.* 2001; Shapira *et al.* 2003; Bresler *et al.* 2004). Examples for such AZ precursor vesicles are presumably SV packets destined to be transported to new presynaptic sites in parallel to other presynaptic molecules as voltage-dependent calcium channels, synapsin, and amphiphysin (Ahmari *et al.* 2000). Axonal dense-core vesicles of 80 nm

of size named Piccolo-Bassoon transport vesicles (PTVs, see Fig. 7) were also reported to assemble at newly forming AZs. PTVs were shown to contain several CAZ components as Basson, Piccolo and CAST as well as RIM1/UNC10, Munc13/UNC-13 and Munc18/UNC-18 (Zhai *et al.* 2001; Shapira *et al.* 2003). The results demonstrate that a major fraction of building material for AZs is pre-assembled somatically so that it can be easily transported and fused with the presynaptic membrane. Considering that these targets are predominantly formed at remote axonal sites, far from the somatic and dendritic biosynthetic center respectively, the prepacking of AZ components in small modular units seems only logical and appropriate. Previous work used a GFP-tagged Basson to address the role of the PTVs *in vitro*. Single Basson-GFP patches were reported to move rapidly along the axon. To form an AZ several of these came to rest at a new synaptic site (Bresler *et al.* 2004). The interval from the first detection of stationary Basson-GFP at a future synaptic site to the acquisition of a capacity for activity-evoked endocytosis and exocytosis ranged from 15 to 45 min (Bresler *et al.* 2004), which is coherent with similar studies based on retrospective immunolabelings (Friedman *et al.* 2000; Zhai *et al.* 2001). Similar experiments also showed that it takes about one hour for the major postsynaptic proteins PSD-95, GluR1 and NMDAR1 to accumulate at synapses positive for styryl dye staining, which indicates vesicle recycling (Friedman *et al.* 2000). The mechanisms for the postsynaptic assembly are even less understood when compared to the presynaptic compartment. Postsynaptic compartments usually originate from dendrites and are therefore rather close to the somatic biosynthetic center, which probably reduces the need for elaborate transport mechanisms. Further works reported discrete mobile SAP90/PSD-95 particles, leading to assumption that these structures might be modular PSD units (Marrs *et al.* 2001; Prange and Murphy 2001). Washbourne and co-workers described the aggregation of NMDAR1 and GluR1 transport vesicles at synapses in young hippocampal cultured neurons (Washbourne *et al.* 2002). However in studies using older neurons, none of these finding could be reproduced (Guillaud *et al.* 2003; Bresler *et al.* 2004). These lightly controversial results speak against the

hypothesis that general precursor vesicles, as described for the presynapse, are used to transport glutamate receptors to synaptic target sites. It is therefore most likely that postsynaptic proteins assembly from diffuse protein pools. The recruitment of SAP90/PSD-95, PSD-Zip45/Homer 1c, NMDR1, ProSAP1 and ProSAP2 to new synaptic sites has been reported to occur in a gradual manner and not from discernible precursor particles (Bresler *et al.* 2001; Marrs *et al.* 2001; Okabe *et al.* 2001a; Okabe *et al.* 2001b; Bresler *et al.* 2004), findings that also strengthen the latter hypothesis. It seems as if PSD components might form multimolecular complexes in the postsynaptic membrane prior to being actually trapped or cross-linked in PSDs. Another possible mechanism consists of the proteins assembling at the PSD in a hierarchical manner. The position in the hierarchy and the molecular kinetics of the aggregate would then be rate limiting for the specific protein incorporation into the postsynaptic site (Fig 7).

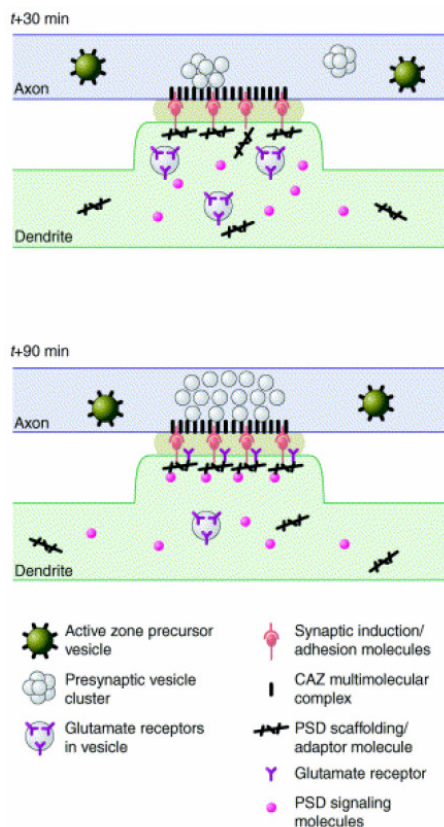


Fig. 7 Synaptic maturation by fusion of preassembled precursor vesicles versus sequential *in situ* recruitment of synaptic components.

In this simplified 'time-lapse sequence', presynaptic differentiation is shown to occur by the insertion of precursor vesicles containing full complements of CAZ complexes, which leads to the formation of functional AZs in a "quantal mode". Postsynaptic differentiation is shown to occur by the sequential recruitment of PSD scaffolding molecules followed by glutamate receptors and PSD signaling molecules. The differentiation processes are presumed to be initiated by interactions between the external aspects of axonal and dendritic membrane molecules. The time points represent the approximate time course of these processes in minutes starting from the point of first axodendritic contact. (Taken from Ziv and Garner 2001)

2.2 Synaptic plasticity

2.2.1 Learning and memory is based on neuronal connectivity and synaptic modulation

It is an undisputed fact that information deriving from innumerable senses is acquired, stored, processed and retrieved by the brain. By analyzing the setup of a neuron, it is most unlikely that each single cell, even when considering the huge amount and diversity, is responsible for one specific memory 'slot'. It is more conceivable that ensembles of many interconnected neurons participate in maintaining an environment representation, which is finally interpreted as memory. The creation of new synaptic contacts and modulation in existing synapses are thought to be the basis for memory, which implies a need for developmental and activity-dependent changes in synaptic function. These changes in synaptic interactions are thought to derive from "neuronal growth" as proposed by Santiago Ramón y Cajal already in 1893 (Cajal, 1893). In 1949 this idea was further refined by Donald O. Hebb who postulated that both the formation of new synapses and alterations in synaptic strength are responsible for memory storage (Banister *et al.* 1949). Further on, Peter Milner showed in 1966 that lesions in the hippocampus produce retrograde amnesia (Anderson *et al.* 1966). These findings were shortly followed by the first experimental induction of synaptic long-term potentiation (LTP) in the mammalian hippocampus in 1973 (Bliss and Lomo 1973). In their experiments they used short tetanic stimuli to induce synaptic strengthening, which persisted for several hours. Since these extraordinary findings and since the development of the patch-clamp technique many synapses in the mammalian CNS were studied, with much emphasis put on the hippocampus, believed to be a major information processing center of the mammalian brain. Thereby a striking diversity of functional performance was revealed (larger and smaller signals as synaptic facilitation and depression, Markram *et al.* 1998; Atwood and Karunanithi 2002).

Modulation in synaptic strength can be attributed to several properties as for synaptic inhibition, experience dependent remodeling of neurons, specific

pre- and postsynaptic features, structural organization and molecular differentiation. Depending of their cause, synapse modulation can vary from rapid, short lasting to slow, long lasting changes in the synaptic potential (Bliss and Lomo 1973; Thomson 2000). It is important to state that the size of the synaptic potential which is produced by a presynaptic neuron in one of the following cells relies on several criteria that include the number of contributing AZs in the synaptic terminal, the amount of neurotransmitter released at each synapse and the scale of the resulting current at each synapse. Each compartment (pre- and postsynaptic) plays a distinct role in the signal transduction and influences the synaptic strength in its own way (Atwood and Karunanithi 2002).

2.2.2 Presynaptic contribution for synaptic modulation

There are basically two ways of how synaptic transmission may be influenced by the presynaptic terminal, but both result in changes in the amount of neurotransmitter released into the synaptic cleft. The first one deals with the probability with which one (or many) synaptic vesicle fuses with the membrane. The amount of transmitter released varies according to the number of released vesicles. The second way can be explained by variances in the amount/concentration of neurotransmitter contained in each synaptic vesicle, resulting in modulation at the level of a single vesicle (also called quantal size, see Fig. 8c).

The release probability is a general term and comprises various factors that influence the number of fusing vesicles by intervening into the trajectory of synaptic vesicles from the recruitment to the fusion. The main factors are: the amount of AZs in the synaptic terminal (Fig. 8a), the number of docked/primed vesicles in the 'readily releasable pool' (Fig. 8e) and the dependence of Ca^{2+} influx and the vesicle release machinery, either by the amount of Ca^{2+} invading the synaptic terminal (Fig. 8b), by the distance of docked/primed vesicles to the Ca^{2+} -channels (Fig. 8d) or by the calcium sensor properties (Fig. 8f).

It would therefore stand to reason that the molecular architecture of the presynapse is of undeniable importance in mediating the synaptic strength in

transient (e.g. vesicle depletion → short-term depression; distance to Ca²⁺-channels → short-term facilitation) and permanent (e.g. assembly of new AZ → LTP; changes in the molecular composition of the CAZ → LTP and LTD) ways.

The modulations due to the depletion of synaptic vesicle pools and the vesicle recycling machinery are evidently as important as all factors mentioned above and their implications were nicely reviewed by Neher and coworkers (Schneppenburger *et al.* 2002).

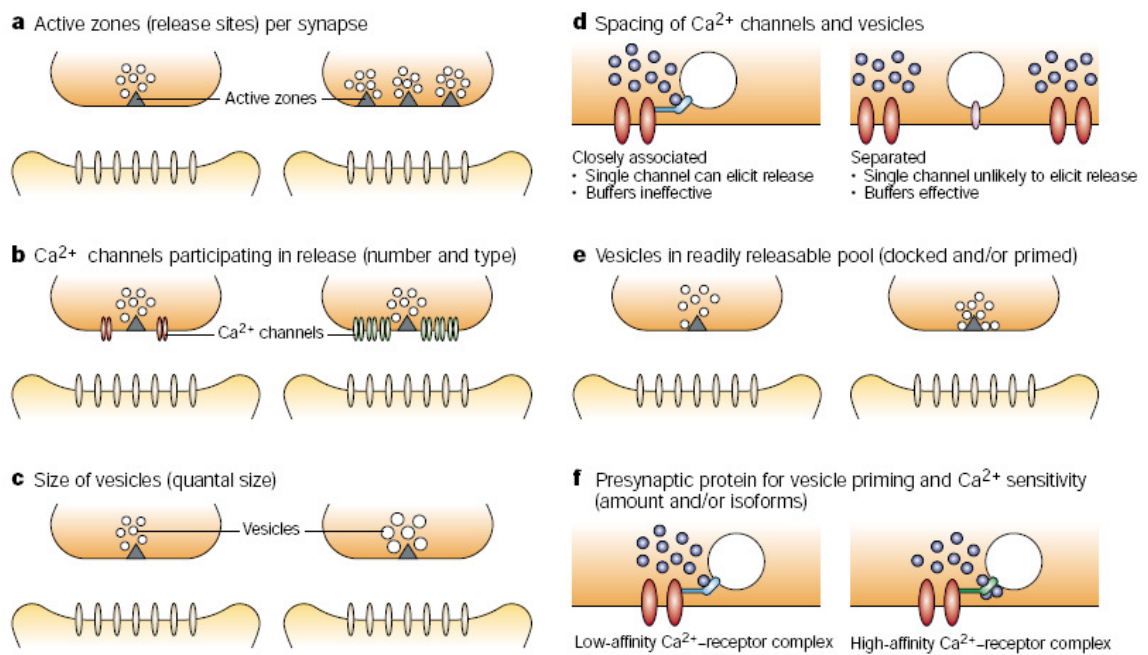


Fig. 8 Presynaptic determinants of synaptic modulation

a) Different synapses have different numbers of release sites (AZ). **b)** Voltage-dependent Ca²⁺-channels at AZs vary in number and/or type, allowing different Ca²⁺ concentrations to invade the presynaptic terminal after a nerve impulse, causing the fusion of more/less synaptic vesicles. **c)** Synaptic vesicles differ in size, generating correspondingly different quantal units, which also depend on their content. **d)** The release probability depends on channel-vesicle spacing. Calcium binding buffers influence the transmission more significantly when channels and vesicles are more separated. **e)** Synaptic vesicles that are ready (primed) for release affects the properties of signal transduction. **f)** Differences in presynaptic protein cytomatrix affect the vesicle release probability. (adapted from Atwood and Karunanithi 2002)

2.2.3 Postsynaptic contribution for synaptic modulation

The postsynaptic determinants of synaptic strength are mainly characterized by the physiological characteristics of the population of neurotransmitter receptors present in the PSD (e.g. activation/inactivation, desensitization and size of the current), the amount of receptors integrated into the postsynaptic membrane (also described through the level of saturation of the transmitter) and distance to the release site of presynaptic vesicles (Bekkers and Stevens 1990; Harris and Sultan 1995; Auger and Marty 2000; Renger *et al.* 2001; Lu *et al.* 2002).

It has been demonstrated by electrophysiological and molecular biological approaches that NMDA and AMPA receptors can be recruited to postsynaptic membranes independently of each other, by both constitutive and experience-dependent pathways (Carroll *et al.* 1999; Luscher *et al.* 1999; Shi *et al.* 1999; Grosshans *et al.* 2002; Xia *et al.* 2002). Actually, even single subunits belonging to the same receptor type (e.g. AMPA-receptor subunits GluR1 and GluR2) showed different dynamics while assembling at the postsynaptic membrane and in activity dependent remodeling at PSDs (Passafaro *et al.* 2003). The AMPA receptor is a heterooligomeric complex composed of several subunits (Seeburg 1993). In the mouse hippocampus, a well established mammalian plasticity model, the expression of subunits GluR1 to 4 could be demonstrated (Hollmann and Heinemann 1994). Investigations were able to indicate that physiological alterations of AMPA receptor-mediated transmission apparently play an important role in the induction and stabilization of long-term potentiation (Linden and Connor 1992; Bliss and Collingridge 1993; Nicoll and Malenka 1995). Interestingly, the composition of the AMPA receptors based on their subunits was described to mediate distinct functions during synaptic plasticity. GluR1/GluR2 receptors are thought to be transported from intracellular compartments to synapses (Shi *et al.* 2001), which could be a viable mechanism for converting silent synapses into active ones during LTP. Furthermore, GluR1/GluR2 receptor complexes are continuously exchanged by GluR2/GluR3 receptor complexes, which could represent a method of stabilizing previously established synapses (Shi *et al.* 2001).

The cellular mechanisms for the transportation of vesicular pools containing AMPA receptors are still poorly characterized. Recently, the glutamate receptor interacting protein (GRIP) was shown to interact with AMPA receptors, and also to associate with cargo-binding domains of the motor protein kinesin (Setou *et al.* 2002). The transport of different AMPA receptor complexes to the synapse also holds mechanistic differences (Sheng and Lee 2001). Proteins with PDZ-domains (e.g. GRIP) are probably responsible for such subunit-specific regulation of both the recruitment (transport) and the incorporation of receptor subunits at the PSD. There are also hints for local translation of glutamate receptors as evidences were gathered, which showed that increased synaptic activity triggered the local synthesis of the ionotropic glutamate receptor subunit DGluRIIA (Sigrist *et al.* 2000), which in turn promotes the formation of additional active sites at the *Drosophila* NMJ (Sigrist *et al.* 2002). In fact, most recently work in rodent neuronal culture has suggested the occurrence of local synthesis of AMPA receptors in dendritic compartments (Ju *et al.* 2004).

2.2.4 The role of synapse formation and retraction for LTP and LTD

Although vesicle release properties, molecular composition of the synapse, and the synthesis of new proteins were shown to be critical for the short and long-term modulation of synaptic strength, little is known about the cellular mechanisms that initiate and maintain long-term structural changes (Bailey and Kandel 1993; Bliss *et al.* 2003). Furthermore, there is a lack of clear evidence showing which structural changes are really required to establish long-term modulation. It is believed that alterations in synaptic strength that underlie LTP and LTD result from structural changes of pre-existing synapses. These alterations are described as modulation of existing synapses, activation of non-functional (silent) synapses or splitting of existing AZs. It is also conceivable that the outgrowth or retraction of dendritic spines is required to establish long-term modulation.

First indications came from a long-term sensitization, simulating the gill drawal reflex, of cultured neurons in the marine mollusk *Aplysia californica* (Bailey and Chen 1989; Abel and Kandel 1998). After an 18 h stimulation a

significant increase in functional synapses was shown (Kim *et al.* 2003). About two third of these new synapses appeared after stimulation, while one third of the activated synapses had previously been silent synapses (Kim *et al.* 2003). This activation of non-functional synapses, which occurred 3 - 6 h after stimulation might contribute to the early phase of LTP, while the addition of new synapses (occurring 12 - 18 h after stimulation) might be responsible for the late phase of LTP (Kim *et al.* 2003).

In vivo imaging revealed that postsynaptic spines are very mobile (see also 2.1.5). Changes in spine neck length (Yuste and Bonhoeffer 2001) and in size or width of the synaptic cleft (Liu *et al.* 1999) are likely to influence synaptic efficacy. One possible role of spines is to isolate inputs physically and equip them with an independent calcium regulation. Since diffusion through the spine neck scales with its length and diameter (Denk *et al.* 1996), changes in the length thereby alter the accessibility of calcium in the cell, which is important for input specific synaptic plasticity (Malenka *et al.* 1988; Engert and Bonhoeffer 1997). Especially the enlargement of spine heads has been shown to occur in response to repeated stimulation (Matsuzaki *et al.* 2004). As spine enlargement could be induced with little time delay (Matsuzaki *et al.* 2004), it is thought to be necessary for the early phase LTP (Gustafsson and Wigstrom 1990).

On the other hand, new filopodia or spines require at least 20 min to emerge from dendrites after the induction of LTP. These results are consistent with obtained observations that the formation of new synapses was delayed compared to the activation of existing silent ones in *Aplysia* (Kim *et al.* 2003). Therefore, the rapid onset of LTP (Engert and Bonhoeffer 1999; Maletic-Savatic *et al.* 1999) may not be explained by the formation of new dendritic spines. The formation of new spines might therefore contribute to a later phase of LTP. Once reaching a mature state, the synaptic spines can be reliably followed over months in the intact mouse cerebral cortex (Trachtenberg *et al.* 2002).

2.3 The *Drosophila* NMJ as a model for glutamatergic synapses

2.3.1 Strengths of the fly as a model system

The fruit fly *Drosophila melanogaster* has been used as a genetic model system for almost a century. Despite its small genome of only 165Mbp divided into four chromosome pairs, most *Drosophila* genes (estimated around 14.000) are in some extent evolutionary conserved in vertebrates. One of the main advantages of breeding *Drosophila* is its short generation time of about 10 days at 25°C (Fig. 9), its undeniably easy and robust handling and its genetic accessibility. The establishment and realization of various transgenic and knockout strategies is fast and straightforward compared to vertebrates, as not much gene redundancy can be encountered due to the size of the genome. Additionally, the well established UAS/Gal4 system allows tissue specific and temporally defined expression of a gene of interest (Brand and Perrimon 1993) and a wide variety of driver lines (see Lai *et al.* 2008; Tanaka *et al.* 2008 for examples in the *Drosophila* brain). Morphologically, most developmental stages are easily accessible with a huge variety of physiological, histological and microscopic techniques allowing numerous approaches addressing questions regarding genetics, neurobiology, and developmental biology, between others.

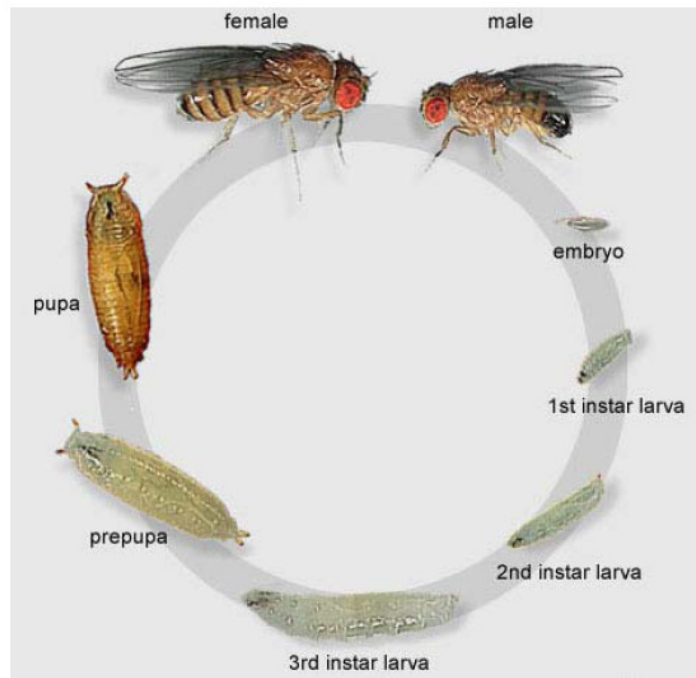


Fig. 9 *Drosophila* life cycle

After cellularization of the blastoderm, gastrulation, germ band elongation and retraction the embryo hatches about 24h after the egg laying (at 25°C). The following 1st and 2nd instar larval stages last again roughly one day each and end with the molt of the larva. After another two days the 3rd instar larvae reach the wandering stage, which is followed by the pupation. The subsequent metamorphosis takes three days and is finished with the eclosion and the hatching of the adult fly.

2.3.2 Development of the *Drosophila* NMJ

The embryonic development of the NMJ in which motoneurons diversify from neuroblasts and contact their pre and postsynaptic target cells can be divided into three stages (Fig. 10): the growth cone stage, the prevaricosity stage and the varicosity stage. During the growth cone stage, 13 to 16 hours after egg laying (AEL), the motoneuron growth cone reaches its target zone and contacts muscle myopodia belonging to future innervating cells/muscles (Ritzenthaler *et al.* 2000). During this period contacts are still transient and inappropriate contacts again withdraw (Broadie and Bate 1993b). The prevaricosity stage (16 h AEL) is characterized by the enlargement of the central region of the growth cone, more precisely at the nerve entry point into the muscle, and the formation of first visible branches. In the varicosity stage (17 h AEL) distinct varicosities (the boutons) develop from the general swelling of the prevaricosity (Rheuben *et al.* 1999).

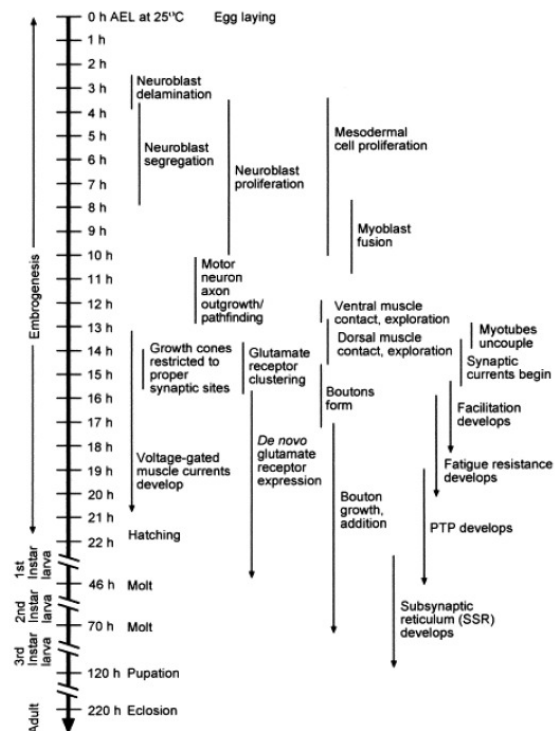


Fig. 10. *Drosophila* NMJ development

The first contact between the presynaptic motoneurons and the postsynaptic muscle cells can be observed after about 13h of embryogenesis. At this time point glutamate receptors start to cluster and synaptic currents begin. The formation of boutons and the commencing *de novo* glutamate receptor expression result in a facilitation of the synaptic transmission. (Modified from Featherstone and Broadie 2000).

The initial contact of the growth cone onto the target cell requires stabilization factors mediated by several cell adhesion molecules. Among them is Fasciclin II (FasII), which comprises certain homologies to vertebrate NCAMs (neuronal cell adhesion molecules). It is initially abundantly present at the surface of innervating motoneurons, and also at comparable low levels in the muscle cell (Schuster *et al.* 1996). As soon as the neuromuscular connection is established, FasII clusters at both the pre- and postsynaptic membrane can be observed. In later developmental stages FasII localization is thought to be mediated by the protein Discs large (Dlg), a PSD-95 homolog (MAGUK family, Thomas *et al.* 1997; Zito *et al.* 1997).

In contrast to the vertebrate NMJ, where Agrin secretion from the presynaptic nerve terminal presumably initiates the clustering of postsynaptic proteins, no homologue to Agrin was found at the *Drosophila* NMJ. However, recent studies showed that specific proteins such as Wnt and TGF β (transforming growth factor β), which are known to play a role during embryo morphogenesis, are also relevant for the cellular differentiation of synaptic terminals (Packard *et al.* 2003).

While the assembly of presynaptic AZs can take place independently of the muscles (Prokop *et al.* 1996), the postsynaptic clustering of glutamate

receptors, which feature homologies to the vertebrate non-NMDA receptors, requires the initial axon-muscle contact (Broadie and Bate 1993a). Interestingly, the suppression of neurotransmission does not influence PSD formation in any way (Featherstone and Broadie 2000). In agreement with that, it has been shown that embryonic synapse assembly remained apparently unaltered in Munc-13 or Munc-18 null mutant mice, which lacked any neurotransmission (Verhage *et al.* 2000; Varoqueaux *et al.* 2002).

2.3.3 The structural organization of the *Drosophila* NMJ

The *Drosophila* larval NMJ is a particularly interesting system due to its optic accessibility, which is a fundamental reason why it is used for this study. The larval cuticula is transparent, which allows an easy visualization of the neuromuscular terminals (located just beneath the cuticula), even in intact animals (see Fig. 11). The repeating muscle pattern in every abdominal segment makes it easy to navigate through the body and enables the viewer to reliably find a selected region over and over again (see segments A2 to A4 in Fig. 11). The axon terminals of motoneurons are completely embedded in the muscle and form typically branched innervations for every muscle. Distinctive for the NMJs are also the compartmentalization into smaller roundish substructures, the so called boutons (Fig. 11). In every bouton, when staining for synaptic markers (presynaptic Bruchpilot - green; postsynaptic glutamate receptors - red), one can find 5 to 20 small discrete structures that are the actual synapses and at which signal transduction takes place (Fig. 11). The synaptic ultrastructure of *Drosophila* NMJ synapses is characterized by a close apposition and a high electron density of the pre- and postsynaptic membranes over several hundred nanometers (synaptic cleft span: 10- 20nm). Moreover, presynaptic active zones are typically associated with electron-dense specializations (T-bars, Atwood *et al.* 1993; Zhai and Bellen 2004)

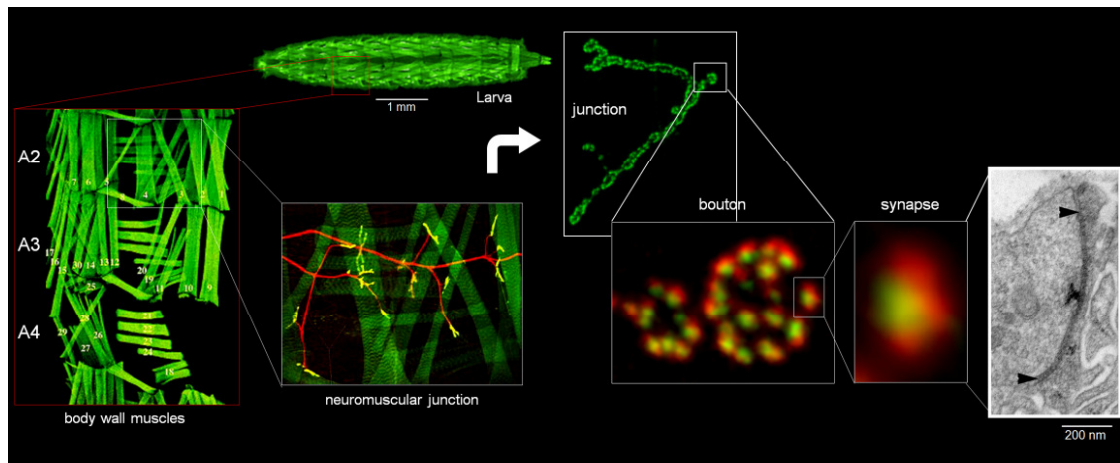


Fig. 11 Schematic overview of the larval NMJ

Representation of the *Drosophila* NMJ from the larva to the synapse, depicting the main structural features of this model system (Adapted from Gorczyca, Budnik, 2006 and Aberle et al., 2002).

The CAZ is required for the efficient release of synaptic vesicles (Kittel *et al.* 2006) and comprises several proteins showing a high degree of homologies (CAST, voltage-gated calcium channels, Neurexins and Neuroligins, Liprins, SNARE proteins and CSP to name a few). The postsynaptic density juxtaposed to the AZ provides the clustering of glutamate receptors (DGluRs), voltage-gated ion channels, scaffolding and regulatory molecules as PAK (p21-activated kinase, Albin and Davis 2004; Qin *et al.* 2005; Prokop and Meinertzhagen 2006). Individual synapses are surrounded by the perisynaptic region which harbors adhesion proteins as FasII, which is linked to synaptic stabilization and growth (Schuster *et al.* 1996; Sone *et al.* 2000). Beneath the PSD the muscle membrane is highly convoluted forming the subsynaptic reticulum (SSR). Various scaffolding and adhesion proteins as Dlg, which might play a role in the structural organization and signaling mechanisms of cell adhesion molecules and ion channels, are found at the SSR membrane (Thomas *et al.* 1997).

The primary structure of glutamatergic synapses at the *Drosophila* NMJ is very similar to excitatory vertebrate CNS synapses, not only ultrastructurally as described earlier in 2.1.2, but also concerning the molecular composition of the presynaptic release machinery (Fernandez-Chacon and Sudhof 1999), and the postsynaptic PSD organization, as described above.

2.3.4 Experience and activity-dependent synapse plasticity

A broad set of mutants, both suppressing and enhancing the outgrowth of the *Drosophila* NMJ, have been identified. As mentioned in 2.3.2 the cell adhesion molecule FasII is a crucial mediator for axonal pathfinding, synaptic stabilization and growth (Fambrough and Goodman 1996; Schuster *et al.* 1996; Thomas *et al.* 1997). It was also demonstrated that higher neuronal activity, decreases synaptic FasII levels, and finally, that loss-of-function and gain-of-function alleles of FasII influenced the sprouting of NMJs (Schuster *et al.* 1996). Therefore, the regulation of cell adhesion is thought to be a prerequisite for the junctional outgrowth and consequently for the addition of novel synaptic contacts resulting from neuronal activity. An artificial elevated presynaptic activity could be genetically achieved by creating a double mutant animal, lacking both *eag* (ether a go-go) and *shaker* (Sh) encoding potassium channels. The absence of these genes leads to an increased frequency of nerve-evoked action potentials. This in turn resulted in elevated cAMP levels, which finally affects the morphological NMJ outgrowth (Zhong *et al.* 1992). The involvement of cAMP signaling in NMJ plasticity could be independently confirmed using the learning mutant *dunce* (Dudai *et al.* 1976; Zhong *et al.* 1992; Cheung *et al.* 1999), which lacks a cAMP phosphodiesterase and increases the concentration of cAMP in the cell (Davis and Kauvar 1984; Zhong *et al.* 1992). The junctional outgrowth was thereby inhibited using a concomitant knockout of *rutabaga*, which encodes for the adenylycyclase (Dudai and Zvi 1985; Livingstone 1985). The cAMP signaling furthermore plays a role in the regulation of synapse formation and structure, as a deletion of *rutabaga* lead to increased synapse size and a decrease synapse number (Renger *et al.* 2000; Shayan and Atwood 2000). *Dunce* mutants, on the other hand, displayed no significant differences in synapse architecture and number when compared to the controls (Renger *et al.* 2000). Instead the presynaptic overexpression of *Dunce* resembled the *rutabaga* deletion (Shayan and Atwood 2000).

Another way of regulating activity of *Drosophila* larvae without genetic intervention may be achieved through the modulation of rearing temperature, which influences their locomotion (Sigrist *et al.* 2003; Zhong and Wu 2004).

The elevated locomotion resulted for keeping the animals at 28 °C, increased the arborization of the NMJ and boosted the formation of new boutons and the synapse number respectively (Sigrist *et al.* 2003; Zhong and Wu 2004). Another interesting fact was raised as the overexpression of the *Drosophila* glutamate receptor subunit IIA (DGluRIIA) was shown to elevate the number of synapses forming per NMJ (Sigrist *et al.* 2002).

2.4 Principles of stimulated emission depletion (STED)

When considering the size of a *Drosophila* NMJ synapse (of about 500 nm in diameter) it only appears logical that in order to visualize its spatial architecture the resolution of image acquisition methods need to be accordingly high. The resolving capacity of conventional visible light microscopy in the focal plane (x, y) ranges between 180 nm to 250 nm and is limited by the numerical aperture of the objective and light diffraction, restricted by the wavelength properties of the light (Pawley 1997; Hell *et al.* 2004). Owing to their diffraction limited resolution, confocal and epifluorescence microscopes cannot properly display subsynaptic organization in a satisfying manner. Electron microscopy, which makes use of much smaller wavelengths, provides sufficient resolution, but the desired labeling efficiency in order to attribute specific proteins to their corresponding structure, requires elaborate staining protocols, which are only moderately successful.

Recent findings in optical physics have shown that the so thought rigid diffraction barrier of far-field microscopy (elaborated by Ernst K. Abbe and published around the 1870s) can be elegantly supplemented by the use of specific molecular characteristics of fluorescent dyes (fluorophores). In their experiments Hell and coworkers demonstrated through a quantum mechanical phenomenon named stimulated emission (Saleh *et al.* 1991) that the resolution in light microscopy could be reduced significantly by partly depleting fluorophores located at the edge of the focal spot (Dyba *et al.* 2003; Hell *et al.* 2004; Willig *et al.* 2006). This method was therefore called stimulated emission depletion microscopy (STED, see Fig. 12).

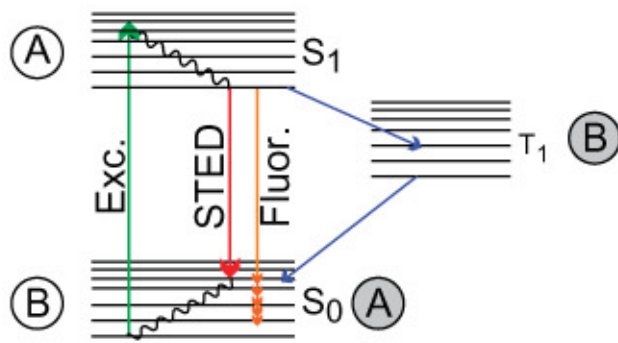


Fig. 12 Principle of stimulated emission

A fluorophore in its excited state (S_1 , A) can be quenched back to its ground state (S_0 , B) by light absorption. This quantum mechanical feature is denominated stimulated emission (adapted from Dyba et al. 2003)

In the STED microscope the excitation beam is overlapped with a doughnut-shaped beam (depleting beam) that is capable of quenching fluorophores by stimulated emission (Fig. 13a). The precise alignment of both beams ensures that fluorescence is allowed only at the very center of the excitation spot where the intensity of the depleting beam is at zero (Fig. 13b). Scanning with a narrowed spot across the sample readily yields images with subdiffractional resolution. With a sufficiently intense depleting beam, the fluorescing spot in a STED microscope can be sharpened down to the molecular scale (80 - 90 nm).

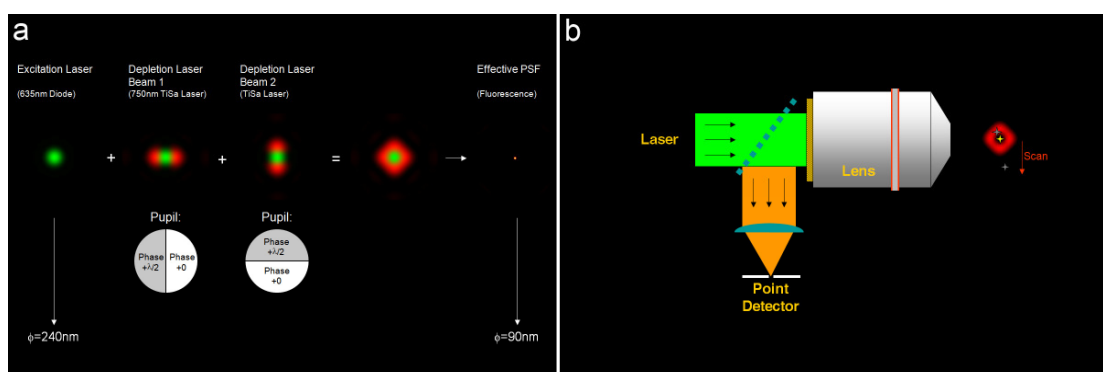


Fig. 13 Technical features of the Leica TSC STED (Leica Microsystems)

a) Generation of the doughnut shaped depleting beam. By a $\lambda/2$ phase shift plate signal intensity in the center of the ring is reduced to zero increasing the effective resolution from 250 nm down to 90 nm (at a wavelength of 635 nm). **b)** By superimposing both excitation and depletion Laser, fluorophores only located in the center of the beam are allowed to release their fluorescence (yellow star), while molecules located at the edge of the excitation beam or outside the scanning region are either not excited or quenched back into the ground state (gray stars). Images kindly provided by M. Dyba, Leica Microsystems.

2.5 Study objectives

Aim of this work is to further explore of how the presynaptic architecture influences the vesicle release machinery by using the fly neuromuscular junction as a model system. By characterizing the localization and dynamics of several important presynaptic proteins meant to play a role in assembly (DLiprin- α and DSyd-1), vesicle release efficiency (Bruchpilot and Ca^{2+} -channels) in relation to already well characterized glutamate receptors (Qin *et al.* 2005; Rasse *et al.* 2005; Schmid *et al.* 2006; Schmid *et al.* 2008), it is the ambition of this thesis to use the latest advances in fluorescence microscopy to correlate the synaptic structure to its function. Thus we want to shed light into whether the reorganization or impairment of AZ substructures may play its part in the control of vesicle release, synapse modulation and ultimately for the proper neuronal function.

3 Material and Methods

3.1 Molecular biology

3.1.1 Material

The following plasmids were used for molecular cloning:

- pBluescript® II KS + (pKS+; Stratagene, La Jolla, USA)
- pEGFP N1 (Clontech, Palo Alto, USA)
- pSL1180 (Fig. 56; Amersham Pharmacia Biotech, Buckinghamshire, England)
- pSL fa1180fa (Horn and Wimmer 2000)
- pUAST (Brand and Perrimon 1993)
- pTWG (Carnegie Institution of Washington)
- pTGW (Carnegie Institution of Washington)

All chemicals were, if not stated elsewhere, purchased from Roth (Karlsruhe, Germany), Sigma (St. Louis, USA) or Merck (Darmstadt, Germany). Agarose was obtained from Peqlab (Erlangen, Germany). Alkaline phosphatase, T4 DNA ligase, T4 polynucleotide kinase, Taq Polymerase and various restriction endonucleases were purchased from Roche (Mannheim, Germany). The restriction endonuclease *Ascl* as well as Vent DNA-Polymerase was obtained from New England Biolabs (Beverly, USA). Elongase® enzyme mix used for overlap-extension PCRs was purchased from Invitrogen (Karlsruhe, Germany). All oligonucleotides were synthesized by MWG Biotech (Ebersberg, Germany). Unless stated elsewhere all molecular biology kits for RNA or DNA extraction and purification were obtained from Qiagen (Hilden, Germany). Chemically competent *E. coli* XL1 blue cells were produced in the lab with standard procedures. All PCRs were performed with the PCR System GeneAmp 9700 (Applied Biosystems, Foster City, USA).

3.1.2 Cloning of fluorescently tagged proteins

The molecular cloning of transgenes was performed using standard molecular biology procedures (Sambrook and Gething 1989). All constructs were double stranded sequenced (MWG Biotech, Ebersberg, Germany). DNA sequences were verified with Sci-Ed Central (Scientific & Educational Software, NC, USA). Overlap-extension PCRs (Fig. 16) were executed according to the Elongase® kit protocol (Invitrogen, Karlsruhe, Germany) with ~30 overlapping base pairs in between the two respective DNA templates.

3.1.2.1 Primer extension method

Mixture 1:

- 10 mM dNTP-Mix
- 10 µM forward primer
- 10 µM reverse primer
- 50 µg DNA template 1
- 50 µg DNA template 2
- add 20 µl H₂O

Mixture 2:

- 5x buffer A
- 5x buffer B
- 2 µl Elongase® enzyme mix
- add 30 µl H₂O

The mixtures 1 and 2 were combined and the PCR was performed as follows:

30x	Denaturation	30''	94 °C
	Annealing	30''	54 °C
	Extension	1' per kbp	68 °C

Step 1: Produce single PCR fragments A, B and C

Step 2: Produce fragment AB



Step 3: Produce fragment ABC



Step 4: Restriction



Fig. 14 Overlap extension PCR

First, three single PCR fragments with roughly 30 overlapping base pairs (striped and checkered regions) are produced using Vent DNA-polymerase. Then, the resulting PCR fragments A and B are combined and subjected to Elongase® overlap-extension PCR creating fragment AB. The enzyme mix, which contains the *Taq* polymerase and the *Pyrococcus* species GB-D polymerase with 3'-5' exonuclease activity, ensures both the fill-up reaction and the rapid template amplification. Finally, a PCR of the AB fragment and the fragment C creates the designated full length PCR product ABC. In order to integrate the final ABC product back into the full length gene the unique restriction sites RS1 and RS2 are needed.

3.1.2.2 Gateway method

The *Drosophila* Gateway Vector collection is a combination of 68 Gateway®-based vectors designed to express fluorophore-tagged proteins in *Drosophila* flies (Carnegie Institution of Washington). Its main tool consists of Invitrogen's Gateway® recombination cassette, which enables the recombination of an Open Reading Frame (ORF) of interest into any of the destination vectors using a simple but efficient recombinase reaction. This reaction results in a fusion gene consisting of your ORF placed in frame with many different fluorescent proteins tags (GFP, CFP, Venus and mRFP, between others) and expressed by the UAS promoter.

Gateway® technology uses lambda integrase to recombine the desired ORF, flanked by attL1 and attL2 recombination sites, with the attR1 and attR2 recombination sites of a destination vector (Fig. 15). The result is a highly efficient and reliable 'swap' of your ORF with the cassette containing the *ccdB* reporter gene in the destination vector. Successfully swapped vectors

can be selected based on their resistance to ampicillin and cell lethality derived from the *ccdB* gene.

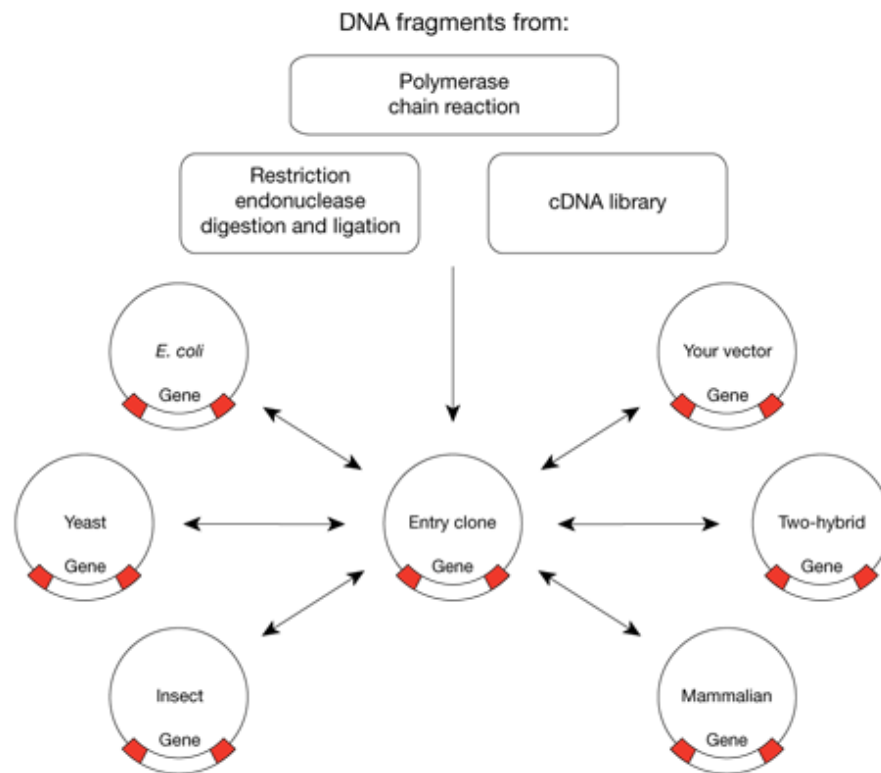


Fig. 15 Gateway® technology facilitates cloning of ORF into destination vectors

Once the desired ORF is brought into an entry vector, it can be easily moved into several different destination vectors, suited with different fluorescent proteins either adding a fluorophore at the very N-Term or the very C-Term of the cloned protein. Red regions represent the *att* recombination sites. (adapted from invitrogen's website)

3.1.2.3 List of cloned vectors and transgenes

- pTWStraw (gateway destination vector created with the primer extension method, substituting the EGFP of the pTWG for mStrawberry, see Shu *et al.* 2006)
- pTWCherry (gateway destination vector created with the primer extension method, substituting the EGFP of the pTWG for mCherry, see Shu *et al.* 2006)

The transgenes used in this study were exclusively developed previously with the methods presented above in 3.1.2.1 and 3.1.2.2.

- DLiprin- α ^{GFP}: constructed by Sara Mertel using the gateway method (Fouquet et al., submitted)
- ^{GFP}DSyd-1 and ^{mStraw}DSyd-1: constructed by David Oswald using the gateway method (Fouquet et al., submitted)
- Cacophony^{GFP}: created by Richard Ordway's laboratory (Kawasaki *et al.* 2004)
- DGlurIIA^{mRFP}: constructed by Tobias Rasse via primer extension method (Rasse *et al.* 2005)
- BRP-short^{GFP} and BRP-short^{mStraw}: created by Sara Mertel via gateway recombination (Fouquet et al., submitted; Schmid and Sigrist 2008)

3.2 *Drosophila melanogaster*

3.2.1 Fly culturing

Fly strains were, if not otherwise stated, reared at 25°C in plastic bottles (Greiner Bio-one, Kremsmünster, Austria) containing cultivation medium (195 g agar, 200 g soy flour, 360 g yeast, 1600 g corn flour, 440 g beet syrup, 1600 g malt, 30 g nipagine, 126 ml propionic acid, add 18 l H₂O). Embryonic collections for intense care rearing were performed in plastic cylinders placed on apple agar plates (1 l apple juice, 100 g saccharose, 85 g agaragar, 40 ml nipagine (15%), add 3 l H₂O). First instar larvae were collected from agar plates 24h AEL and transferred to small (5.5 cm diameter) Petri dishes containing a small amount of mashed cultivation medium. The Petri dishes were sealed with parafim® (American Nation Can Company) and kept at 25°C. Petri dish conditions were checked every 12 h for medium moisture and larval fitness.

3.2.2 Transgenesis

Drosophila germ line transformation was performed with an Eppendorf InjectMan (Hamburg, Germany) as described previously (Rubin and Spradling 1982) using 300 ng/μl P-element DNA (pUAST with inserted

transgene) and 100 ng/μl helper plasmid (pΔ2-3). Transgenic animals were established in the following genetic backgrounds:

- w1 (w^-/w^- ; $+/+$; $+/+$, Castiglioni 1951)
- Df(2R)BSC29 (w^-/w^- ; Df(2R)BSC29, cn^1 , bw^1 , sp^1 /CyO; $+/+$, Mason *et al.* 2004)

3.2.3 The UAS/Gal4 system and drivers

The UAS/Gal4 expression system is broadly used in *Drosophila* for the ectopic expression of transgenic insertions. The yeast transcription factor Gal4, is not present and therefore presumably inactive in the fruit fly. The expression system utilizes the yeast *gal4* insertion and its associated upstream activating sequence (UAS) to which Gal4 binds in order to enable gene transcription. Gal4 may be expressed in many different patterns and tissues by creating enhancer trap lines and placing it under control of specific endogenous promoters. Since UAS promoter sequences cannot be found in the fruit fly, the transcription of the transgenic insertion will only be activated in tissues in which Gal4 is expressed (Brand and Perrimon 1993).

In this project motoneuron/neuron specific driver lines (expressing Gal-4 exclusively in motoneurons/neurons) were used to overexpress fluorescently tagged proteins in order to visualize its synaptic localization in living animals and in fixed samples, in case no antibody were available for the specific protein.

Used driver lines: *ok6*-Gal4; *elav*-Gal4 and *D42*-Gal4

3.2.4 Transgenic lines used in thesis

dsyd-1 mutants (*dsyd-1*^{ex3.4}, eliminating the complete *dsyd-1* and partially the 3' *heph* locus and *dsyd-1*^{ex1.2} eliminating the complete *dsyd-1* locus and partially the 5' *ferrochelatase* locus) were constructed and validated by genomic PCR according to Parks and coworkers (Parks *et al.* 2001). For *dliprin-α* mutants, *dliprin-α*^{EPexR60}/*dliprin-α*^{F3ex15} (Kaufmann *et al.* 2002), for *brp*, *brp*⁶⁹/DfBSC29 (Kittel *et al.* 2006) was used.

For live imaging, Ca²⁺-channels: *ok6-Gal4/+*; *Cac^{GFP}/+* (control); *ok6-Gal4, Cac^{GFP}/+*; *dsyd-1^{ex1.2}/dsyd-1^{ex3.4}* (*dsyd-1* background); DfBSC29, *ok6-Gal4/brp⁶⁹*; *Cac^{GFP}/+* (*brp* background); *elav-Gal4/y; dliprin-α^{EPexR60}/dliprin-α^{F3ex15}*; *Cac^{GFP}/+* (*dliprin-α* background). For temporal analysis of AZ assembly: *ok6-Gal4/+; BRP^{GFP}/DGluRIIA^{mRFP}*, *ok6-Gal4/+; DLiprin-α^{GFP}/DGluRIIA^{mRFP}*; *ok6-Gal4, BRP^{mStraw}/+*; *DLiprin-α^{GFP}/+*, *ok6-Gal4, BRP^{mStraw}/+*; *DSyd-1^{GFP}/+* and *ok6-Gal4/+; DLiprin-α^{GFP}/DSyd-1^{mStraw}*. For DLiprin-α STED stainings: *ok6-Gal4/+; DLiprin-α^{GFP}/+*.

3.3 Immunohistochemistry

3.3.1 Material

For all dissections hemolymph-like (HL-3) saline without Ca²⁺ (Stewart *et al.* 1994) was used: NaCl 70 mM, KCl 5 mM, MgCl₂ 20 mM, NaHCO₃ 10 mM, trehalose 5 mM, sucrose 115 mM, HEPES 5 mM, pH adjusted to 7.2.

3.3.2 Larval body wall preparation

3rd instar larvae were fixed on a rubber dissection pad with fine insect pins (0.1x10 mm, Thorns, Göttingen, Germany) and covered with a drop of ice cold HL-3 solution. Then, the larvae were opened dorsally along the midline from the posterior to the anterior end with dissection spring scissors (FST, Vancouver, Canada). Subsequently, the epidermis was stretched and pinned down with two to three pins on each side and all internal organs including the central nervous system were removed carefully with fine forceps (FST, Vancouver, Canada).

3.3.3 Fixation and staining procedures

The dissected samples were fixed either for 10' with 4% paraformaldehyde (PFA) in PBS (8 g NaCl, 2 g KCl, 2 g KH₂PO₄, 1.15 g Na₂HPO₄ x 2H₂O, add 1 l H₂O, pH 7.4) or for 5' with 98% ethanol at -20 °C (for *Cac^{GFP}* stainings). After 30' of blocking with PBT (PBS with 0.05% Triton TX100, except for anti-DSyd-1 stainings, which used 0.3% Triton TX100) containing 5% goat serum

(NGS), the PBT/NGS solution was refreshed, primary antibodies were added and the dissections were incubated over night at 4°C. The next day the samples were rinsed three times shortly and washed three times for 20' with PBT. Then, fluorescence-labeled secondary antibodies were applied for at least 3 h and at most for 12 h in PBT with 5% NGS. The dissections were washed as after the appliance of the first antibodies and mounted on an object slide in VectaShield Mounting Medium for fluorescent samples (Vector Laboratories, Burlingame, USA).

Primary antibodies were used at the following concentrations:

- mouse anti-GluRIIA (8B4D2; Developmental Studies Hybridoma Bank, Iowa City, USA), 1:250
- rabbit anti-GluRIID (Qin *et al.* 2005), 1:500
- mouse anti-BRP^{Nc82} (gift of E. Buchner, University of Würzburg, Würzburg, Germany), 1:250
- rabbit anti-BRP^{N-term} (Fouquet *et al.*, submitted)
- rabbit anti-DSyd-1 (Fouquet *et al.*, submitted)
- mouse anti-GFP 3E6 (A-11120; Molecular Probes, Eugene, USA), 1:500
- rabbit anti-GFP (A-11122; Molecular Probes, Eugene, USA), 1:500
- goat anti-HRP Cy5 (Dianova, Hamburg, Germany), 1:200

Secondary antibodies were used at the following concentrations:

- goat anti-mouse Alexa488 (A-31560, Invitrogen, Karlsruhe, Germany) 1:500
- goat anti-rabbit Alexa488 (A-11034, Invitrogen, Karlsruhe, Germany), 1:500
- goat anti-mouse Cy3 (A-10521, Invitrogen, Karlsruhe, Germany), 1:500
- goat anti-rabbit Cy3 (A-10520, Invitrogen, Karlsruhe, Germany), 1:500
- goat anti-mouse Atto647N (50185, Sigma-Aldrich, St. Luis, USA), 1:200
- goat anti-rabbit Atto647N (40839, Sigma-Aldrich, St. Luis, USA), 1:100

3.3.4 Atto-647N NHS-Ester antibody conjugation

Antibodies were dissolved in bicarbonate buffer (0.1 M, preferably of pH 8.3) at a final concentration of 2 mg/ml. Values below this concentration will decrease labeling efficiency. Antibody solutions should be free of amine-containing substances such as Tris, glycine or ammonium salt, otherwise the NHS-Ester will react with it. Dissolve Atto 647N NHS-ester in amine-free, dry DMF or DMSO at 2 mg/ml (e.g. 1 mg Atto 674N NHS in 500 µl). For better results this solution should be prepared immediately before conjugation. The dye/protein ratio varies according to the amount and localization of amine groups in the antibodies. In order to get the optimal dye/protein ratio, different concentrations should be tested. Normally a ratio of 1-2 should lead to satisfying results. To obtain a ratio in this range, add a twofold molar excess of reactive dye to the antibody/bicarbonate buffer solution. In case of our experiments, 10 mM of dye solution to 1 mM protein solution were used. Incubate the reaction at room temperature for 60 min under constant stirring. Finally, the labeled antibody can be separated from freely floating dye by gel permeation chromatography, using a SephadexTM G-25 column. It should be equilibrated with 22 mM phosphate buffer of pH 7.2 or another similar buffer of choice, which will be the same buffer used for elution. The first blue band is the labeled protein, while the floating Atto 647N will elute in a second band.

3.4 Image Acquisition

3.4.1 Procedures for fixed samples imaging

Conventional confocal images were acquired with a 63x, 1.4 N.A. oil objective suited in a Leica TCS SP5 or TCS SP2 confocal microscope (Leica Microsystems, Mannheim, Germany). Images taken from fixed samples were exclusively from third instar larval NMJs 6/7 (segments A2, A3). The fluorescence detection was set with the AOBs between 500-530 nm for Alexa 488, between 575-620 nm for Cy3, and 650-700 nm for Cy5. PMT gain was set between 800 and 1100 V for maximum sensibility thereby avoiding the bleaching of fluorescent proteins. Alexa 488 was excited using the 488

nm ArKr laser line, while Cy3 were excited with a 561 nm DPSS laser and Cy5 was excited using the 633 nm HeNe laser. The pinhole ranged between 0.5 to 1 airy units, depending on signal strength. Scanning speed was kept at 400 Hz and pixel size varied between 75 nm and 120 nm.

3.4.2 Procedures for in-vivo imaging (time images / FRAPs)

In vivo imaging was performed on a Leica DMI6000 inverted microscope equipped with a Leica TCS SP5 AOBS scan head and a HCX PL Apo CS 63x 1.32 N.A. OIL objective. The following settings were applied:

- GFP:
 - Excitation: 488 nm (Ar/ArKr laser)
 - Detection: 500 – 540 nm, gain 1250 V
- mRFP, mStrawberry and mCherry:
 - Excitation: 561 nm (He/HeNe laser)
 - Detection: 575 – 620 nm, gain 1250 V
- format: 512 x 512 pixel
- pixel size: 97.75 x 97.75 nm
- z-distance: 500 nm
- line averaging: 4
- pinhole: 1 – 1.5 airy units

All *in vivo* imaging experiments were done as recently presented (Rasse *et al.* 2005; Fuger *et al.* 2007; Schmid and Sigrist 2008). In short, early 3rd instar larvae with a size between 3.0mm and 3.5mm were selected and mounted inside an airproof anaesthetization chamber between two 0.12 mm coverslips. The damaging of the larvae was avoided by placing them in a slit of a thin plastic film, which also held the larvae in place until anaesthetization. The thickness of the film and the size of the slit were adjusted according to the size of the larvae. Both coverslips were covered with Voltalef H 10S oil (Lehman & Voss, Hamburg, Germany) to enable optimal optical access to the ventral larval body wall muscles. Further, a metal ring was placed onto the upper coverslip to fix the animal position and to flatten the larvae as much

as possible to improve optic accessibility. To anesthetize the larvae a mixture of air and Suprane® containing the anesthetic desflurane (Baxter, Unterschleißheim, Germany) was lead into the chamber for about 20 to 30 seconds. Desflurane stops all internal movement, including gut peristaltic and heart beating, which is necessary for undisturbed high resolution imaging of the NMJ synapses. It has been demonstrated, that even several rounds of anaesthetization do not interfere with further growth and function of the synaptic system (Rasse *et al.* 2005; Fuger *et al.* 2007). To focus on a specific NMJ (usually NMJ 27 and 26 in abdominal segment A2 and A3), normal halogen light was used to identify the respective muscle. For FRAP (fluorescence recovery after photobleaching) experiments either the mRFP/mStrawberry (high intensity 561nm laser) or both the GFP and mRFP/mStrawberry channel (high intensity 488nm laser) were bleached until residual fluorescent signals were no longer detectable in the respective NMJ part. After each imaging session (maximally 30 min, ideally 15 min) single larvae were placed inside Petri dishes containing standard fly cultivation medium and raised at 25° as before. After the fist imaging session the same NMJs were recovered within regular time intervals (3 h, 6 h, 12 h or 24 h) and subjected to live imaging again. In experiments composed of imaging intervals shorter than 30 min, the larvae was wakened inside the anaesthetization chamber by briefly applying fresh air, kept in the chamber for the given interval and re-anaesthetized just before the next image acquisition.

3.4.3 The LCS STED microscope and its acquisition settings

For the STED images the Leica TCS STED setup was used in combination with a 100x, 1.4 n.a. oil objective (Leica Microsystems, Mannheim, Germany). Detection of the Atto-647N fluorophore was performed with APDs and filters for wavelengths between 650 and 710 nm. APD gain was continuously set to 310 V. Excitation laser power varied according to the sample, but always ranged between 5.0 and 5.6 V. Pinhole was kept at 0.5 airy units, when possible, to decrease background, but never passed 1 airy units. Scan speed was set to 5 Hz. The pixel size was kept at 25.22 nm

Confocal co-images in STED experiments were acquired sequentially and had the same settings as described in 3.4.1, except for the scanning speed, which varied between 10 and 100 Hz, according to the fluorophore characteristics.

3.5 Image processing and analysis

3.5.1 Software

The image analysis itself was led through with ImageJ (NIH, Bethesda, USA). All calculations were performed with Microsoft Excel (Microsoft Corporation, Redmond, USA). Graphics and statistics were produced with Prism 4 (GraphPad Software, San Diego, USA). Image transformation and compilation was done with Adobe Photoshop (Adobe Systems, San Jose, USA).

3.5.1.1 Confocal imaging. Confocal stacks were mainly processed with ImageJ software (see above). Image quality enhancing procedures (deconvolutions) were used for single slices and confocal stacks available as ImageJ plug-ins: 'iterative deconvolution' and 'iterative deconvolution 3D' respectively (Bob Dougherty, OptiNav, Inc.). A representation of the point-spread-function (PSF) was created using the 'Diffraction PSF 3D plug-in' (Bob Dougherty, OptiNav, Inc.).

3.5.1.2 STED imaging. STED images were processed via a linear deconvolution tool implemented into the ImSpector Software bundle (Max-Planck Innovations GmbH, Munich). Regularization parameters ranged from $1e^{-10}$ to $1e^{-12}$. The PSF was created with the 'Arithmetics' tool also comprised in ImSpector using the three dimensional Lorentz function ($a / (a^2 + x^2 + y^2)$), while 'a' represents the half width half maximum (HWHM) value of the PSF.

3.5.2 Image Quantifications

All images comprising the synapse number quantification were acquired using the same microscope settings, control and mutant dissections were stained in the same vial.

3.5.2.1 Defining the synapse number

To count the number of synapses per NMJ, first the original stack was scaled up two-fold. A Gaussian filter with a radius of two pixels was applied. The contrast of the maximum projection of that image stack was adjusted in such way, that the intensity maximum of the picture was set to 255 (min/max contrast function, ImageJ). Afterwards a threshold was set excluding all pixels with a value inferior to 51. The segmentation of single synapses was done by hand with the pencil tool and a line thickness of 2 pixels. The processed image was then transformed into a binary picture with all pixels with a value lower than 51 receiving the value “0” and all pixels with a value higher and equal to 51 were reassigned to a value of “255”. This binary mask was then projected onto the original unmodified image using the “min” operation from the ImageJ image calculator. The synapses of resulting image were counted with the help of the “analyze particle” function with the threshold set to 1, thereby measuring the number, the size and the mean intensity for every synapse.

3.5.2.2 Measuring the peak-to-peak distances

The quantification was exclusively performed on ImageJ. In order to measure the peak-to-peak distances between to labels, images were acquired with optimal sampling rates (pixel size of 75 nm). The acquired pictures were scaled to 2x of their original size and a gaussian blur filter was applied with a radius of 2 pixels. Only synapses were selected that were placed at the very edge of boutons, which are more likely to be visualized horizontally. A strait line was placed over the intensity maxima of both labels and the distance in pixels was measured.

3.5.2.3 Defining the temporal sequence

In order to identify which synaptic label precedes which, images of two consecutive time points, acquired in an interval of 12 h, were analyzed. Protein agglomerations were defined as Synapses, which were 2.5 times

brighter than the mean background level. New synapses were scored if spots defined as synapses in the second time point were not detectable (less intense than 2.5 x the background) in the same area in the first time point. When imaging two distinct labels synapses were screened, which had only one detectable label in the first acquisition, but both labels in the second time point. Therefore conclusions about the assembling sequence could be made, as some synaptic proteins were detected earlier than others.

3.5.2.4 Averaging of synapses

With the intuition to generate a representation of an image engulfing the information of several synapses, merged pictures were created. Therefore several synapses were aligned regarding their AZ center (BRP) and projected using the 'sum' function in ImageJ. The images were not quantified and attend only to display the probability where selected proteins reside at the AZ.

3.5.3 Statistical analysis

The nonparametric Mann-Whitney rank sum test was used for statistical analysis of all linear independent data groups. The data are reported as mean \pm s.e.m., n indicates the sample number, and p denotes the significance: * p<0.05, ** p<0.01, ***p<0.001. Linear and non-linear (Gaussian fit) regression was used to determine significant data correlation.

4 Results

4.1 Structural organization of the presynaptic active zone

4.1.1 The monoclonal antibody Nc82 labels Bruchpilot

The monoclonal antibody Nc82 reliably labels the presynaptic AZs of seemingly all *Drosophila* synapses and has been used as a tool to identify synaptic contacts both in central and peripheral neurons (Kittel *et al.* 2006; Wagh *et al.* 2006). Thereby it has been demonstrated by the lab of Erich Buchner (Universität Würzburg) that Nc82, which derived from a monoclonal library created against *Drosophila* head extracts, recognizes an epitope within the C-terminal tail of a large protein named Bruchpilot (Nc82 will therefore be named BRP^{C-Term}) (Wagh *et al.* 2006). BRP expression is thereby confined to postmitotic, differentiated neurons and the protein is encoded by a large complex locus that consists of several coiled-coil domains distributed over its entire length (Wagh *et al.* 2006). Thereby, its N-terminal part encodes a sequence, which features homologies over the whole extend of the mammalian AZ protein family CAST/ERC, while the C-terminal is highly conserved between all insects but not found elsewhere (Kittel *et al.* 2006; Wagh *et al.* 2006). In short, the BRP N-terminal half encodes a full length CAST, but the protein is extended at its C-term in comparison to other CAST-family members (see Fig.16).

The CAST/ERC proteins have been described to localize close to the AZ in close range to electron dense projections of photoreceptors of the rat, while their functions still remain to be elucidated (Ohtsuka *et al.* 2002; Ko *et al.* 2003; Deguchi-Tawarada *et al.* 2006). Thus, an investigation of the fly homologue, BRP, could help to further understand its role in synapses and guide later research for putative functions in vertebrates.

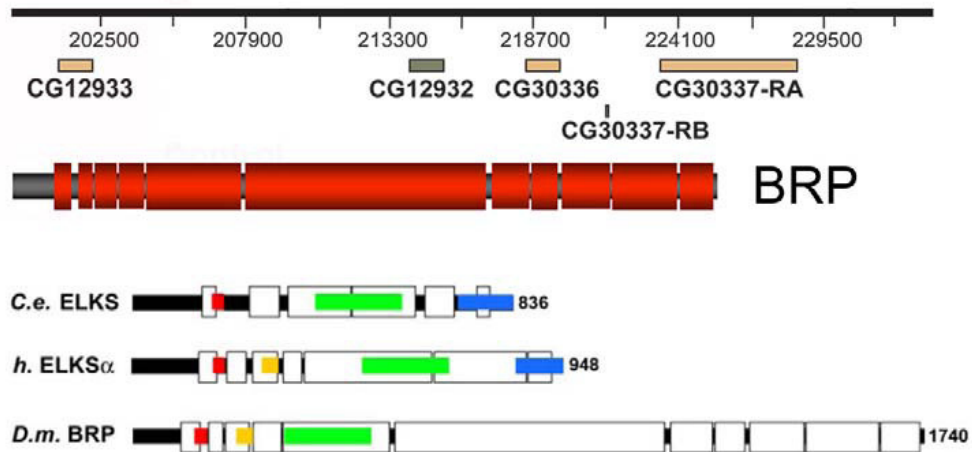


Fig. 16 *Drosophila* BRP shows N-terminal homology to CAST/ERC.

The *brp* locus consists of 18 exons (organized in 3 exon-clusters), which were formerly annotated as three independent genes (CG12933, CG30336 and CG30337). The BRP protein is rich in coiled-coil domains (demarcated in red). Comparisons of predicted coiled-coil domains (white boxes) and conserved regions (colour) for *C. elegans*, human, and *Drosophila* homologues. The N-terminal 480 amino acids of Bruchpilot contain short homologous stretches of up to 67 % identity with both mammalian and *C. elegans* CAST/ERC (colored bars), but Bruchpilot lacks the IWA motif (blue, Wagh *et al.*, 2006).

4.1.2 AZ proteins localize at different distances from the AZ membrane

We were interested to study the cyto-architecture of AZ proteins by localizing proteins within this arrangement. The distance to the AZ membrane could reveal whether the protein in question could be associated, e.g. to exocytotic function or, on the other hand, play an important role in vesicle recruitment and scaffolding functions. A protein localized distant from the AZ membrane (and not directly associated to vesicles) would less likely be considered to have a function in vesicle docking and priming, as they would be expected to gather closely to the AZ membrane. In contrast, if localized far from the membrane, it might have a function in guiding vesicles from internal pools to the release site.

At *Drosophila* NMJ boutons, the orientation of synapses relative to the optical axis can be readily defined, since bouton surfaces are nearly spherical. Thus, one could use proteins known to bind to the membrane (either pre- or postsynaptically) as markers to measure the distances to other protein clusters (see also 3.5.2.2).

In order to estimate how far away synaptic proteins are in relation to other membrane markers we performed confocal peak-to-peak distance measurements. The monoclonal antibody Nc82 (BRP^{C-Term}) identified

diffraction-limited spots in images opposite the center of postsynaptic receptor fields (PSDs, DGlurIID signal) (Fig. 17a). BRP^{C-Term} and GluRIID signals were separated by about 150 nm along an axis vertical to the bouton surface (Fig. 17a and e). The distance between BRP^{C-Term} and presynaptic Ca²⁺-channels however measured approximately 100 nm along the vertical axis whereas the distance between Cac^{GFP} and DGlurIID measured approximately 40 nm. Thus, the epitope recognized by BRP^{C-Term} is oriented away from the presynaptic AZ membrane. We co-labeled BRP^{N-Term} and BRP^{C-Term} (Fig. 17c) and quantified the centre-to-centre intensity maxima of each signal. BRP^{N-Term} label was found to be approximately 75 nm closer to the plasma membrane than the C-terminal label (Fig. 17e). The centre-to-centre location between BRP^{N-Term} and Cac^{GFP} however was only about 65 nm apart (Fig. 17e). Thus, not only are different synaptic proteins localized at different distances from the plasma membrane, but BRP seems to establish an elongated structure as BRP^{C-Term} and BRP^{N-Term} in fact are segregated along an axis perpendicular to the AZ membrane.

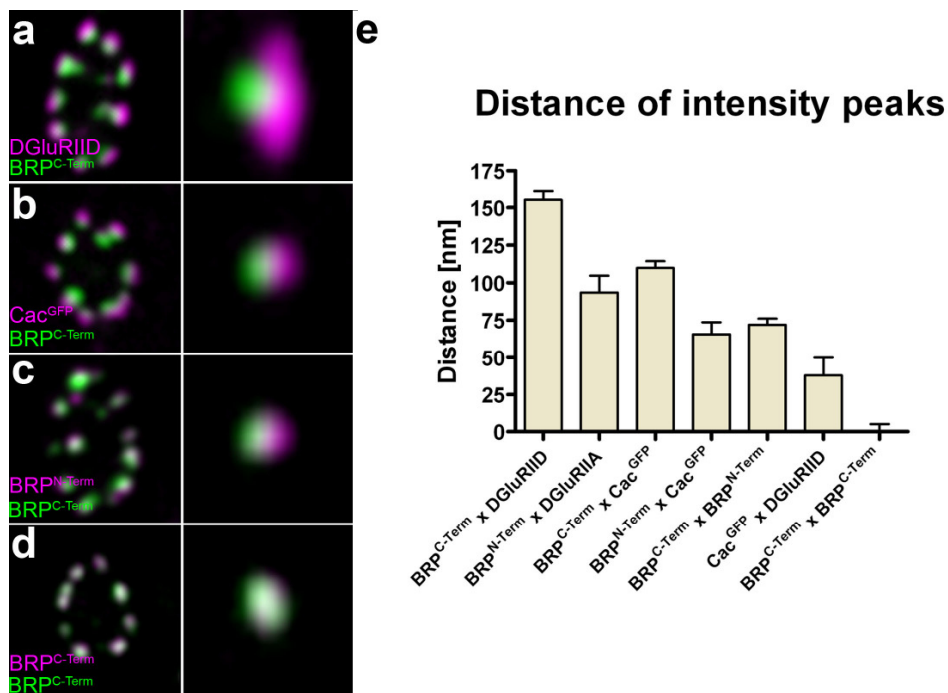


Fig. 17 Synaptic protein localization regarding their distances to the membrane
(a - d) Confocal images of an immunocytochemically stained single synapse with the bouton lumen facing towards the left, stained for **a)** GluRIID, magenta and BRP^{C-Term}, green, **b)** Cac^{GFP}, magenta and BRP^{C-Term}, green; **c)** BRP^{N-Term}, magenta and BRP^{C-Term}, green and as a control **d)** BRP^{C-Term}, magenta and BRP^{C-Term}, green. Scale bars: 500 nm and 100 nm. **e)** Distance of center-to-center intensity maxima for different synapse labels (n=30 for each group).

4.1.3 BRP extends vertical to AZ membrane

When analyzing the structure of BRP, confocal microscopy recognized diffraction limited spots located at the center of AZs, consistent with the AZ size of about 300 nm (Fig. 18a and b).

As mentioned above (4.1.1), the Nc82 epitope was mapped to the C-terminal part of the nearly 2000 amino acid BRP protein. At *Drosophila* NMJ boutons, the orientation of synapses relative to the optical axis can be readily defined, since bouton surfaces are nearly spherical, as also described in 4.1.2. Through the high resolution of stimulated emission depletion fluorescence microscopy (STED), donut-shaped BRP structures were reproduced from tangentially imaged AZs (Fig. 18b and Fig. 19a arrow and b) reaching an effective point spread function of 80 nm full-width-half-maximum (FWHM). From here on, tangentially imaged AZs are called planar AZs (Fig. 19b-f left, arrow in Fig. 19a) whereas vertically imaged AZs are referred to as vertical AZs (Fig. 19b-f right, arrow head in Fig. 19a). Planar synapses, were comprised of structures consisting of both single and multiple 'rings', which were of similar size to freeze-fracture-derived estimates of fly AZs. Average length of isolated rings (Fig. 18b, arrows) was $0.191 \pm 0.002 \mu\text{m}$, $n = 204$; average length of single rings within double ring structures (Fig. 18b, arrow heads) was $0.148 \pm 0.002 \mu\text{m}$. Average length of double rings was 0.297 ± 0.005 , (fig. 18c) (Kittel *et al.* 2006). The donuts were up to $0.16 \mu\text{m}$ high, as judged by images taken parallel to the synaptic plane (not shown).

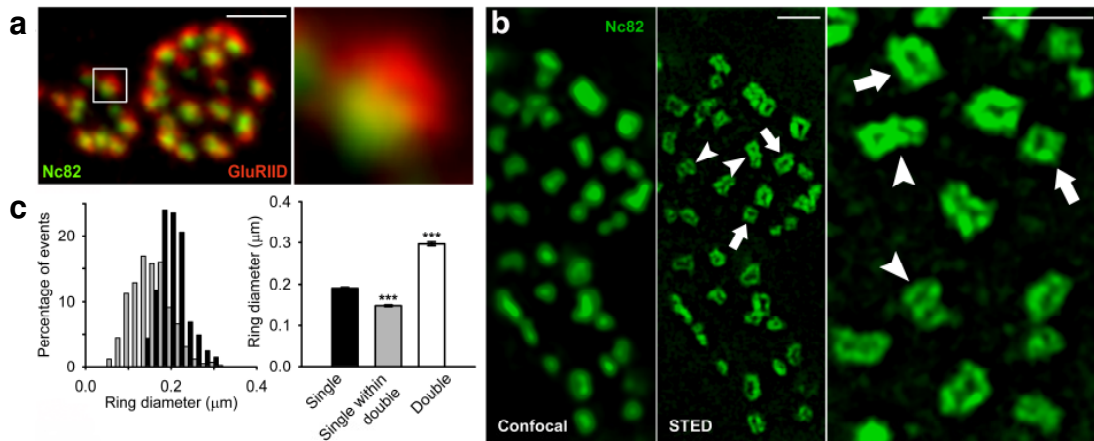


Fig. 18 BRP^{Nc82} localizes at AZ in a polygonal ring-like structure

a) The active zone marker Nc82 labels the presynaptic area opposite postsynaptic glutamate receptor fields stained with the glutamate receptor subunit GluRIID. Scale bar: 1 μm **b)** Unlike confocal, STED microscopy reveals ring-like structures recognised by Nc82. Both single rings (arrows) and clusters of multiple rings (arrowheads) were identified. Scale bar: 500 nm **c)** The quantification of ring length illustrates that individual rings (black) were larger than single rings contained within assemblies of double rings (grey, $p < 0.001$). Adapted from Kittel *et al.* 2006.

In order to probe BRP substructure Sara Mertel raised a polyclonal antibody directed against an N-terminal peptide sequence of BRP (BRP^{N-Term}; Fouquet *et al.* submitted). Other than BRP^{C-Term}, BRP^{N-Term} did not show a donut-shaped distribution when imaged with STED (Fig. 19d). The combination of STED-resolution for BRP^{C-Term} and confocal resolution for BRP^{N-Term} (STED is confined to one channel) rather revealed a 'funnel-like' distribution of BRP epitopes (Fig. 19a and b). Notably, the BRP^{C-Term} signal appeared not fully continuous but instead to consist of discrete foci (Fig. 19b and e).

In order to extend our picture of AZ organization, and as BRP has been shown to be crucial for Ca²⁺-channel clustering (see 4.3.1), we wanted to verify the structural organization according to these findings. Confocally imaged Ca²⁺-channel spots (GFP-labeled Cacophony, Cac^{GFP}; Kawasaki *et al.* 2004) were found in the center of BRP^{C-Term} donuts at planar AZs, and localized towards the membrane at vertical AZs (Fig. 19b). With STED resolution (Fig. 19c), Ca²⁺-channels were found in small patches (about 100-150 nm in longest axis) at the AZ center. In vertical AZs, BRP^{N-Term} localized further towards the bouton interior compared to Ca²⁺-channels, but closer to the membrane than BRP^{C-Term} (Fig. 19d and e). In order to probe whether the observed distances might be due to differential distributions of potential BRP

isoforms, we expressed full-length *brp*^{CDNA} in *brp* mutants (Wagh *et al.* 2006). Displacement between BRP^{N-Term} and BRP^{C-Term} was similar to that observed in control AZs (Fig. 19f). Thus, individual BRP molecules indeed take up an elongated conformation, vertical to the AZ membrane.

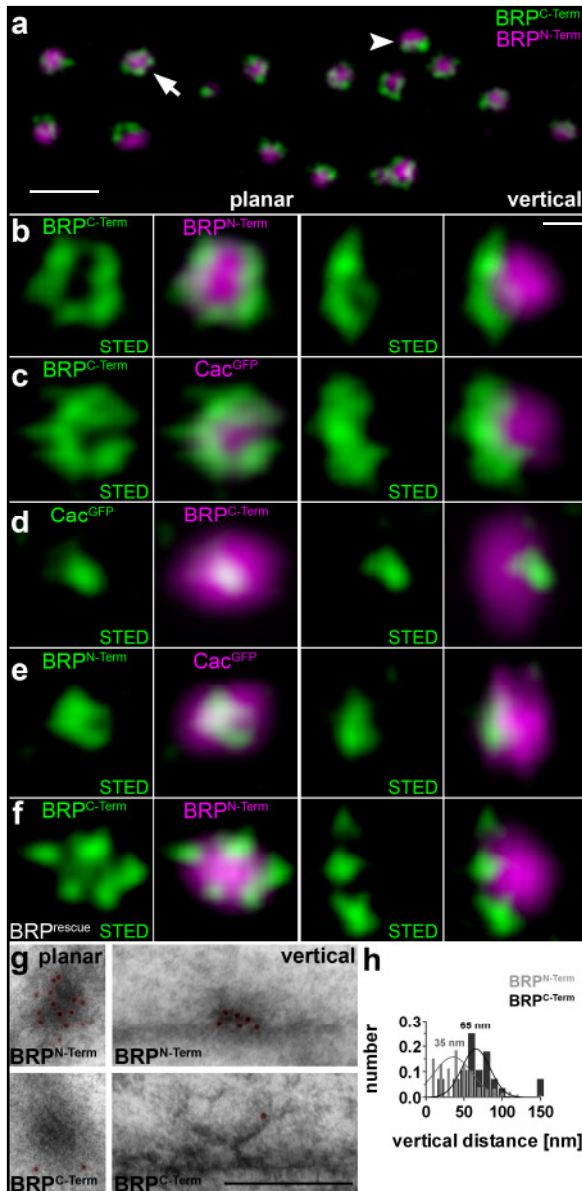


Fig. 19 STED and immuno-EM analysis of AZ organization at *Drosophila* NMJ synapses

a) Overview of a typical bouton stained for BRP^{N-Term} (confocal, magenta) and BRP^{C-Term} (STED, green). The arrow indicates a planar and the arrowhead a vertical AZ. Scale bar: 500 nm **b – f)** Magnifications of individual planar (left) and vertical (right) AZs, stained for: **b)** Cac^{GFP} (confocal) and BRP^{C-Term} (STED), **c)** Cac^{GFP} (STED) and BRP^{C-Term} (confocal), **d)** Cac^{GFP} (confocal) and BRP^{N-Term} (STED), **e)** BRP^{N-Term} (confocal) and BRP^{C-Term} (STED), **f)** BRP^{N-Term} (STED) and BRP^{C-Term} (STED) after re-expression of full length *brp*-cDNA in *brp* null background. **g)** Immunogold labeling of planar (left) and vertical (right) AZs with antibodies against either BRP^{N-Term} or BRP^{C-Term} (for clarity gold particles are highlighted by red circles). Scale bar: 100 nm **h)** Quantification of the gold particle distribution found with BRP^{N-Term} and BRP^{C-Term}. The BRP^{N-Term} signal is found closer to the AZ membrane (35 nm) in comparison to the BRP^{C-Term} signal (65 nm, peak of Gaussian fit).

4.1.4 BRP localizes to the electron dense T-bar matrix

It still remained to be elucidated whether BRP epitopes are directly associated with the T-bar dense body using immuno-electron microscopy (performed by Dr. Carolin Wichmann; Fouquet *et al.* submitted). The antibodies to both epitopes, BRP^{N-Term} and BRP^{C-Term}, clearly bound to the

electron dense T-bar matrix (Fig. 19g), with higher labelling efficacy of the BRP^{N-Term} antibody. In vertical sections (right panels), the BRP^{N-Term} antibody was found to thoroughly label the pedestal region of the CAZ. This indicates that BRP is an integral component of the *Drosophila* CAZ. As expected from STED images, the N-terminal epitope appeared considerably closer to the AZ membrane than the C-terminal epitope. In vertical sections, the BRP^{C-Term} epitope was typically found at the edge of the electron dense structures (Fig. 19g, bottom right panel). To quantify the spatial distribution of the N-terminal and the C-terminal BRP label, the vertical distances of individual gold particles to the corresponding AZ membrane were determined (Fig. 19h). We found that the N-terminal label was closer to the AZ membrane compared to the C-terminal label (the peaks of the Gaussian fits were separated by roughly 30 nm).

When combining these findings with the previously shown STED images, BRP localization was tightly associated with the T-bars in a polarized conformation with N- and C-term segregated along an axis perpendicular to the AZ membrane and parallel to the T-bar longitudinal axis. As no T-bars form in the absence of BRP (see chapter 4.3; Kittel *et al.* 2006), BRP most likely is a direct T-bar component, with the protein extending throughout the T-bar ribbon, thereby giving the dense body its shape.

4.1.5 Proteomics identify *Drosophila* DSyd-1 via biochemical interaction to Bruchpilot

In order to gain further insights into the AZ architecture, BRP was used to search for further synaptic interactors (performed by Manuela Schmidt and David Oswald). Using Nc82, which recognizes an epitope close to the C-terminus of BRP (Wagh *et al.* 2006), BRP was immuno-precipitated from adult fly head extracts. Bands of co-precipitating proteins were subsequently analyzed by MS/MS analysis in order to identify putative interaction partners. One band delivered several peptides (Fig. 20) corresponding to a putative protein named CG1976 also known as RhoGAP100F. This protein was predicted to encode a *Drosophila* orthologue of *C.elegans* Syd-1 (Hallam *et al.* 2002). Syd-1 has been implicated in playing a role in both axon/dendrite

identity formation and AZ assembly (Dai *et al.* 2006; Patel *et al.* 2006). As the first functional analysis was performed on the worm orthologue, the *Drosophila* gene will be referred in the following as *dsyd-1*. DSyd-1 is predicted to comprise a calcium-sensing/lipid/protein binding C2 domain, a PDZ protein-protein interaction domain and a putative RhoGAP domain (Fig. 20b; Fouquet *et al.* submitted).

In order to elucidate whether DSyd-1 might directly interact with BRP, overlapping constructs of either proteins were used as bait or prey in a yeast-two-hybrid (Y2H) assay (performed by David Oswald, Harald Depner and Sara Mertel). Thereby multiple interactions between both proteins were found (Fig. 20c). In addition, to confirm the interaction in native cells, *Drosophila* Schneider S2R cells were co-transfected with Myc-tagged *dsyd-1* cDNA and the C-terminal 1152 –1740 amino acids of *brp* tagged with GFP, which showed colocalization (Fig. 20d). As well as in the Y2H experiments, BRP and DSyd-1 were efficiently co-precipitated reciprocally. This results likely suggests that both proteins do biochemically interact.

Previously a direct interaction between the mammal homologue of BRP, CAST, and Liprin- α has been reported (Ko *et al.* 2003). Taking these results into consideration preliminary Y2H experiments using both proteins, BRP and DLiprin- α were performed and an interaction could thereby be determined (data not shown).

These findings were suggestive of a direct biochemical interaction between Bruchpilot, DSyd-1 and DLiprin- α , indicating that these proteins are part of the specialized protein meshwork present in the presynaptic AZ.

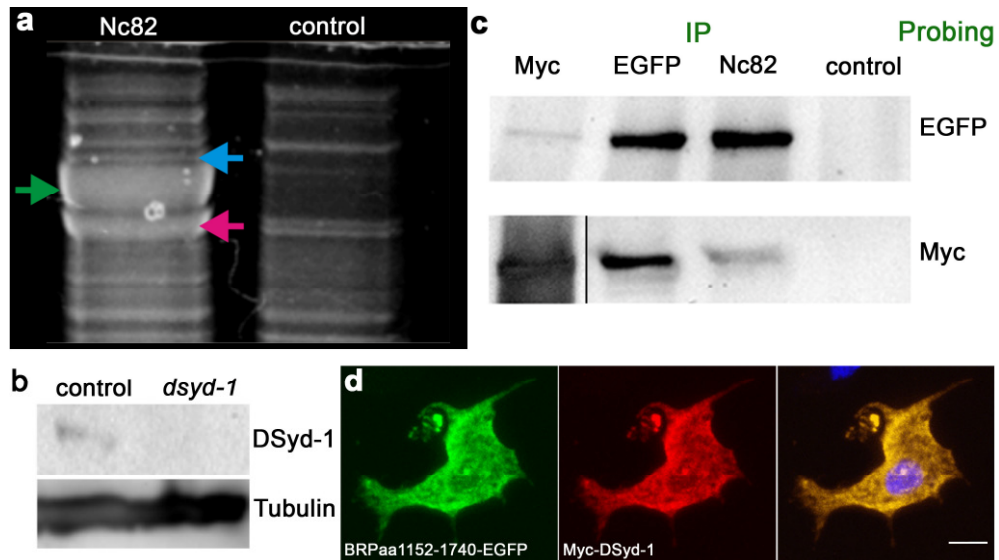


Fig. 20 DSyd-1 physically interacts with BRP

a) Nc82 efficiently precipitates BRP (left lane, green and magenta arrows) as seen in this Cypro Ruby stained SDS-gel. Amongst others DSyd-1 was found to co-precipitate with BRP (blue arrows) as confirmed by MS/MS analysis **b)** The polyclonal anti-DSyd-1 antibody recognizes a band at the predicted molecular weight of 195 kDa on immunoblots of control fly head lysate. This band is lacking in *dsyd-1* deficient flies (upper panel). The lower panel shows the same immunoblot probed with anti-tubulin antibody as loading control. **c)** Immunoblots of co-immunoprecipitates obtained from Myc-DSyd-1 and BRPaa1152-1740-EGFP co-transfected *Drosophila* Schneider S2R cells. Anti-Myc, -EGFP, -Nc82 and control IPs are shown. Blots incubated with ECL were developed for 30 minutes, except for the anti-Myc IP probed with anti-Myc antibody which was exposed for 10 minutes. **d)** Immunostainings of Myc-DSyd-1 and BRPaa1152-1740-EGFP co-transfected *Drosophila* Schneider S2R cells. The nucleus was counter-stained with DAPI as seen in the merge picture. Scale bar: 10 μ m.

4.1.6 DLiprin- α and DSyd-1 are localized in 'quantal' clusters at the AZ edge

To extend our AZ map including these BRP interactors, DLiprin- α ^{GFP} was expressed in motoneurons and visualized with α GFP-stainings (compare confocal and STED resolution in Fig. 21a). In order to visualize DSyd-1 a polyclonal antibody was raised against a C-terminal peptide recognizing a band of about 195 kDa on *Drosophila* head extract immunoblots, which was absent in *dsyd-1* mutant animals (David Oswald, Fig. 20b). STED resolution revealed that both DLiprin- α and DSyd-1 formed four to five discrete clusters at the edge of single mature AZs (Fig. 21b and c).

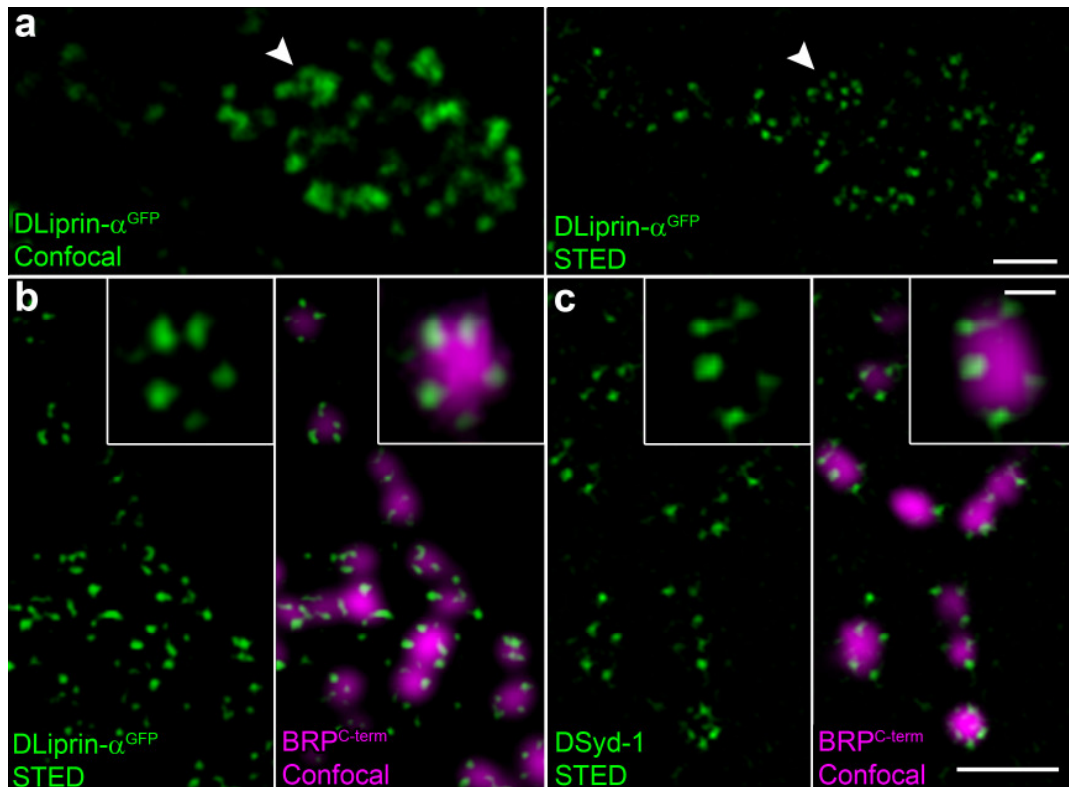


Fig. 21 Discrete DLiprin- α^{GFP} / DSyd-1 clusters surrounding the AZ core
a) STED image of DLiprin- α^{GFP} displays structures beyond diffraction-limited resolution obtained with confocal microscope (arrow heads). Scale bar: 1 μm
b) Single confocal slices of junctions expressing DLiprin- α^{GFP} . STED images of α^{GFP} show DLiprin- α^{GFP} as discrete dots arranged around the AZ core labeled by BRP (magenta), ranging from 1-2 dots at small AZs to four to five dots at matured AZs.
c) Single confocal slices of NMJs stained for endogenous DSyd-1 (green, STED) and BRP (magenta, confocal). Distinct separable DSyd-1 dots are arranged around the AZ comparable to the DLiprin- α localization. Scale bar: 1 μm (lower magnification) and 250 nm (higher magnification). Images were deconvolved using ImInspector software.

We quantified the distribution and size of these modules gathered from planar STED-imaged AZs displaying three DLiprin- α or DSyd-1 clusters and freely floating clusters (Fig. 22a and b). Individual DLiprin- α and DSyd-1 dots were found to have a very similar diameter of approximately 100 nm. As STED resolution was about 80 nm in our experiments, the relation between the structure and the microscopy resolution should be high enough to sample these structures properly. Standard deviations were surprisingly small for the dot diameters suggesting them to reflect discrete building ‘quanta’ of AZs. Center-to-center distances between DLiprin- α or DSyd-1 signals were around 250 to 300 nm, respectively (Fig. 22a and b). As this value is comparable to ultrastructural estimates for AZ diameter (Govind and Pearce 2003), these ‘quanta’ seemed localized at the AZ edge. DLiprin- α and DSyd-1 quanta,

however, were not solely restricted to established AZs characterized by BRP expression. As the average size of these clusters found outside mature sized AZs was strikingly similar to quanta confined to mature AZ (Fig. 22a and b), it appears likely that these dots belong to a pool of clusters that navigate through the NMJ boutons, associating to existing AZs or being transported to newly forming ones.

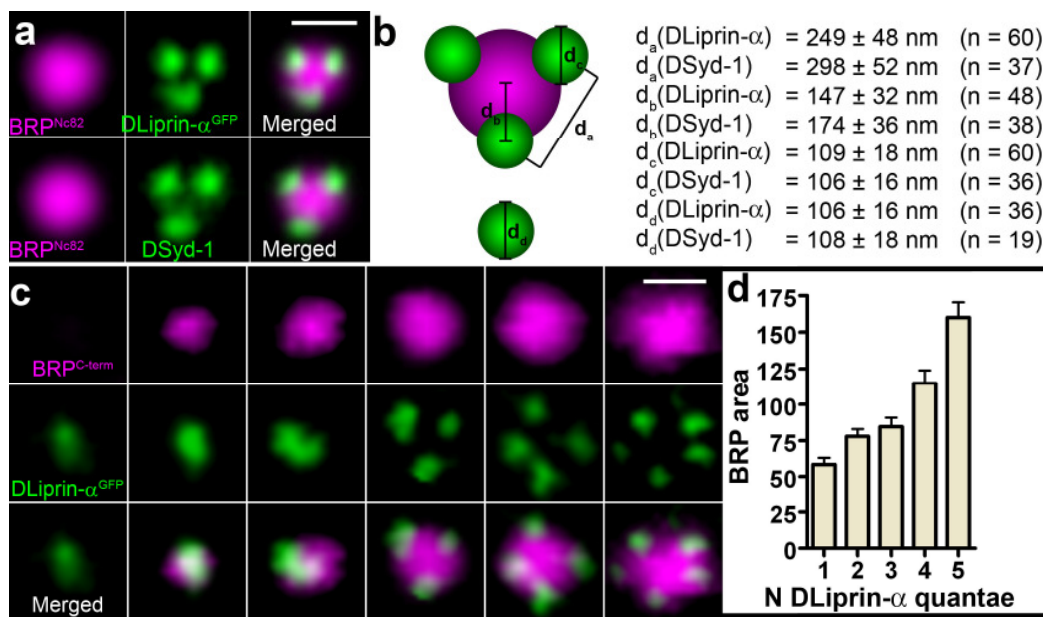


Fig. 22 Quantification of AZ architecture using STED

a) Merged picture of several aligned planar imaged AZs of mid-size associated with three DLiprin- α and DSyd-1 clusters. BRP^{C-term} in confocal resolution, α -GFP for DLiprin- α ^{GFP} or for endogenous DSyd-1 imaged with STED. **b)** Quantification of images as in A). Discrete DLiprin- α cluster centers are similar in diameter compared to DSyd-1 cluster centers. d_a : distance between single clusters associated with the AZ; d_b : distance between AZ associated cluster and AZ center; d_c : diameter of clusters associated with AZs; d_d : diameter of cluster not associated with AZs. **c)** Predicted sequence of AZ assembly based on STED images. **d)** Average area of BRP clusters regarding the number of DLiprin- α spots associated to the AZ. The BRP size thereby increases corresponding to the number of DLiprin- α dots.

4.2 Observing synapse assembly *in-vivo*

4.2.1 A temporal sequence of *in vivo* AZ assembly

The spatial organization of synaptic proteins is not the only important feature for a deeper understanding. Knowing *when* synaptic proteins cluster at AZs is

also relevant. Thus, we were interested in characterizing AZ assembly *in vivo*. We recently devised ways to visualize protein traffic at identified individual synapses over extended periods in intact living larvae (Rasse *et al.* 2005; Fuger *et al.* 2007; Schmid and Sigrist 2008). Here, we used these protocols to study developmental formation of AZs. As our previous work had characterized synaptic dynamics of glutamate receptor subunit DGluRIIA in detail (Rasse *et al.* 2005; Schmid *et al.* 2008), we used this protein as a reference point for our time line of synapse assembly. Here, we imaged larvae co-expressing two fluorescently tagged synaptic proteins (Fig. 23), and extracted quantitative data (see 3.5.2.3) to construct a temporal sequence of 'protein arrival' at forming AZs (Table I). For a given larval NMJ, two *in vivo* images were acquired with a time interval of 12 hours. Sites were regarded as new synapses if *both* protein-labels exceeded the average background by a factor of 2.5 at the second (t=12h) but not the first time point (t=0h). At these new sites, we scored whether one of the two protein labels had exceeded the background level (if yes scored as "+" in Table 1) at the first time point (t=0h).

We first compared BRP and DGluRIIA accumulation. For visualization of BRP we used a fragment of the protein, whose AZ label fully matched the Nc82 label of endogenous BRP (BRP-short; Schmid *et al.* 2008). This was expressed as fusion with GFP or mStrawberry (BRP^{GFP}, Fig. 3A; BRP^{mStraw}, Fig. 23c, d). As expected (Rasse *et al.* 2005; Schmid *et al.* 2008), DGluRIIA accumulation clearly preceded BRP accumulation *in vivo* (Fig. 23a, Table I). Furthermore, all postsynaptic DGluRIIA accumulations incorporated presynaptic BRP eventually, showing that DGluRIIA accumulation safely indicates formation of new synapses. When expressed in motoneurons, DLiprin- α clearly localized to presynaptic AZs opposite DGluRIIA positive PSDs (Fig. 23b, Table I). In clear contrast to BRP, DLiprin- α preceded the arrival of DGluRIIA (Fig. 23b, Table I). Consistently, BRP accumulation invariably followed DLiprin- α incorporation (Fig. 23c, Table I). In line with this, DSyd-1 also preceded BRP arrival at synaptic sites (Fig. 23d, Table I). Finally, DLiprin- α and DSyd-1 accumulation matched closely in time and in some cases DLiprin- α seemed to arrive at the synapse first (Fig. 23e, Table

l). Thus, shorter imaging intervals were needed to temporarily resolve the assembly (See 4.2.5).

In summary, these data provide direct *in vivo* evidence that the assembly of individual new synaptic sites protracts over hours, with an overlapping, defined sequence of pre- and postsynaptic proteins joining in. DLiprin- α and DSyd-1 appeared to be very early players, while the incorporation of BRP seemed to center an AZ maturation process, which followed the incorporation of postsynaptic DGluRIIA dominating glutamate evoked conductance (Petersen *et al.* 1997; DiAntonio *et al.* 1999; Schmid *et al.* 2008).

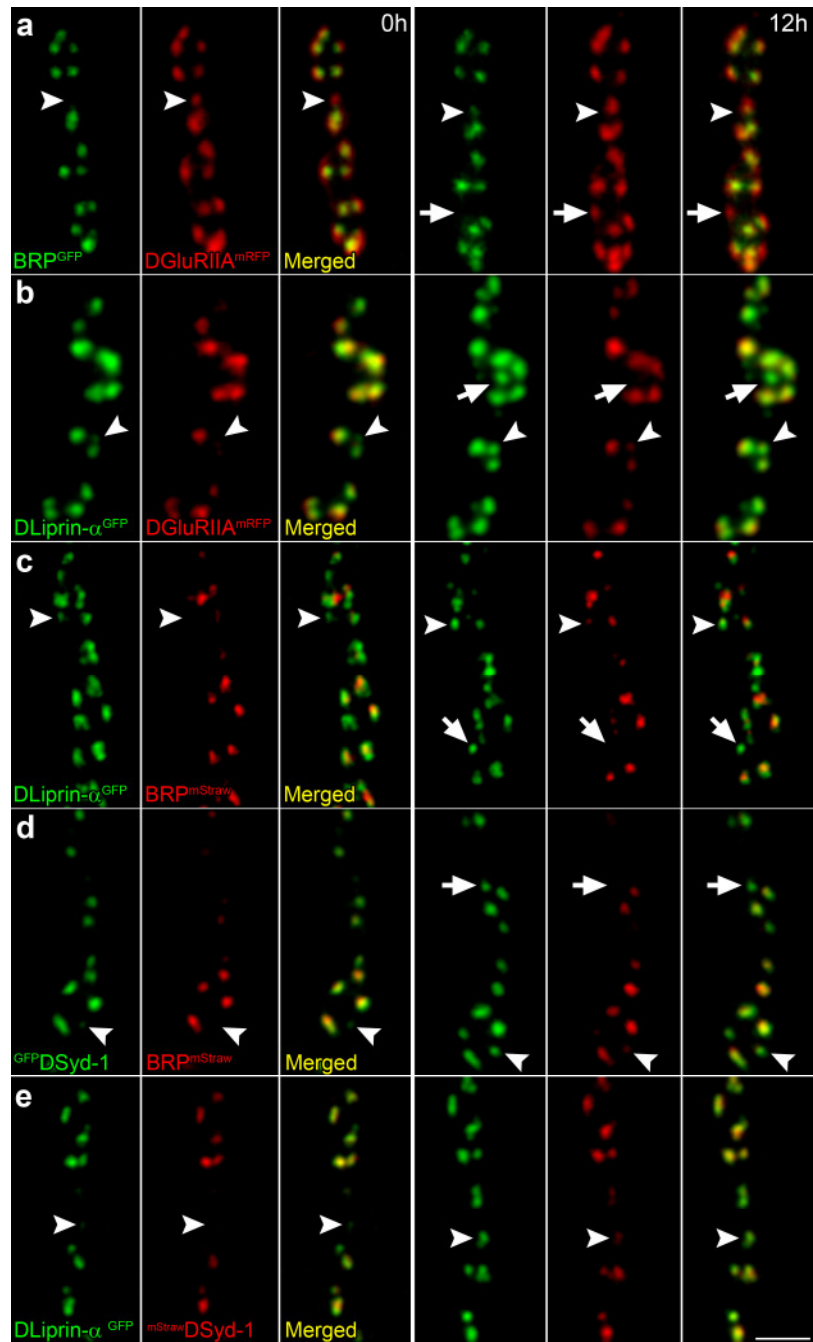


Fig. 23 *In vivo* analysis of synaptic protein accumulation

Shown are developing NMJs of intact living 3rd instar *Drosophila* larvae. (a - e) Confocal stacks of sequentially *in vivo* imaged NMJs (muscle 26), $\Delta t = 12h$. NMJs co-expressing the indicated labels, GFP constructs green, mRFP/mStrawberry constructs red. Arrow heads show synapses positive for only one label at t=0h, but positive for both labels at t=12h. Arrows show a prospective synapse positive for only one label at t=12h. Scale bars: 1 μm . a) BRP^{GFP} / DGluRIIA^{mRFP}, b) DLiprin- α ^{GFP} / DGluRIIA^{mStraw}, c) DLiprin- α ^{GFP} / BRP^{mStraw}, d) GFP^{DSyd-1} / BRP^{mStraw}. e) DLiprin- α ^{GFP} / mStraw^{DSyd-1}

BRP x DGluRIIA	BRP⁻/IIA⁻	BRP⁺/IIA⁻	BRP⁻/IIA⁺
	17/39 (44%)	0/39 (0%)	22/39 (56%)
DLiprin-α x DGluRIIA	DLiprin-α⁻/IIA⁻	DLiprin-α⁺/IIA⁻	DLiprin-α⁻/IIA⁺
	16/39 (41%)	23/39 (59%)	0/39 (0%)
BRP x DLiprin-α	BRP⁻/DLiprin-α⁻	BRP⁺/DLiprin-α⁻	BRP⁻/DLiprin-α⁺
	8/31 (26%)	0/31 (0%)	23/31 (74%)
BRP x DSyd1	BRP⁻/DSyd-1⁻	BRP⁺/DSyd-1⁻	BRP⁻/DSyd-1⁺
	21/48 (44%)	0/48 (0%)	27/48 (56%)
DLiprin-α x DSyd1	DLiprin-α⁻/DSyd-1⁻	DLiprin-α⁺/DSyd-1⁻	DLiprin-α⁻/DSyd-1⁺
	25/32 (74%)	7/32 (26%)	0/32 (0%)

Table I. Quantification depicting the relation of temporal assembly between synaptic proteins observed within a time interval of 12 h.

The table describes events in which no or only one label was detectable (higher than 2.5x the mean background level) at the first time point, while a correlation of both labels was seen in the second imaging session. Labels not present in the first image were scored negatively (-), whereas labels already present in the first time point were scored positively (+). The results suggest that DLiprin- α reaches the synapse at an early time point, as no event was found in which another synaptic protein preceded DLiprin- α in assembly. BRP arrived after all analyzed proteins were already present at the synaptic terminal.

4.2.2 BRP shows fast protein turn-over but no changes in its steady state signal

When following the localization of BRP over short time intervals (30 – 60 min) no significant change in the steady state signal was observed (Fig. 25), which suggested BRP being a rather stable protein assembly.

To complement these results, fluorescence recovery after photobleaching (FRAP) experiments were performed. We proceeded by imaging NMJs of muscle 26 and 27 in intact anaesthetized larvae expressing the short version of the *brp* cDNA (Schmid *et al.* 2008) tagged with mStrawberry at its C-term. By applying high laser intensity in a square region with an edge length of roughly 10 μ m, we were able to bleach 2-3 boutons, thereby leaving a considerable part of the NMJ intact as a reference area (Fig. 24). After a time interval of 30 minutes, the bleached area showed a recovery to about 50% of pre-bleached signal intensity, demonstrating an incorporation of roughly half the amount of protein present in the synaptic region before the bleaching

experiment. As in the control region no increase of AZ size or intensity could be detected (not shown), an equivalent amount of protein must have left the synapse (compare Fig. 24 and Fig. 25).

Despite first assumptions based on the ultrastructure and the steady state intensity levels, FRAP experiments revealed a high motility for BRP.

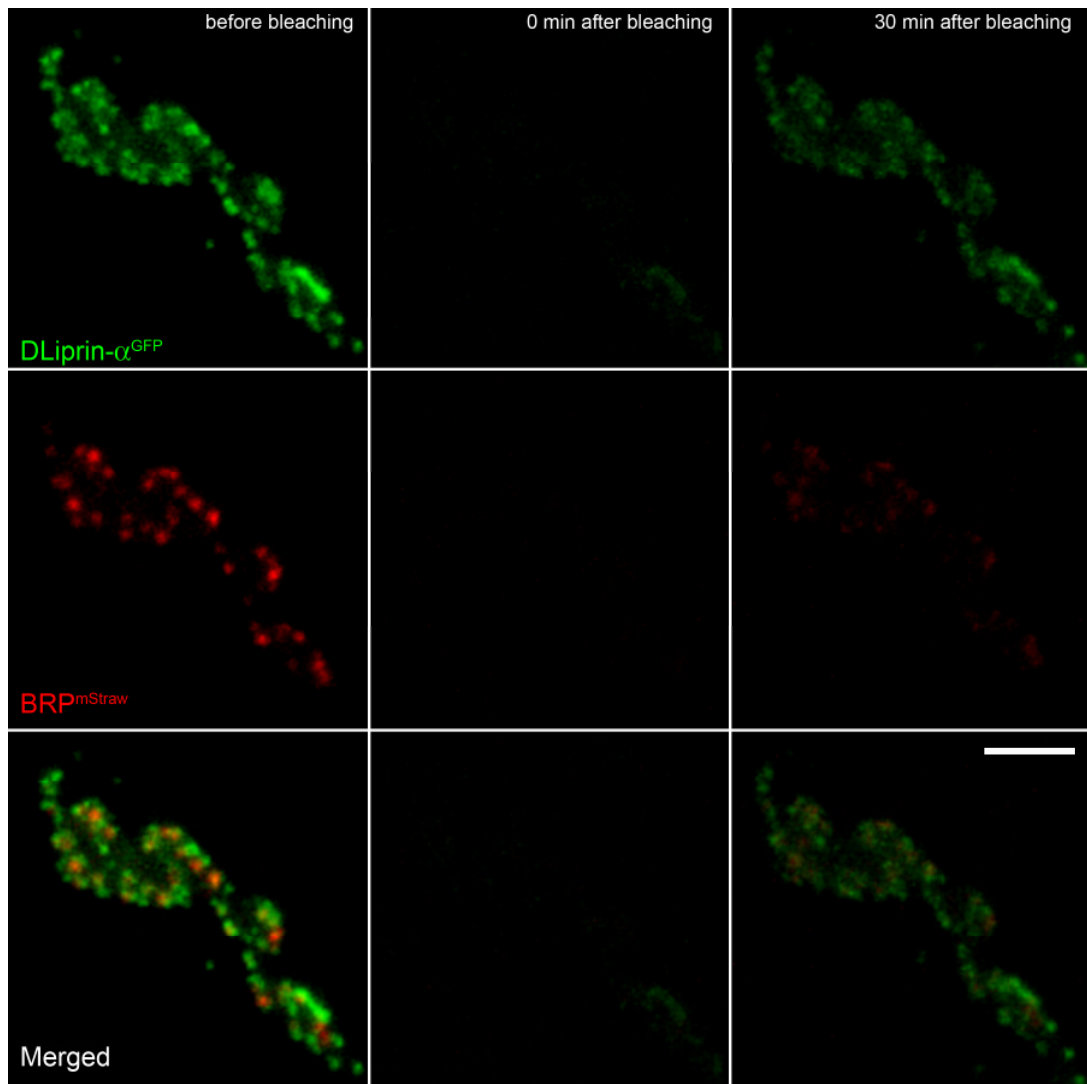


Fig. 24 Similar recovery after FRAP for DLiprin-α and BRP

DLiprin-α (green) and BRP (red) show similar recovery rates after FRAP. Both synaptic proteins display a high protein turnover, when recovering roughly 50 % of the original intensity after only 30 min. Scale bar 2 μm.

4.2.3 DLiprin- α dynamics at AZs are characterized by fast exchange and continuous remodeling

In FRAP experiments with DLiprin- α^{GFP} , the protein showed a similar recovery as BRP as roughly 50% of the signal intensity was restored after 30 minutes (Fig. 24). Even more interestingly, the distribution of the DLiprin- α signal changed drastically within this time interval (Fig. 25). In many cases strong fluctuations in DLiprin- α signal intensity were observed at residual AZs. Furthermore, small particles were seen apart from established synapses appearing and disappearing (Fig. 25 arrows). These changes were equally seen in experiments with even shorter time intervals (10 min, data not shown). These findings not only suggest a fast exchange of DLiprin- α , but also a dynamic remodeling of the DLiprin- α associated architecture.

STED images of DLiprin- α^{GFP} expressing larvae revealed discrete dots arranged around the edge of AZs (see 4.1.6). In many cases dots of the same size (100 nm) were also observed distant from established AZs (positive for BRP). It appears most likely that these clusters found outside AZs represent the 'fluctuating' clusters of DLiprin- α described in this chapter (Fig. 25, arrows). Thus, similar sized clusters of DLiprin- α might operate at nascent as well as at mature size AZs. It is conceivable that these clusters are transported to the junction as discrete objects, but the resolution of conventional confocal microscopy is not high enough to properly visualize it. New advances in STED technology in living organisms could lend a helping hand in future experiments, as demonstrated by Hell and coworkers (Hein *et al.* 2008).

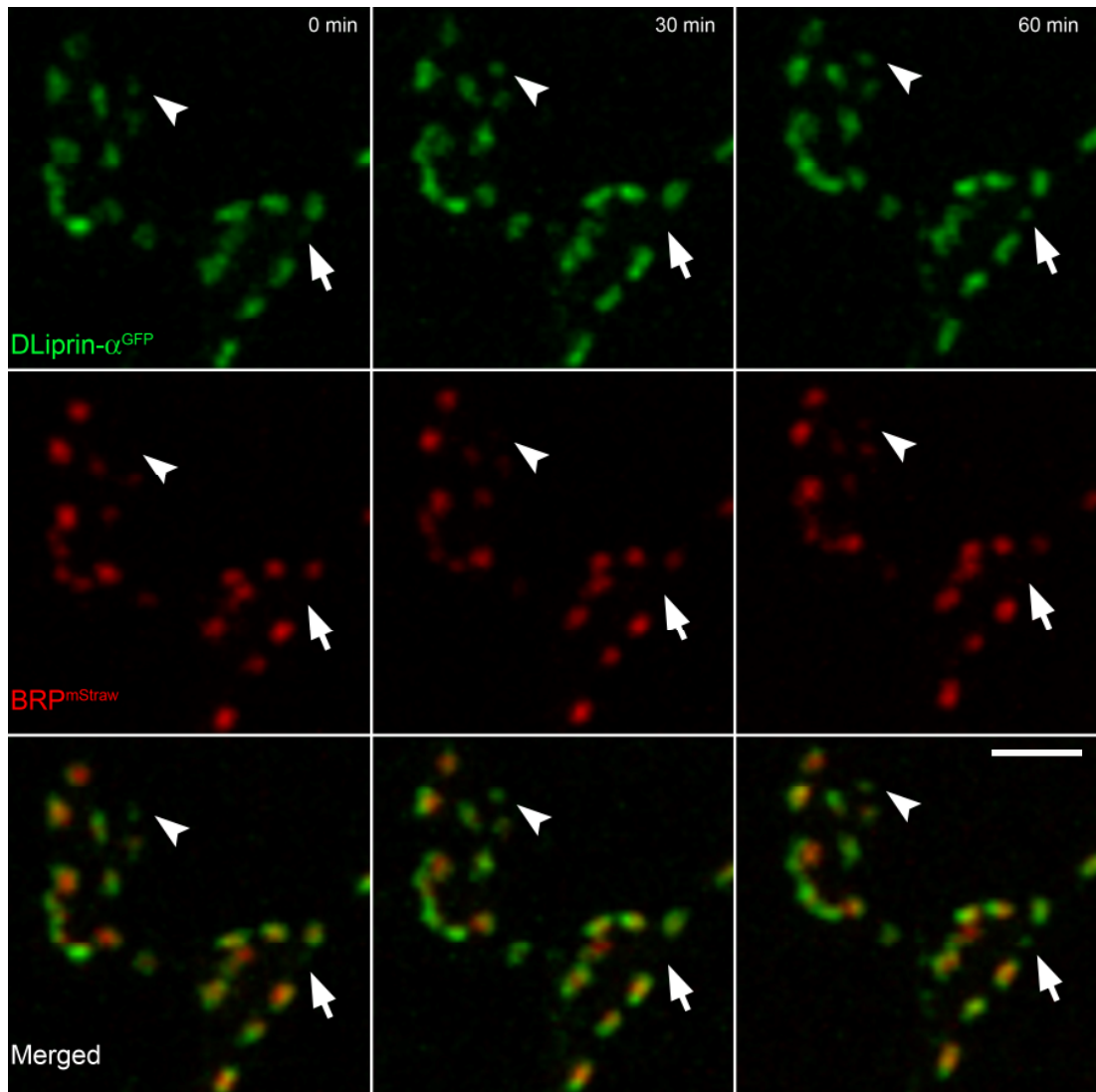


Fig. 25 Drastic DLiprin- α reorganization within short time intervals compared to BRP
 Fluctuating clusters of DLiprin- α can be observed during short time intervals (arrows), while BRP aggregates appear unaltered. This figure also retains an example of a newly forming AZ (arrow heads) depicting a DLiprin- α positive spot accumulating BRP. BRP accumulation appears rather slow, when compared to new DLiprin- α accumulations (arrows) suggesting a different assembly mechanism. Scale bar 1 μ m.

4.2.4 BRP accumulates late, in the AZ center, from diffuse pools

When co-imaging DLiprin- α with BRP at high temporal resolution (Fig. 25) the DLiprin- α clusters typically seemed to surround BRP, which clustered in the AZ center (Fig. 25 and Fig. 21). Moreover, discrete, dynamic spots were observed distant from matured AZs (Fig. 25, arrows). In contrast, BRP appeared restricted to maturing AZs (Fig. 25) indicated by an invariant association with the DLiprin- α quanta. Moreover, BRP accumulations, once established, appeared stable in intensity and distribution, while the associated DLiprin- α clusters changed in appearance. When comparing the

speed in which new accumulations of DLiprin- α and BRP gather at synapses (compare Fig 25 arrow heads and arrows) and their distinct localization at the AZ is seems obvious that both proteins reach the target synapse with different transport mechanisms. While clusters of DLiprin- α appear and disappear completely in short time intervals, suggesting an incorporation of discrete quanta, BRP aggregates at synapses gradually, indicating an accumulation from diffuse pools.

4.2.5 DLiprin- α and DSyd-1 co-fluctuate within an early, still reversible AZ assembly phase

To address a more precise conclusion concerning the temporal organization of DSyd-1, which also arrived at putative nascent synapses early, similar experiments as the ones described in the previous chapter were conducted. On the level of single mature AZs, DLiprin- α^{GFP} strictly co-localized with $\text{mStraw}^{\text{DSyd-1}}$ ($R = 0.814$) but less with $\text{BRP}^{\text{mStraw}}$ ($R = 0.656$; also compare Fig. 25 and 26). When followed over time, DLiprin- α and DSyd-1 positive accumulations frequently dissolved again (Fig. 26b, arrows). While, in some occasions, DLiprin- α seemed first to advent (Fig. 26a, arrows) and last to leave (Fig. 26b, arrows), the overall timing of both proteins reaching AZs appeared very similar. Moreover, shape and intensity of these clusters co-fluctuated over time.

Taking their high degree of co-localization (in confocal experiments), similar organization at AZs (STED, see Fig. 21) and co-fluctuation into account, it appears likely that DLiprin- α and DSyd-1 are aggregated in the same clusters (DLiprin- α /DSyd-1 cluster – LSC). Thus, while DLiprin- α and DSyd-1 positive clusters are stereotypically involved in the early assembly of stable AZs (Fig. 23 and Table I), obviously not all such clusters lead to mature synapses. Instead, we find that some of them disappear within tens of minutes (Fig. 26b, arrows).

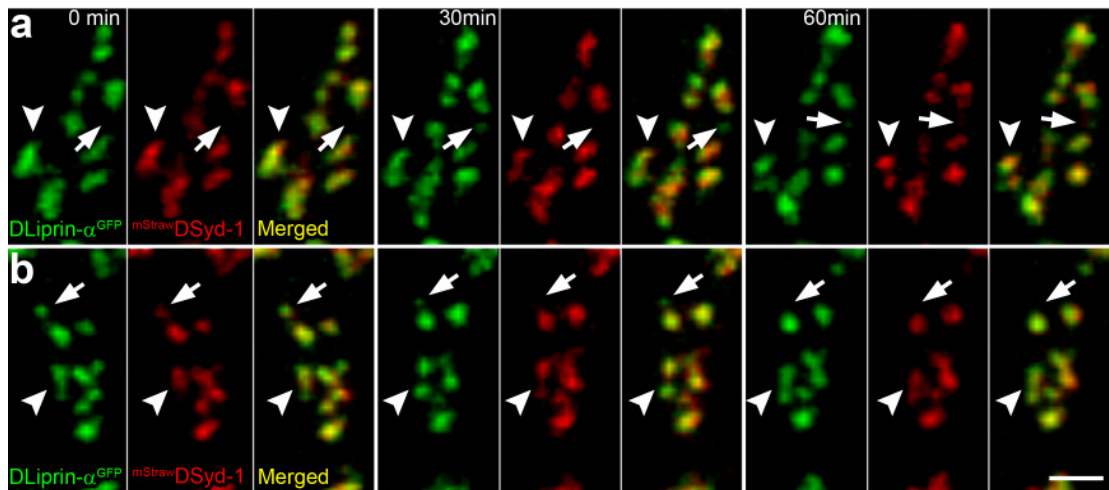


Fig. 26 DLiprin- α and DSyd-1 show tightly correlated structural rearrangements
 High magnification *in vivo* images acquired in 30 min time intervals of junctions located on muscles 26 and 27. **a - b)** Time series of larvae expressing DLiprin- α^{GFP} and $\text{mStraw}^{\text{DSyd-1}}$. DSyd-1 (red) behavior was highly dynamic and comparable to that of DLiprin- α (green), displaying structural rearrangements in short time intervals. DLiprin- α was detected slightly before DSyd-1 (**a**, arrows). DSyd-1 however left established nascent sites earlier than DLiprin- α (**b**, arrows). Scale bar: 1 μm .

Taken together, DLiprin- α and DSyd-1 form fluctuating clusters (LSCs). As these clusters however do not move on scales of seconds as judged from our *in vivo* imaging experiments, they might well mark early stages of AZ assembly and thus may demark putative nascent synaptic sites. Some of these gradually increase in size and enter into a more stable state. At the time BRP gets incorporated to detectable levels, AZs have entered an apparently irreversible maturation process.

4.3 Dissecting functional and structural roles of AZ proteins

4.3.1 Brp mutants lack T-bars and have a reduced vesicle release probability

The specific distribution of BRP suggested a role of this factor in defining AZs structure and/or composition. To test this hypothesis, we sought to eliminate BRP function. Transposon-mediated mutagenesis allowed us to isolate a mutant chromosome (*brp*⁶⁹, Kittel *et al.* 2006), in which nearly the whole open reading frame of BRP was deleted (Fig. 27).

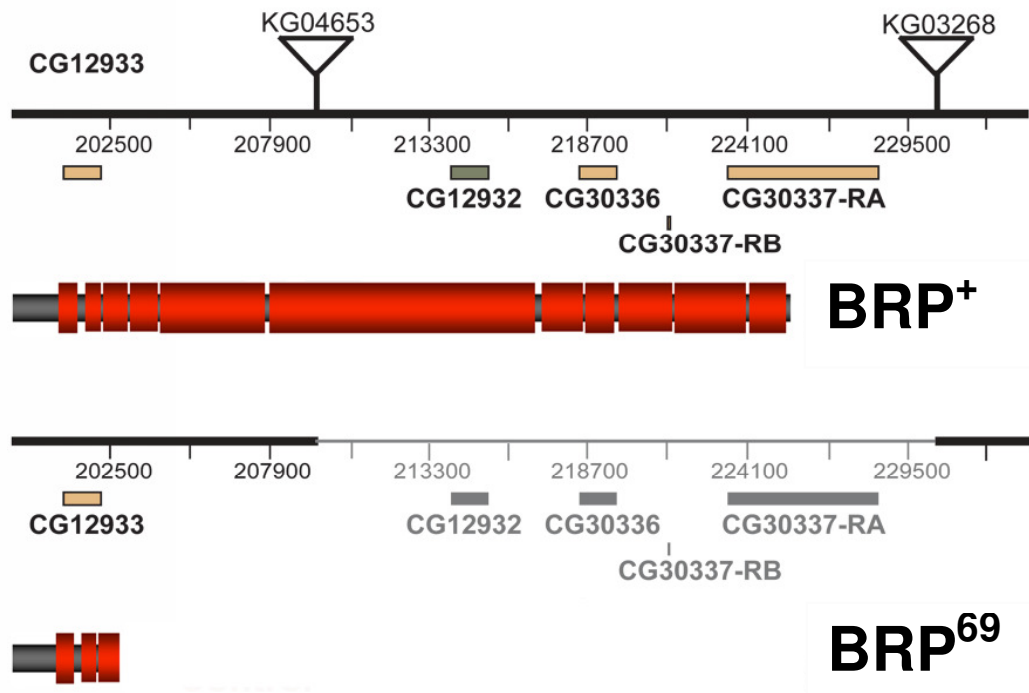


Fig. 27 Transposon mediated deletion of the BRP locus

Through transposase mediated deletion a major region between KG04653 and KG03268 of the *BRP* locus could be deleted generating the mutant allele *brp*⁶⁹.

brp mutants (*brp*⁶⁹/*df(2R)BSC29*) could still develop into mature larvae but only rarely formed pupae. Previous investigations (Wagh *et al.* 2006) had shown that the Nc82 epitope maps to the C-terminal half of BRP. Consistently, the Nc82 label was completely lost from the AZs of *brp* mutant NMJs, but could be partially restored by re-expressing the *brp* cDNA (Wagh *et al.* 2006) in the *brp* background using the neuron-specific driver lines *ok6-Gal4* (Kittel *et al.* 2006) or *elav-Gal4* (not shown). This neuron-specific re-expression of BRP using neuronal promoter elements also partially rescued from larval lethality (Kittel *et al.* 2006). In *brp* mutant larvae, the morphological size of NMJs, as determined by the projected surface area of α HRP staining, was slightly but significantly reduced (control: $780.0 \pm 35.8 \mu\text{m}^2$, $n = 14$; *brp*: $593.3 \pm 29.1 \mu\text{m}^2$, $n = 12$; $P = 0.0013$), and in accord with this, *brp* mutant NMJs also had somewhat less individual synapses (control: 411.1 ± 41.5 , $n = 9$; *brp*: 296.3 ± 28.9 , $n = 8$; $P = 0.036$), as judged by staining against the glutamate receptor subunit GluRIID. However, individual receptor fields were enlarged in *brp* mutants (control: $0.43 \pm 0.02 \mu\text{m}^2$, $n = 9$; *brp*: $0.64 \pm 0.03 \mu\text{m}^2$, $n = 8$; $P < 0.001$) and surrounded by the characteristic

perisynaptic expression of the NCAM homologue FasII. In summary, principal synapse formation proceeded normally in *brp* mutants, with individual postsynaptic receptor fields increased in size but moderately decreased in number.

Electron microscopy was then used to study the synaptic structure in more detail (performed by Dr. Carolin Wichmann, Kittel *et al.* 2006). *brp* mutants, synapses were present at normal density, and consistent with the enlarged glutamate receptor fields. In contrast, severe defects in the ultrastructural organisation of the presynaptic AZ were observed at mutant synapses. *brp* mutants completely lacked presynaptic dense projections. However, after re-expressing the BRP protein in the mutant background, T-bar formation could be partially restored, though these structures were occasionally somewhat aberrant in shape (Kittel *et al.* 2006). In conclusion, BRP assists in correctly assembling the CAZ, and is essential for T-bar formation at *Drosophila* NMJ synapses.

The physiological consequences of BRP and subsequently T-bar loss were analyzed by employing two-electrode voltage clamp (TEVC) recordings of postsynaptic currents (performed by Robert Kittel). A drastic decrease of eEJC amplitudes in *brp* mutant larvae at low stimulation frequencies was discovered. This drop in current amplitude could be partially rescued through BRP re-expression within the presynaptic motoneurons using either *elav-Gal4* or *ok6-Gal4*. The decrease of evoked and, further, the increase of miniature EJC amplitudes implicates that the number of vesicles released per presynaptic action potential (quantal content) was severely compromised at *brp* mutant NMJs. Moreover these defects could not be solely attributed to a 28 % decrease in synapse number. Together with absence of T-bars, the reduced quantal content strongly suggested that *brp* mutants had a major impairment of synaptic vesicle release.

As described in (2.1.3) the exact amplitude and time course of the action potential (AP) triggered Ca^{2+} -influx in the nerve terminal governs the amplitude and time course of vesicle release, and has a profound effect on short-term plasticity. It is therefore conceivable that the described altered short-term plasticity of *brp* mutant synapses suggests a change in the highly

Ca²⁺-dependent vesicle release probability (Kittel *et al.* 2006). Previous studies have demonstrated that vesicle release is sensitive to the spacing between Ca²⁺-channels and vesicles at release sites (Neher and Sakaba 2008). In fact, the probability of a synaptic vesicle to undergo secretion following the opening of a single Ca²⁺-channel has been calculated to decrease threefold when this distance is doubled from 25 to 50 nm.

The presynaptically expressed N-type $\alpha 1$ Ca²⁺-channel subunit Cacophony (Cac) dominates release at *Drosophila* neuromuscular junctions. By utilizing a fully functional, GFP labelled variant of Cac (Cac^{GFP}), Ca²⁺-channels were visualized at the NMJ using *in vivo* imaging of *Drosophila* larvae. In controls, Cac^{GFP} was confined to small spots, indicating Ca²⁺-channel clusters at presynaptic AZs (Fig. 28). Calculations of the mean GFP-intensity illustrated that in *brp* animals the expression level of Cac^{GFP} was reduced at the NMJs (control: 31.1 ± 2.4 a.u., $n = 13$; *brp*: 18.0 ± 2.0 , $n = 10$; $P = 0.0017$) and within synapses (control: 52.6 ± 1.2 , $n = 421$ synapses; *brp*: 25.3 ± 0.8 , $n = 320$ synapses; $P < 0.001$ according to student t-test; Fig. 28). Considering the results, it can be said that *brp* mutants suffered from a diminished vesicle release probability due to a decrease in the density of Ca²⁺-channels and an increase in the average distance between Ca²⁺-channels and vesicle release sites. Hence, BRP seems essential for organizing the appropriate membrane composition at the AZ, illustrated by the defective clustering of Ca²⁺-channels in membranes of *brp* mutants.

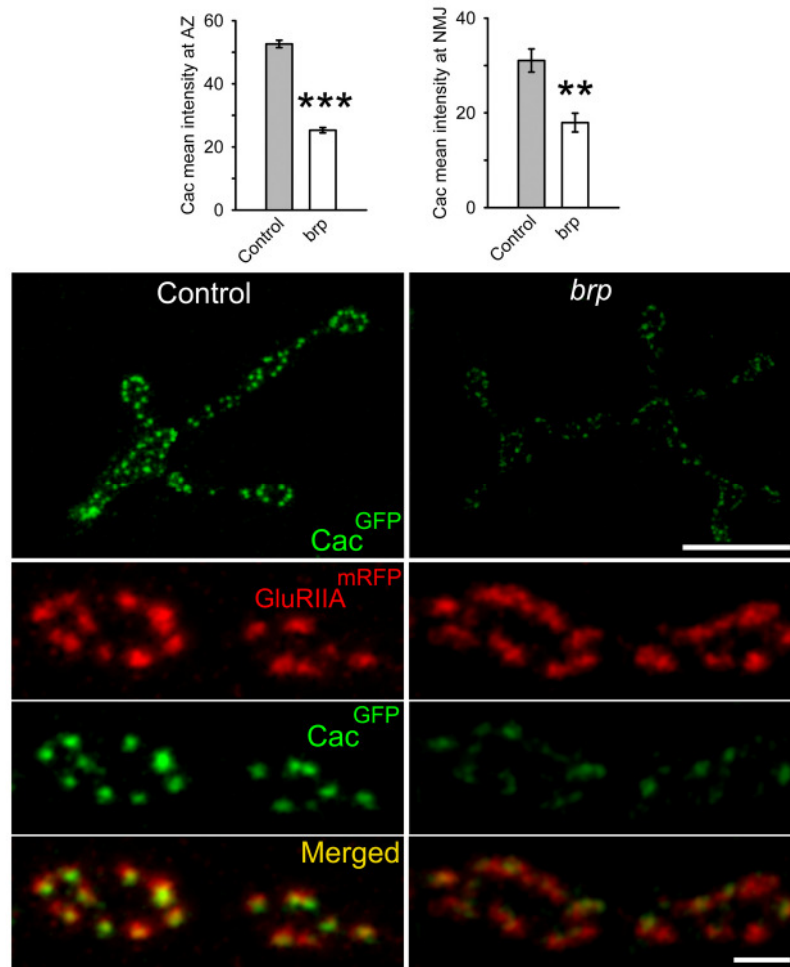


Fig. 28 Ca²⁺-channel delocalization impairs vesicle release in *brp* mutants

Projections of confocal stacks displaying the NMJ (top images; scale bar, 10 μ m) and several boutons (lower images; scale bar, 2 μ m) reveal weak Cac^{GFP} signal at *brp* mutant synapses. Quantification of Cac^{GFP} intensity averaged over the entire NMJs [control, 31.1 ± 2.4 arbitrary units (a.u.); $n = 13$; *brp*, 18.0 ± 2.0 a.u.; $n = 10$; $P = 0.0017$] or only synaptic areas (control, 52.6 ± 1.2 a.u.; $n = 421$ synapses; *brp*, 25.3 ± 0.8 a.u.; $n = 320$ synapses; $P < 0.001$, student *t* test) included as bar charts. One asterisk indicates $P \leq 0.05$; two asterisks, $P \leq 0.01$; and three asterisks, $P \leq 0.001$. Error bars indicate SEM

Taken together, it could be demonstrated that BRP plays an important role in the organization of the AZ at this glutamatergic model synapse. BRP may form a matrix, to which AZ components including Ca²⁺-channels, DLiprin- α and Dsyd-1 are anchored, which in turn sets the prerequisite for proper CAZ assembly and vesicle release. Similar arrangements have been defined electron microscopically at AZs of mammalian CNS synapses (particle web) (Zampighi *et al.* 2008) and frog NMJs (ribs) (Harlow *et al.* 2001), and though these structures have also been proposed to organise Ca²⁺-channel clustering, so far this could not be functionally proven.

Synapses lacking BRP and T-bars exhibited a defective coupling of Ca^{2+} influx with vesicle fusion. The results imply an involvement of BRP and related factors in synaptic plasticity by promoting Ca^{2+} -channel clustering at the AZ membrane. The elongated, polarized spatial organization of BRP at the presynaptic terminal, comprised of several densely packed filaments, also suggests a tethering function for synaptic vesicles. If part of the reduction in vesicle release is due to an impaired tethering function still remains to be elucidated.

4.3.2 DSyd-1 is important for efficient AZ formation

The *Drosophila* homologue of *C. elegans* Syd-1 (DSyd-1) has been identified through sequence alignments (Hallam *et al.* 2002). With *in situ* hybridization we found nervous system specific expression of *dsyd-1* (also known as RhoGAP100F or CG1976, Kiger *et al.* 2003) throughout embryonic development (Fouquet *et al.* submitted). Expression had a similar onset as BRP (Wagh *et al.*, 2006) and coincided with neuronal differentiation. David Oswald went on to construct *dsyd-1* deficient animals using Flippase-mediated trans-deletions of FRT-sites containing transposon lines (Parks *et al.* 2004) flanking the *dsyd-1* locus (Fig. 29).

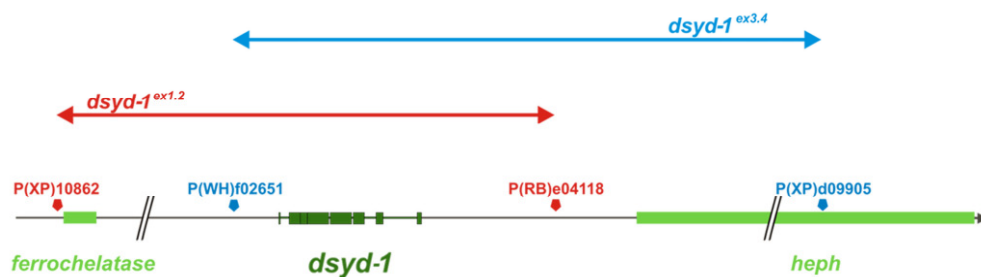


Fig. 29 Generating *dsyd-1* mutants

Genomic location of *dsyd-1* on chromosome arm 3R at 100D2-100D3. *dsyd1* deficient animals were generated using *Drosophila* lines carrying transposon mediated FRT sites (Parks *et al.* 2004) that are in close neighborhood to the *dsyd1* locus (for *dsyd-1*^{ex1,2} depicted in red and for *dsyd-1*^{ex3,4} in blue). We obtained two deficiencies that were confirmed with genomic PCR. In both cases the entire *dsyd-1* locus (dark green) was excised, whereas in one case (*dsyd-1*^{ex1,2}, blue line), the 5' *ferrochelatae* and in the other case the 3' *heph* (*dsyd-1*^{ex3,4}, red line) locus (both light green) were affected. Taking these deficiencies in trans eliminates both copies of *dsyd-1*, however leaves one intact copy of each *heph* and *ferrochelatae*.

Two *dsyd-1* deficient lines (*dsyd-1^{ex1.2}* and *dsyd-1^{ex3.4}*) were isolated and deletions were confirmed by genomic PCR (Parks *et al.* 2004). Combining both lines resulted in flies specifically deleted in *dsyd-1* (from here on short *dsyd-1*). In larval and adult brains, neuropil-specific staining was observed (Fouquet *et al.* submitted). This staining was completely absent in *dsyd-1* mutant animals. In order to perform rescue experiments, Manuela Schmidt and David Oswald cloned a *dsyd-1* cDNA (*dsyd-1^{cDNA}*) following an existing partial cDNA clone (LD28013, BDGP) and computer-based exon predictions (flybase.org). Pan-neuronal expression (*elav-Gal4*) of the *dsyd-1^{cDNA}* in *dsyd-1* restored DSyd-1 antibody staining.

Given that DSyd-1 localized to AZs (see 4.1.6), we asked whether DSyd-1 might be important for AZ formation. We performed quantitative analysis of synapse numbers at NMJs of third instar larva by counting both, individual BRP dots (AZs) and the opposite postsynaptic glutamate receptor fields (PSDs) independently (Fig. 30). In *dsyd-1* mutant larvae, a significant reduction of both AZ and PSD numbers was observed. This reduction was rescued by motoneuron-specific expression of the *dsyd-1^{cDNA}* (Fig. 30b, c, e and f).

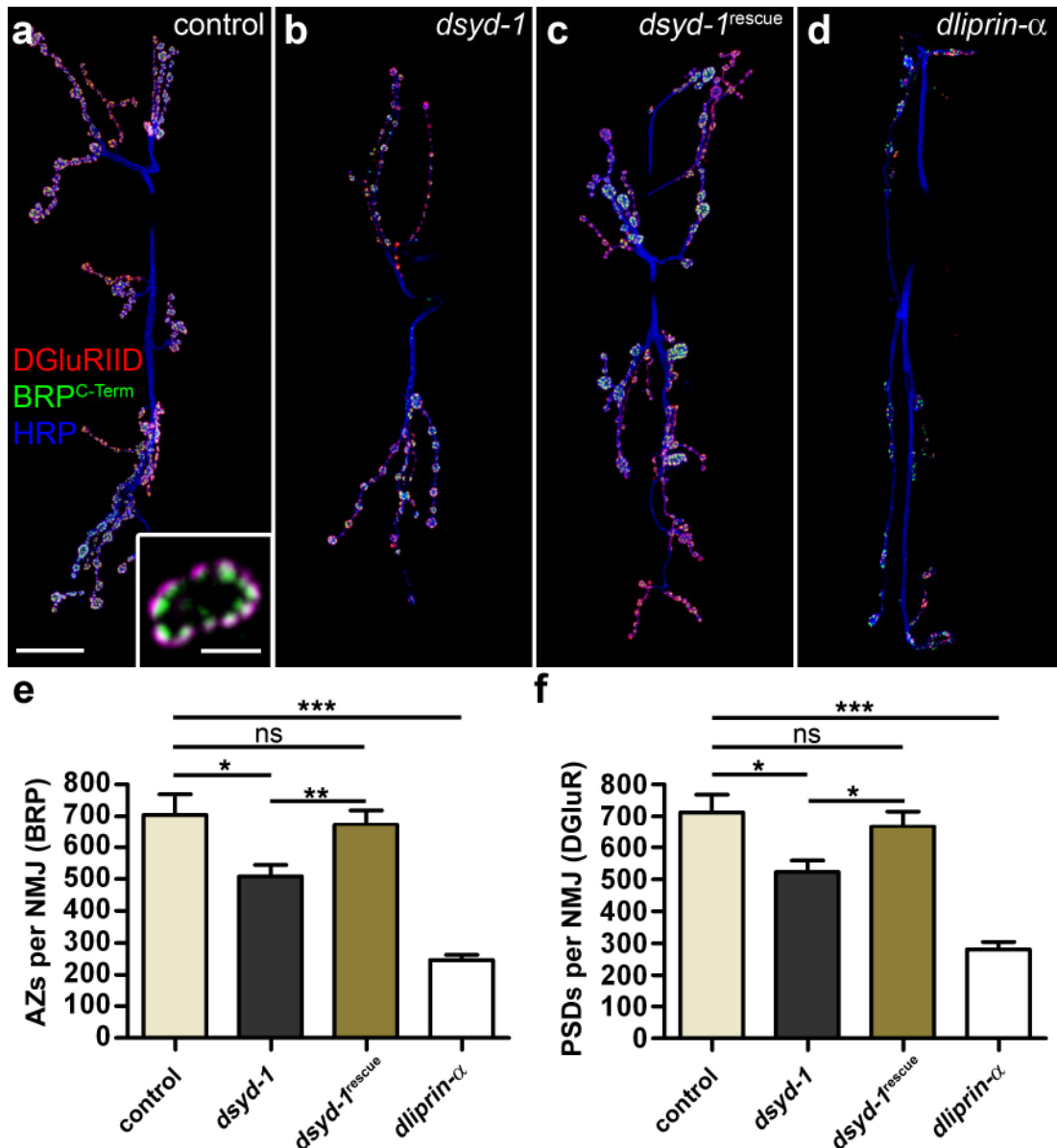


Fig. 30 Comparative analysis of NMJ morphology in *dsyd-1* and *dliprin-α* mutant animals.

a – d) Projection of confocal stacks of muscles 6 and 7 NMJs, labeled with antibodies recognizing BRP (BRP^{C-Term}, green), glutamate receptor subunit GluRIID (red) and HRP (blue). *dsyd-1* mutants **b)** showed a reduction in NMJ size compared to controls **a)**, which was rescued by motoneuron-specific re-expression of *dsyd-1*^{cDNA} **c)**. **d)** *dliprin-α* junctions showed a strong reduction in NMJ size. **e)** Number of AZs counted with αBRP^{C-Term} label. In both *dsyd-1* and *dliprin-α* mutants, synaptic sites were reduced compared to controls. The reduction seen in *dsyd-1* mutants was rescued by presynaptic *dsyd-1* cDNA expression (n: control=14; *dsyd-1*=14; *dsyd-1*^{rescue}=10; *dliprin-α*=8). Scale bars: 20 μm and 2 μm. **f)** Number of PSDs defined by using postsynaptic glutamate receptor subunit GluRIID. The results were comparable to (e). (n: control=14; *dsyd-1*=14; *dsyd-1*^{rescue}=10; *dliprin-α*=8)

Placing this finding into context, we scored *dliprin-α* mutant NMJs, with the same assay. AZ and PSD numbers were also reduced in *dliprin-α* animals (Fig. 30d - f), consistent with a reduction in bouton numbers (Kaufmann *et al.* 2002, also compare HRP signals in Fig. 30d and 30a).

We next performed TEVC recordings on third instar larval NMJs (performed by David Oswald). Evoked excitatory postsynaptic currents (eEJCs) were significantly reduced in *dsyd-1* mutant larvae ($59.2 \text{ nA} \pm 5.9 \text{ nA}$ and $99.3 \text{ nA} \pm 9.6 \text{ nA}$; $p=0.01$). These were nearly restored to control levels by presynaptic expression of *dsyd-1*^{cDNA} using the motoneuron specific driver *ok6-Gal4* ($81.4 \text{ nA} \pm 4.5 \text{ nA}$; $p=0.003$ to *dsyd-1* and $p=0.162$ to control). Mini current amplitudes, on the other hand, did not differ from controls (Fouquet *et al.* submitted). We thus conclude that the number of vesicles released at *dsyd-1* mutant NMJs is reduced. As expected, *dliprin- α* eEJCs were reduced to a similar degree as in *dsyd-1*, while mini current amplitudes were comparable to those of control animals (Fouquet *et al.* submitted).

Apart from a reduction of synapse numbers, the release defect due to presynaptic loss of *dsyd-1* might principally have its origin in defective AZ organization, as e.g. T-bar assembly, Ca^{2+} -channel localization (Kaufmann *et al.* 2002), or synaptic vesicle number and distribution respectively. Thus, we studied AZ assembly at an ultrastructural level (performed by Carolin Wichmann). In *dsyd-1* mutants, the average size of dense bodies (T-bars), the average diameter of AZs (not shown) and number and distribution of synaptic vesicles relative to the AZ membrane appeared comparable to controls (Fig. 31a - c). In contrast to *brp* mutants which as expected (Kittel *et al.* 2006) showed diffuse Ca^{2+} -channel clusters, Ca^{2+} -channel clustering appeared proper at *dsyd-1* as well as at *dliprin- α* AZs (Fig. 31d). Thus reduced vesicle release per NMJ in both *dsyd-1* and *dliprin- α* is likely correlated to the reduction in synapse numbers.

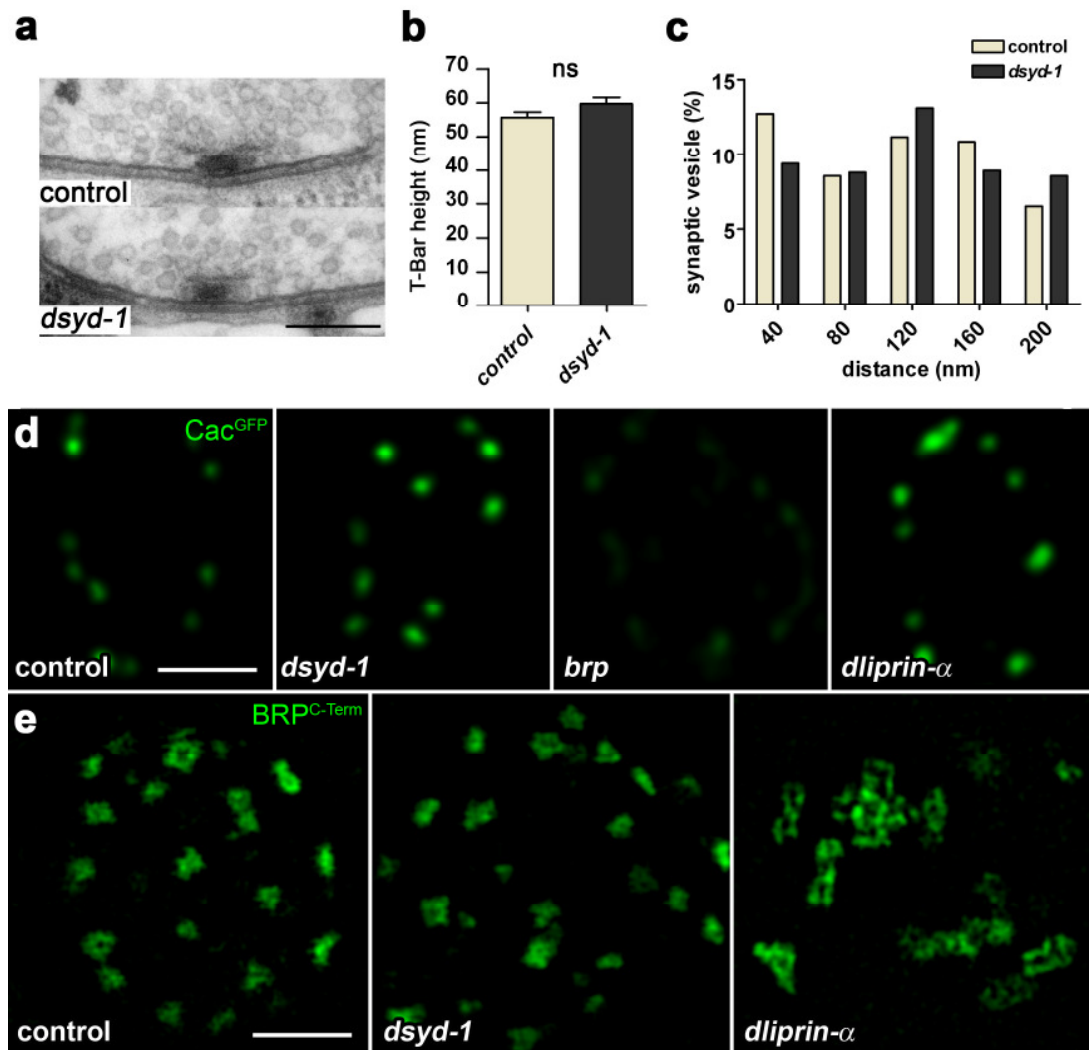


Fig. 31 Ultrastructural mutant characterization

a) Ultrastructure of *dsyd-1* mutant larval synapses. Scale bar: 200 nm. **b)** T-bar height (n: control=13, *dsyd-1*=19) and **c)** distribution of synaptic vesicles relative to the plasma membrane (n: control=322, *dsyd-1*=427) of *dsyd-1* NMJs are comparable to controls. **d)** Localization of Cac^{GFP} is not altered from controls in *dsyd-1* and *dliprin- α* animals. *brp* animals show delocalized Cac^{GFP} as expected (Kittel et al., 2006). Scale bar: 1 μm . **e)** Comparative STED images of BRP stainings (BRP^{C-Term}) in controls, *dsyd-1* and *dliprin- α* . Structure of BRP donuts in controls and *dsyd-1* are similar in shape and size, while *dliprin- α* mutants show denser AZs consisting of several BRP donuts. Scale bar: 1 μm .

Above, we scored the number of discrete AZ/PSD punctae with standard resolution light microscopy. The reduction of AZ numbers was more pronounced in *dliprin- α* than in *dsyd-1* mutant larvae (Fig. 30). However, vesicle release was reduced to an equal extent at *dsyd-1* and *dliprin- α* NMJs. Notably, AZs were described to stay partially interconnected in *dliprin- α* mutants using electron microscopy (Kaufmann et al. 2002) which might have lead to an underestimation of AZ numbers for *dliprin- α* due to limited resolution.

The size of individual AZs is in the range of 200 nm making light microscopic analysis of synapse substructure difficult. Recently, stimulated emission depletion microscopy (STED; Hell *et al.* 2004) has proven to be valuable for dissecting AZ architecture and synaptic vesicle movement (Kittel *et al.* 2006; Jin and Garner 2008; Westphal *et al.* 2008). Thus, STED uncovered donut-shaped distribution of BRP when using monoclonal antibody BRP^{C-Term} (Kittel *et al.* 2006). Here (Fig. 31e), segregated donuts were reproduced in controls and observed in *dsyd-1* mutant NMJs. At *dliprin-α* NMJs, however, BRP donuts often appeared connected, and the actual reduction of AZ numbers might be similar to that observed in *dsyd-1* mutants.

Thus, both *dliprin-α* and *dsyd-1* NMJs show reduced vesicle release and form fewer AZs. However, from what we can tell, these AZs if anything appeared only mildly affected on an ultrastructural level (Kaufmann *et al.* 2002) and still efficiently released vesicles. As described, *brp* mutants, although also forming less synapses, show grave functional defects with impaired ultrastructural AZ organization (Kittel *et al.* 2006). Thus, all analyses so far agree that DSyd-1 and DLiprin-α, different from BRP, are predominantly needed for efficient AZ formation at *Drosophila* NMJ synapses. Nonetheless, synapse formation still continues to a certain degree in both mutants, consistent with the generally observed cooperativity and partial functional redundancy between AZ proteins (Jin and Garner 2008).

5 Discussion

Efficient neurotransmission is meant to crucially depend on the structural and functional integrity of the presynaptic AZ compartment (Schoch and Gundelfinger 2006). A basic core of AZ components seems to be functionally and structurally conserved between *Drosophila*, *C. elegans* and mammals, allowing the analysis of AZ protein properties and characteristics in these efficient genetic models (Jin and Garner 2008).

Understanding the architectural organization and assembly mechanisms of the AZ is an initial step towards unraveling the physiological implications resulting from missing or malformed proteins located at the synapse. In order to get to a better understanding of AZ assembly, reconstructing the 'assembly sequence' by *in vivo* tracking of components appears important to complement the genetically and biochemically retrieved information. Here we capitalize on the specific advantages of the *Drosophila* NMJ system (Rasse *et al.* 2005; Fuger *et al.* 2007) to follow the history of assembling AZs with molecular resolution over extended periods *in vivo*. Apart from BRP and DLiprin- α , we included DSyd-1 into the spatio-temporal dissection of forming synapses.

Being able to directly 'see' structural changes on a light microscope nicely contributes to other, more abstract research fields as electrophysiology and proteomics. Current advances in light microscopy are creating new intriguing applications including the visualization of structures far below the resolution of classical fluorescence microscopy.

5.1 The role of Bruchpilot at the active zone

5.1.1 Localization of Bruchpilot within the AZ

As indicated in *brp* mutant analysis the presence of Bruchpilot appears to be a prerequisite for the formation of T-bars. Based on the STED images for BRP^{C-Term} and BRP^{N-Term}, BRP tightly associates with these elongated dense aggregates (Fig. 18 and 19). In fact, it could be suggested that BRP extends along the T-bar dense body as filaments of a polarized funnel-like structure. Notably, the C-terminal half of BRP consists of about 1000 amino acids of essentially contiguous coiled-coil sequence (Wagh *et al.* 2006), resembling Golgi/ER-resident 'tethering' factors, such as e.g. GM130 (Lupashin and Sztul 2005). Typically, coiled-coil domains form rod-like structures when dimerized. Thus, proteins consisting of 100 amino acid residues are known to extend for about 150 nm, such as Uso1p (Slayter and Lowey 1967; Yamakawa *et al.* 1996), which sometimes even exceeds 150 nm (Lupashin and Sztul 2005). It might be interesting to search for structural similarities between these proteins and BRP.

5.1.2 The function of T-bars

The question of how BRP influences the clustering of Ca²⁺-channels still remains unanswered. No direct biochemical interactions between BRP and Ca²⁺-channels were found in our assays, which could mean two things: either BRP's interaction with Ca²⁺-channels is too weak to be detected with our current procedures, or BRP recruits other proteins, which help stabilizing the channels in the center of the AZ. When BRP is missing in the system, the specific protein cannot be recruited and Ca²⁺-channel localization collapses. Based on our current tools, it remains challenging to dissect further functions of BRP independently from defective Ca²⁺-channel clustering at the AZ. The structural arrangement of dense bodies indicates that this presynaptic structure is involved in the tethering of synaptic vesicles and to direct them to their destined position for efficient release at the base of the T-bar (Koenig and Ikeda 1996; Feeney *et al.* 1998; Prokop 1999; Zhai and Bellen 2004; Atwood 2006; Prokop and Meinertzhagen 2006). Physiological analyses of

brp mutants show that synapses lacking BRP are still functional to some degree (Kittel *et al.* 2006). Further, more subtle defects in mutant animals regarding the recruitment, presentation and endocytosis of synaptic vesicles may be masked by the strong phenotype resulting from defects in Ca²⁺-channel clustering. However, an impaired vesicle transport machinery may be indicated by the slightly reduced number of vesicles docked to the AZ (Kittel *et al.* 2006).

The larvae of the flesh fly *Sarcophaga bullata* feature similar synaptic architectural properties as *Drosophila melanogaster* (Feeney *et al.* 1998). Electron micrographs of freeze fractures through the presynaptic membrane of *Sarcophaga* showed small intra-membranous structures, believed to be Ca²⁺-channels. The structural organization of the channels at the membrane are very similar to EM sections of the base of the T-Bar, further suggesting a close correlation between the dense bodies and Ca²⁺-channels. Previous findings are reinforced through STED microscopy showing the N-Terminal region of BRP in close range to Cac^{GFP}.

Previous experiments at the fly NMJ indicated a correlation between the number of T-bars and the modulation of the synaptic strength (Jia *et al.* 1993; Stewart *et al.* 1996). In line with this, at the crayfish NMJ, the activity-induced increased number of dense bodies has been proposed to elevate the release efficiency (Wojtowicz *et al.* 1994). Our findings are in agreement with these hypotheses. In fact, not only are Ca²⁺-channels structurally related to the T-Bar but the absence of BRP alone is sufficient to hinder the T-Bar formation and reduce the synaptic efficiency respectively.

The synaptic protein Bassoon has been linked to the structural assembly of AZs at vertebrate synapses (Khimich *et al.* 2005; tom Dieck *et al.* 2005). In murine inner hair cells mutant for Bassoon, the large dense bodies (ribbons, see Chapter 2.1.2.) were detached from the presynaptic membrane and observed afar from the synapse, floating in the cytoplasm. As a result, the number of docked vesicles was reduced and Ca²⁺ influx was impaired, but principally, the process of exocytosis was mainly preserved (Khimich *et al.* 2005). No floating electron-dense structures were detected in BRP mutants (personal communication with Carolin Wichmann; Kittel *et al.* 2006), BRP

thereby appears to be an integrand of the T-Bar, rather than required for its anchoring.

Until now, no homolog to Piccolo and Bassoon could be found in *Drosophila*. Considering the N-terminal homology of BRP to mammalian CAST/ ELKS proteins which are known to interact with Bassoon (see Fig. 2), and the structural similarity (coiled-coil domains) of the C-terminal part of BRP to large structural proteins, BRP may engulf functions, which are carried out by several interconnected vertebrate proteins.

An additional putative function of ribbons at sensory synapses consists of getting v- SNAREs of vesicles into reach of t-SNAREs on the plasma membrane (Zhai and Bellen 2004). This could increase the number of docked vesicles and further the amount of transmitter released at calcium influx. Following this line of reason, the 'ribs' of the cytomatrix at the frog neuromuscular AZ have been suggested to facilitate the association of v- and t-SNAREs to Ca²⁺-channels (Harlow *et al.* 2001). Such mechanisms may be similar in *Drosophila* synapses.

5.2 A sequential model of AZ formation

Taking into consideration the results described in this work, a model of the AZ architecture and its assembly at the *Drosophila* NMJ synapse may be formulated (Fig. 32). DLiprin- α and DSyd-1 are very early players during the AZ assembly, preceding both BRP accumulation and postsynaptic glutamate receptors. Notably, DLiprin- α and DSyd-1 cluster (LSCs) localization appeared highly dynamic, and many LSCs disappeared from certain locations in turn (Fig. 26). At both *dliprin- α* and *dsyd-1* deficient NMJs, formation of AZs and PSDs respectively was impaired but not abolished (Fig. 30). As DSyd-1 (Fig. 30) and DLiprin- α mutants (Kaufmann *et al.* 2002) operated presynaptically, the reduction of the amount of PSDs indicates a tight correlation between the pre- and postsynaptic compartment. Moreover, cooperative interactions between AZ proteins ensuring some functional redundancy might be responsible for a basal assembly remaining even in

absence of either one of these proteins. Taken together, the data propose that both proteins co-operate in an early rate-limiting step of synapse assembly in this system.

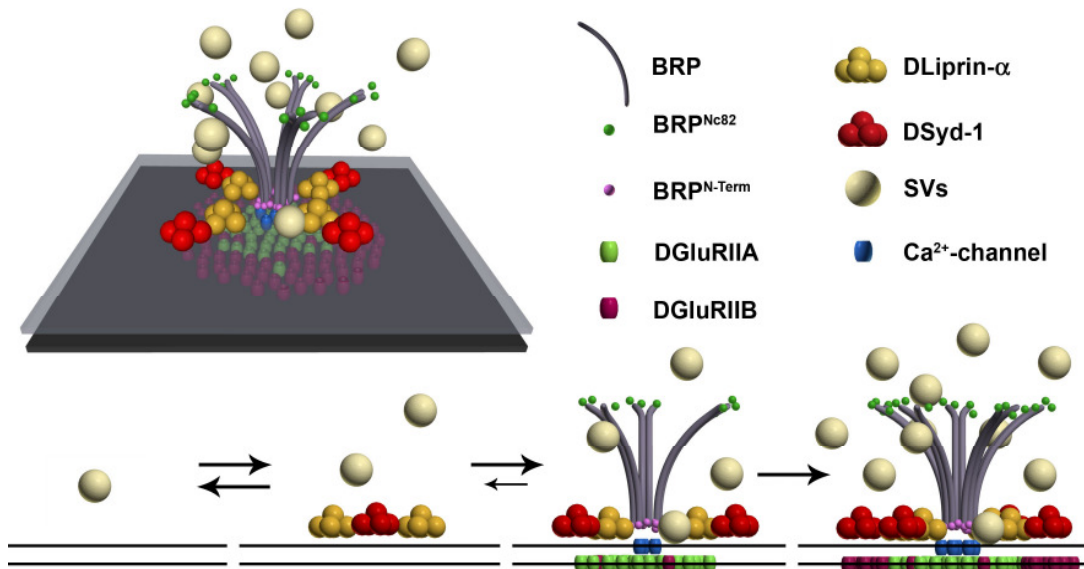


Fig. 32 A model of AZ assembly and structure at *Drosophila* NMJ synapses

On the postsynaptic side, PSDs comprise two different types of glutamate receptor complexes characterized by comprising either the DGluRIIA or DGluRIIB subunit. DGluRIIA containing channels were thereby contributed dominantly to the postsynaptic currents (DiAntonio *et al.* 1999). Our group had previously shown that postsynaptic DGluRIIA containing subunits (located in close apposition to the AZ) accumulates earlier, while DGluRIIB positive receptors followed later in PSD assembly and aggregated predominantly at the edge of PSDs (Rasse *et al.* 2005; Schmid *et al.* 2008) (see also model, Fig. 32). Furthermore, an activity-dependent, site-specific control of DGLuR composition contributes to match pre- and postsynaptic assembly, and GluRIIA can become rate limiting for synapse formation (Sigrist *et al.* 2002; Sigrist *et al.* 2003; Schmid *et al.* 2008). Here, we find that presynaptic DLiprin- α and DSyd-1 clusters clearly precede DGluRIIA accumulation at prospective synaptic sites (Fig. 32).

While initial LSCs appeared and disappeared, synapses were stabilized as soon as DGluRIIA was detected. Thus, the number of presynaptic nascent LSCs forming, and to what extent these assemblies can attract postsynaptic

GluRIIA, seems rate limiting for forming new synapses at expanding NMJs (Fig. 32). Possibly, transsynaptic interactions depending on DGluRIIA might irreversibly prime AZ assemblies for maturation. Hence, it will be interesting to address whether transsynaptic signaling, e.g. through Neurexin-Neuroigin (Li *et al.* 2007; Zeng *et al.* 2007) interactions, contributes here as well. A possible link between DLiprin- α and Neurexin was described in earlier works in which MALS/CASK/Liprin- α complexes were shown to interact with LARs and Neurexins in vertebrates (Olsen *et al.* 2006). How well these protein complexes are conserved in *Drosophila* still remains to be elucidated.

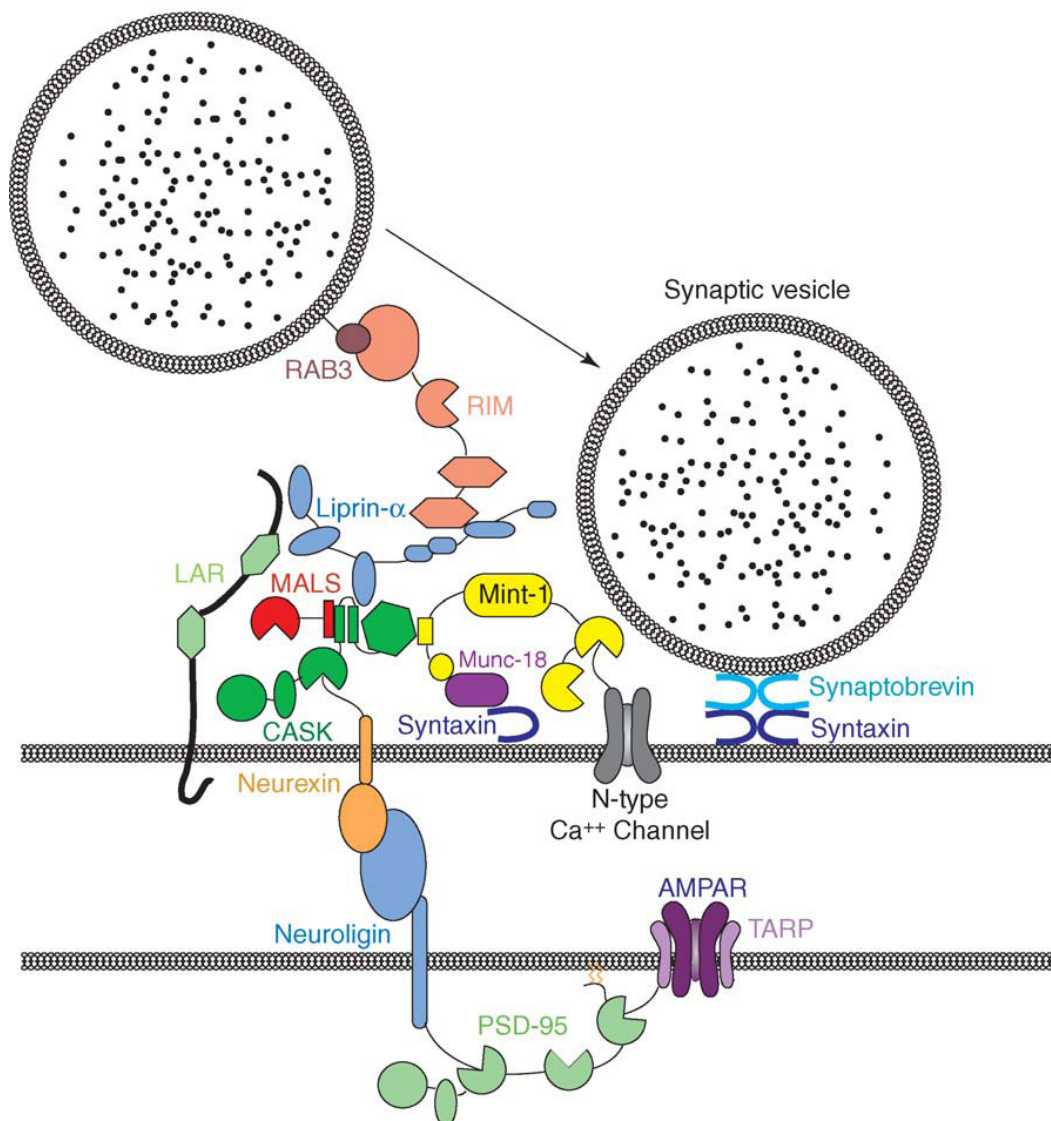


Fig. 33 Interaction of synaptic proteins in both pre- and postsynaptic compartments
 Scheme depicting protein interactions between pre- and postsynaptic compartments. The interaction of the MALS/CASK/Liprin- α complex with Neurexin and LAR could give first hints of how the pre- and postsynaptic assembly may be correlated. Adapted from Olsen *et al.*, 2006.

BRP accumulations were only detected at AZs in an advanced maturation stadium, after LSCs aggregation and also after detecting glutamate receptors (Rasse *et al.* 2005). BRP, however, was demonstrated to exert an unique and crucial role for efficient neurotransmitter release, while maintaining Ca²⁺-channel clusters close to the vesicle release site (see 5.2). These features could not be demonstrated by the absence of any other studied synaptic proteins (see Fig. 31). Regarding our finding of DLiprin- α preceding BRP, *C. elegans* genetics showed that ELKS became relevant for AZ assembly at the HSNL synapse after Syd-1 function was bypassed by a Syd-2 allele with increased affinity to ELKS (Dai *et al.* 2006).

Alongside the temporal sequence of assembling synaptic proteins, it could be demonstrated that synapse assembly extends over several hours, at both sides of the synapse. These findings are in line with ultrastructural studies on vertebrate slice cultures (Nagerl *et al.* 2007). Fast assembly of AZs, on the other hand, has been described while imaging cultured neurons (Garner *et al.* 2006). Nevertheless, it is conceivable that synapse formation could be more tightly controlled, both temporally and spatially *in vivo* than *in vitro*, particularly when synapses are added to strengthen already functional circuits, which is the case in NMJ synapses in later larval stages.

5.3 Discrete dynamic modules at the AZ edge

AZ architecture has been probed on an ultrastructural level using electron microscopy tomography (Harlow *et al.* 2001). In fact, a recent tomography study has identified polyhedral units of electron dense material surrounded by synaptic vesicles (Zampighi *et al.* 2008) revealing a subcompartmentalization at the mammalian synaptic AZs.

When applying STED resolution on *Drosophila* NMJs, discrete quanta of equal intensity and size (LSCs) were spotted both afar and associated to the AZs. Overall, LSCs changed positions in the range of minutes. These findings suggest a fast redistribution of protein modules (presumably containing DLiprin- α and DSyd-1) which loosely associate to established and

newly forming AZs. LSCs could therefore represent small building blocks (compartments) from which synapses are eventually built. Previously, immunolabeling of the AZ proteins Piccolo and Bassoon at light and electron microscopic levels (Zhai and Bellen 2004), as well as live imaging of GFP-Bassoon (Shapira *et al.* 2003) combined with fractionation and immunolabeling, identified an 80 nm diameter dense core vesicle, termed Piccolo/Bassoon transport vesicle (PTV, see 2.1.5). It was suggested that PTVs carry a comprehensive set of AZ materials, and that AZs form by unitary assembly of two or three PTVs (Shapira *et al.* 2003; Dresbach *et al.* 2006; Tao-Cheng 2007). *C. elegans* HSNL synapses deficient for Syd-2 (Liprin- α) or Syd-1 fail to properly target AZ material to their destination sites (Dai *et al.* 2006; Patel *et al.* 2006). Moreover, Liprin-family proteins indeed mediate transport processes both pre- and postsynaptically (Wyszynski *et al.* 2002; van Roessel *et al.* 2004; Miller *et al.* 2005). Thus, LSCs could therefore be DLiprin- α containing transport vesicles. When bringing this information into context, the function of putative homologous structure for PTVs in *Drosophila* (LSCs) would not only be restrained to synapse formation. Compellingly, these LSCs did not evenly dissolve into the AZ but established defined subcompartments, which could be relocated as discrete units to other targets.

On the other hand, the accumulation of specific cell adhesion molecules might prepare the stage for efficient assembly of the AZ center by gradual recruitment of diffuse proteins as e.g. BRP, possibly via direct interactions of certain players. In line with this mammalian ELKS and Liprin- α have been found to biochemically interact (Ko *et al.* 2003).

We thus identify AZ sub-compartments defined by a temporally segregated pathway of assembly, making room for distinct signaling traits. It will be most interesting to address how AZ sub-compartments are held together, which interactions between AZ proteins are rate-limiting for assembly, and how the synaptic vesicle cycle is tied with the AZ cyto-architecture. Moreover, addressing whether plastic changes of AZ function make use of similar pathways as demonstrated for developmental AZ formation here should be warranting.

6 Appendix

6.1 Table of abbreviations

ABP: AMPA receptor-binding protein

AEL: after egg-laying

AMPA: α -amino-3-hydroxyl-5-methyl-4-isoxalone propionic acid

AP: action potential

APD: avalanche photodiode

AZ: Active zone

BRP: Bruchpilot

Cac: Cacophony

CAST: cytomatrix at the active zone-associated structural protein

CAZ: cytomatrix at the active zone

CNS: central nervous system

DGluR: *Drosophila* glutamate receptor subunit

Dlg: *Drosophila* PSD-95/SAP90 orthologue Discs-large

DSyd: *Drosophila* synapse-defective

eag: *ether a go-go*

EGTA: Ethyleneglycol-*bis*(β -aminoethyl)-N,N,N',N'-tetraacetic Acid

eEJC: evoked excitatory junctional current

ER: endoplasmatic reticulum

ERC: ELKS/Rab6-interacting protein/CAST

ex: Excision

FasII: *Drosophila* NCAM homologue Fasciclin II

FRT: Flippase-mediated trans-deletion

FWHM: full-width-half-maximum

GABA: γ -aminobutyric acid

GFP: green fluorescent protein

GRIP: glutamate receptor interacting protein

HRP: Horse-radish-peroxidase

HSNL: Hermaphrodite specific neuron
HWHM: half-width-half-maximum
LSC: DLiprin- α /DSyd-1-cluster
LTD: long-term depression
LTP: long-term potentiation
M: Mouse
MAB: monoclonal antibody
mCherry: monomeric Cherry
mEJC: miniature excitatory junctional current
Munc13: mammalian homologue of Unc13
mRFP: monomeric red fluorescent protein
mStraw: monomeric Strawberry
n.a.: numerical aperture
NCAM: neuronal cell adhesion molecule
NMDA: *N*-methyl-D-aspartate
NMJ: neuromuscular junction
ORF: open reading frame
PBT: Phosphate-buffered saline with Triton
PCR: polymerase chain reaction
PMT: Photomultiplier
PSD: postsynaptic density
PTV: Piccolo-Bassoon transport vesicle
Rb: Rabbit
RIM1: Rab3-interacting molecule-1
RNAi: RNA interference
SAP-97: synapse-associated protein
Sh: *shaker*
SNAP: soluble *N*-ethylmaleimide-sensitive factor attachment protein
SNARE: SNAP receptor
SSR: subsynaptic reticulum
STED: stimulated emission depletion
TEVC: two-electrode voltage clamp
Unc13: uncoordinated protein-13

6.2 Table of Figures

Fig. 1 The electrical and chemical synapse.....	11
Fig. 2 Molecular components of the CAZ and the active zone.....	14
Fig. 3 Ultrastructure of the AZ.....	15
Fig. 4 Molecular components of the postsynaptic density (PSD).....	19
Fig. 5 Dendritic spines as a model for vertebrate synapse.....	20
Fig. 6 Model for dendritic spine development.....	21
Fig. 7 Synaptic maturation by fusion of preassembled precursor vesicles versus sequential <i>in situ</i> recruitment of synaptic components.....	23
Fig. 8 Presynaptic determinants of synaptic modulation.....	26
Fig. 9 <i>Drosophila</i> life cycle.....	31
Fig. 10 <i>Drosophila</i> NMJ development.....	32
Fig. 11 Schematic overview of the larval NMJ.....	34
Fig. 12 Principle of stimulated emission.....	37
Fig. 13 Technical features of the Leica TSC STED (Leica Microsystems).....	37
Fig. 14 Overlap extension PCR.....	41
Fig. 15 Gateway® technology facilitates cloning of ORF into destination vectors.....	42
Fig. 16 <i>Drosophila</i> BRP shows N-terminal homology to CAST/ERC.....	54
Fig. 17 Synaptic protein localization regarding their distances to the membrane.....	55
Fig. 18 BRP ^{Nc82} localizes at AZ in a polygonal ring-like structure.....	57
Fig. 19 STED and immuno-EM analysis of AZ organization at <i>Drosophila</i> NMJ synapses.....	58
Fig. 20 DSyd-1 physically interacts with BRP.....	61
Fig. 21 Discrete DLiprin- α ^{GFP} / DSyd-1 clusters surrounding the AZ core.....	62
Fig. 22 Quantification of AZ architecture using STED.....	63
Fig. 23 <i>In vivo</i> analysis of synaptic protein accumulation.....	66
Fig. 24 Similar recovery after FRAP for DLiprin- α and BRP.....	68
Fig. 25 Drastic DLiprin- α reorganization within short time intervals compared to BRP.....	70
Fig. 26 DLiprin- α and DSyd-1 show tightly correlated structural rearrangements.....	72
Fig. 27 Transposon mediated deletion of the BRP locus.....	73
Fig. 28 Ca ²⁺ -channel delocalization impairs vesicle release in <i>brp</i> mutants.....	76
Fig. 29 Generating <i>dsyd-1</i> mutants.....	77
Fig. 30 Comparative analysis of NMJ morphology in <i>dsyd-1</i> and <i>dliprin-a</i> mutant animals.....	79
Fig. 31 Ultrastructural mutant characterization.....	81
Fig. 32 A model of AZ assembly and structure at <i>Drosophila</i> NMJ synapses.....	87
Fig. 33 Interaction of synaptic proteins in both pre- and postsynaptic compartments.....	88

6.3 References

- Abel, T. and E. Kandel (1998). "Positive and negative regulatory mechanisms that mediate long-term memory storage." Brain Res Brain Res Rev **26**(2-3): 360-78.
- Ahmari, S. E., J. Buchanan, et al. (2000). "Assembly of presynaptic active zones from cytoplasmic transport packets." Nat Neurosci **3**(5): 445-51.
- Albin, S. D. and G. W. Davis (2004). "Coordinating structural and functional synapse development: postsynaptic p21-activated kinase independently specifies glutamate receptor abundance and postsynaptic morphology." J Neurosci **24**(31): 6871-9.
- Anderson, J. M., R. D. Milner, et al. (1966). "Pathological changes in the nervous system in severe neonatal hypoglycaemia." Lancet **2**(7459): 372-5.
- Atwood, H. L. (2006). "Neuroscience. Gatekeeper at the synapse." Science **312**(5776): 1008-9.
- Atwood, H. L., C. K. Govind, et al. (1993). "Differential ultrastructure of synaptic terminals on ventral longitudinal abdominal muscles in *Drosophila* larvae." J Neurobiol **24**(8): 1008-24.
- Atwood, H. L. and S. Karunanithi (2002). "Diversification of synaptic strength: presynaptic elements." Nat Rev Neurosci **3**(7): 497-516.
- Auger, C. and A. Marty (2000). "Quantal currents at single-site central synapses." J Physiol **526 Pt 1**: 3-11.
- Augustin, I., C. Rosenmund, et al. (1999). "Munc13-1 is essential for fusion competence of glutamatergic synaptic vesicles." Nature **400**(6743): 457-61.
- Augustine, G. J. and E. Neher (1992). "Neuronal Ca²⁺ signalling takes the local route." Curr Opin Neurobiol **2**(3): 302-7.
- Bailey, C. H. and M. Chen (1989). "Structural plasticity at identified synapses during long-term memory in *Aplysia*." J Neurobiol **20**(5): 356-72.
- Bailey, C. H. and E. R. Kandel (1993). "Structural changes accompanying memory storage." Annu Rev Physiol **55**: 397-426.
- Banister, J., C. Hebb, et al. (1949). "Stimulating action of NH₄ ions on the perfused superior cervical ganglion of the cat." J Physiol **110**(1-2): Proc, 13.
- Barrett, E. F. and C. F. Stevens (1972). "The kinetics of transmitter release at the frog neuromuscular junction." J Physiol **227**(3): 691-708.
- Barry, M. F. and E. B. Ziff (2002). "Receptor trafficking and the plasticity of excitatory synapses." Curr Opin Neurobiol **12**(3): 279-86.
- Bekkers, J. M. and C. F. Stevens (1990). "Computational implications of NMDA receptor channels." Cold Spring Harb Symp Quant Biol **55**: 131-5.

- Betz, A., P. Thakur, et al. (2001). "Functional interaction of the active zone proteins Munc13-1 and RIM1 in synaptic vesicle priming." Neuron **30**(1): 183-96.
- Bliss, T. V. and G. L. Collingridge (1993). "A synaptic model of memory: long-term potentiation in the hippocampus." Nature **361**(6407): 31-9.
- Bliss, T. V., G. L. Collingridge, et al. (2003). "Introduction. Long-term potentiation and structure of the issue." Philos Trans R Soc Lond B Biol Sci **358**(1432): 607-11.
- Bliss, T. V. and T. Lomo (1973). "Long-lasting potentiation of synaptic transmission in the dentate area of the anaesthetized rabbit following stimulation of the perforant path." J Physiol **232**(2): 331-56.
- Borgdorff, A. J. and D. Choquet (2002). "Regulation of AMPA receptor lateral movements." Nature **417**(6889): 649-53.
- Brand, A. H. and N. Perrimon (1993). "Targeted gene expression as a means of altering cell fates and generating dominant phenotypes." Development **118**(2): 401-15.
- Bredt, D. S. and R. A. Nicoll (2003). "AMPA receptor trafficking at excitatory synapses." Neuron **40**(2): 361-79.
- Bresler, T., Y. Ramati, et al. (2001). "The dynamics of SAP90/PSD-95 recruitment to new synaptic junctions." Mol Cell Neurosci **18**(2): 149-67.
- Bresler, T., M. Shapira, et al. (2004). "Postsynaptic density assembly is fundamentally different from presynaptic active zone assembly." J Neurosci **24**(6): 1507-20.
- Broadie, K. S. and M. Bate (1993a). "Development of larval muscle properties in the embryonic myotubes of *Drosophila melanogaster*." J Neurosci **13**(1): 167-80.
- Broadie, K. S. and M. Bate (1993b). "Development of the embryonic neuromuscular synapse of *Drosophila melanogaster*." J Neurosci **13**(1): 144-66.
- Brodin, L., P. Low, et al. (2000). "Sequential steps in clathrin-mediated synaptic vesicle endocytosis." Curr Opin Neurobiol **10**(3): 312-20.
- Cao, Y. Q., E. S. Piedras-Renteria, et al. (2004). "Presynaptic Ca²⁺ channels compete for channel type-preferring slots in altered neurotransmission arising from Ca²⁺ channelopathy." Neuron **43**(3): 387-400.
- Carroll, R. C., D. V. Lissin, et al. (1999). "Rapid redistribution of glutamate receptors contributes to long-term depression in hippocampal cultures." Nat Neurosci **2**(5): 454-60.
- Castiglioni, M. C. (1951). "[Distribution of pigments in the eye of alleles of white and their compounds in *Drosophila melanogaster*.]" Sci Genet **4**(1-2): 57-60.
- Chad, J., R. Eckert, et al. (1984). "Kinetics of calcium-dependent inactivation of calcium current in voltage-clamped neurones of *Aplysia californica*." J Physiol **347**: 279-300.

- Cheung, U. S., A. J. Shayan, et al. (1999). "*Drosophila* larval neuromuscular junction's responses to reduction of cAMP in the nervous system." J Neurobiol **40**(1): 1-13.
- Couteaux, R. and M. Pecot-Dechavassine (1970). "[Synaptic vesicles and pouches at the level of "active zones" of the neuromuscular junction]." C R Acad Sci Hebd Seances Acad Sci D **271**(25): 2346-9.
- Dai, Y., H. Taru, et al. (2006). "SYD-2 Liprin-alpha organizes presynaptic active zone formation through ELKS." Nat Neurosci **9**(12): 1479-87.
- Davis, R. L. and L. M. Kauvar (1984). "*Drosophila* cyclic nucleotide phosphodiesterases." Adv Cyclic Nucleotide Protein Phosphorylation Res **16**: 393-402.
- Deguchi-Tawarada, M., E. Inoue, et al. (2006). "Active zone protein CAST is a component of conventional and ribbon synapses in mouse retina." J Comp Neurol **495**(4): 480-96.
- Denk, W., R. Yuste, et al. (1996). "Imaging calcium dynamics in dendritic spines." Curr Opin Neurobiol **6**(3): 372-8.
- DiAntonio, A., S. A. Petersen, et al. (1999). "Glutamate receptor expression regulates quantal size and quantal content at the *Drosophila* neuromuscular junction." J Neurosci **19**(8): 3023-32.
- Dresbach, T., V. Torres, et al. (2006). "Assembly of active zone precursor vesicles: obligatory trafficking of presynaptic cytomatrix proteins Bassoon and Piccolo via a trans-Golgi compartment." J Biol Chem **281**(9): 6038-47.
- Dudai, Y., Y. N. Jan, et al. (1976). "dunce, a mutant of *Drosophila* deficient in learning." Proc Natl Acad Sci U S A **73**(5): 1684-8.
- Dudai, Y. and S. Zvi (1985). "Multiple defects in the activity of adenylate cyclase from the *Drosophila* memory mutant rutabaga." J Neurochem **45**(2): 355-64.
- Dyba, M., S. Jakobs, et al. (2003). "Immunofluorescence stimulated emission depletion microscopy." Nat Biotechnol **21**(11): 1303-4.
- Engert, F. and T. Bonhoeffer (1997). "Synapse specificity of long-term potentiation breaks down at short distances." Nature **388**(6639): 279-84.
- Engert, F. and T. Bonhoeffer (1999). "Dendritic spine changes associated with hippocampal long-term synaptic plasticity." Nature **399**(6731): 66-70.
- Fambrough, D. and C. S. Goodman (1996). "The *Drosophila* beaten path gene encodes a novel secreted protein that regulates defasciculation at motor axon choice points." Cell **87**(6): 1049-58.
- Featherstone, D. E. and K. Broadie (2000). "Surprises from *Drosophila*: genetic mechanisms of synaptic development and plasticity." Brain Res Bull **53**(5): 501-11.
- Feeney, C. J., S. Karunanithi, et al. (1998). "Motor nerve terminals on abdominal muscles in larval flesh flies, *Sarcophaga bullata*: comparisons with *Drosophila*." J Comp Neurol **402**(2): 197-209.
- Fenster, S. D., W. J. Chung, et al. (2000). "Piccolo, a presynaptic zinc finger protein structurally related to bassoon." Neuron **25**(1): 203-14.

- Fernandez-Chacon, R. and T. C. Sudhof (1999). "Genetics of synaptic vesicle function: toward the complete functional anatomy of an organelle." Annu Rev Physiol **61**: 753-76.
- Friedman, H. V., T. Bresler, et al. (2000). "Assembly of new individual excitatory synapses: time course and temporal order of synaptic molecule recruitment." Neuron **27**(1): 57-69.
- Fuger, P., L. B. Behrends, et al. (2007). "Live imaging of synapse development and measuring protein dynamics using two-color fluorescence recovery after photo-bleaching at *Drosophila* synapses." Nat Protoc **2**(12): 3285-98.
- Garner, C. C., S. Kindler, et al. (2000a). "Molecular determinants of presynaptic active zones." Curr Opin Neurobiol **10**(3): 321-7.
- Garner, C. C., J. Nash, et al. (2000b). "PDZ domains in synapse assembly and signalling." Trends Cell Biol **10**(7): 274-80.
- Garner, C. C., C. L. Waites, et al. (2006). "Synapse development: still looking for the forest, still lost in the trees." Cell Tissue Res **326**(2): 249-62.
- Geppert, M., Y. Goda, et al. (1994). "Synaptotagmin I: a major Ca²⁺ sensor for transmitter release at a central synapse." Cell **79**(4): 717-27.
- Goda, Y. and G. W. Davis (2003). "Mechanisms of synapse assembly and disassembly." Neuron **40**(2): 243-64.
- Govind, C. K. and J. Pearce (2003). "Active zones and receptor surfaces of freeze-fractured crayfish phasic and tonic motor synapses." J Neurocytol **32**(1): 39-51.
- Grosshans, D. R., D. A. Clayton, et al. (2002). "Analysis of glutamate receptor surface expression in acute hippocampal slices." Sci STKE **2002**(137): PL8.
- Guillaud, L., M. Setou, et al. (2003). "KIF17 dynamics and regulation of NR2B trafficking in hippocampal neurons." J Neurosci **23**(1): 131-40.
- Gundelfinger, E. D. and S. tom Dieck (2000). "Molecular organization of excitatory chemical synapses in the mammalian brain." Naturwissenschaften **87**(12): 513-23.
- Gustafsson, B. and H. Wigstrom (1990). "Long-term potentiation in the hippocampal CA1 region: its induction and early temporal development." Prog Brain Res **83**: 223-32.
- Hagiwara, A., Y. Fukazawa, et al. (2005). "Differential distribution of release-related proteins in the hippocampal CA3 area as revealed by freeze-fracture replica labeling." J Comp Neurol **489**(2): 195-216.
- Hallam, S. J., A. Goncharov, et al. (2002). "SYD-1, a presynaptic protein with PDZ, C2 and rhoGAP-like domains, specifies axon identity in *C. elegans*." Nat Neurosci **5**(11): 1137-46.
- Harlow, M. L., D. Ress, et al. (2001). "The architecture of active zone material at the frog's neuromuscular junction." Nature **409**(6819): 479-84.
- Harris, K. M. and P. Sultan (1995). "Variation in the number, location and size of synaptic vesicles provides an anatomical basis for the nonuniform probability of release at hippocampal CA1 synapses." Neuropharmacology **34**(11): 1387-95.

- Hein, B., K. I. Willig, et al. (2008). "Stimulated emission depletion (STED) nanoscopy of a fluorescent protein-labeled organelle inside a living cell." Proc Natl Acad Sci U S A **105**(38): 14271-6.
- Heintzmann, R. and G. Ficz (2007). "Breaking the resolution limit in light microscopy." Methods Cell Biol **81**: 561-80.
- Hell, S. W., M. Dyba, et al. (2004). "Concepts for nanoscale resolution in fluorescence microscopy." Curr Opin Neurobiol **14**(5): 599-609.
- Hollmann, M. and S. Heinemann (1994). "Cloned glutamate receptors." Annu Rev Neurosci **17**: 31-108.
- Horn, C. and E. A. Wimmer (2000). "A versatile vector set for animal transgenesis." Dev Genes Evol **210**(12): 630-7.
- Jahn, R., T. Lang, et al. (2003). "Membrane fusion." Cell **112**(4): 519-33.
- Jia, X. X., M. Gorczyca, et al. (1993). "Ultrastructure of neuromuscular junctions in *Drosophila*: comparison of wild type and mutants with increased excitability." J Neurobiol **24**(8): 1025-44.
- Jin, Y. and C. C. Garner (2008). "Molecular Mechanisms of Presynaptic Differentiation." Annu Rev Cell Dev Biol **24**: 237-262.
- Ju, W., W. Morishita, et al. (2004). "Activity-dependent regulation of dendritic synthesis and trafficking of AMPA receptors." Nat Neurosci **7**(3): 244-53.
- Katz, B. and R. Miledi (1965). "The Effect of Calcium on Acetylcholine Release from Motor Nerve Terminals." Proc R Soc Lond B Biol Sci **161**: 496-503.
- Kaufmann, N., J. DeProto, et al. (2002). "*Drosophila* liprin-alpha and the receptor phosphatase Dlar control synapse morphogenesis." Neuron **34**(1): 27-38.
- Kawasaki, F., B. Zou, et al. (2004). "Active zone localization of presynaptic calcium channels encoded by the cacophony locus of *Drosophila*." J Neurosci **24**(1): 282-5.
- Khimich, D., R. Nouvian, et al. (2005). "Hair cell synaptic ribbons are essential for synchronous auditory signalling." Nature **434**(7035): 889-94.
- Kiger, A. A., B. Baum, et al. (2003). "A functional genomic analysis of cell morphology using RNA interference." J Biol **2**(4): 27.
- Kim, E. and M. Sheng (2004). "PDZ domain proteins of synapses." Nat Rev Neurosci **5**(10): 771-81.
- Kim, J. H., H. Udo, et al. (2003). "Presynaptic activation of silent synapses and growth of new synapses contribute to intermediate and long-term facilitation in *Aplysia*." Neuron **40**(1): 151-65.
- Kittel, R. J., C. Wichmann, et al. (2006). "Bruchpilot promotes active zone assembly, Ca²⁺ channel clustering, and vesicle release." Science **312**(5776): 1051-4.
- Klar, T. A., S. Jakobs, et al. (2000). "Fluorescence microscopy with diffraction resolution barrier broken by stimulated emission." Proc Natl Acad Sci U S A **97**(15): 8206-10.

- Ko, J., M. Na, et al. (2003). "Interaction of the ERC family of RIM-binding proteins with the liprin-alpha family of multidomain proteins." J Biol Chem **278**(43): 42377-85.
- Koenig, J. H. and K. Ikeda (1996). "Synaptic vesicles have two distinct recycling pathways." J Cell Biol **135**(3): 797-808.
- Koh, T. W. and H. J. Bellen (2003). "Synaptotagmin I, a Ca²⁺ sensor for neurotransmitter release." Trends Neurosci **26**(8): 413-22.
- Lai, S. L., T. Awasaki, et al. (2008). "Clonal analysis of *Drosophila* antennal lobe neurons: diverse neuronal architectures in the lateral neuroblast lineage." Development **135**(17): 2883-93.
- Landis, D. M., A. K. Hall, et al. (1988). "The organization of cytoplasm at the presynaptic active zone of a central nervous system synapse." Neuron **1**(3): 201-9.
- Lang, T. and R. Jahn (2008). "Core proteins of the secretory machinery." Handb Exp Pharmacol(184): 107-27.
- Lenzi, D. and H. von Gersdorff (2001). "Structure suggests function: the case for synaptic ribbons as exocytotic nanomachines." Bioessays **23**(9): 831-40.
- Li, J., J. Ashley, et al. (2007). "Crucial role of *Drosophila* neurexin in proper active zone apposition to postsynaptic densities, synaptic growth, and synaptic transmission." Neuron **55**(5): 741-55.
- Linden, D. J. and J. A. Connor (1992). "Long-term Depression of Glutamate Currents in Cultured Cerebellar Purkinje Neurons Does Not Require Nitric Oxide Signalling." Eur J Neurosci **4**(1): 10-15.
- Liu, G., S. Choi, et al. (1999). "Variability of neurotransmitter concentration and nonsaturation of postsynaptic AMPA receptors at synapses in hippocampal cultures and slices." Neuron **22**(2): 395-409.
- Livingstone, M. S. (1985). "Genetic dissection of *Drosophila* adenylate cyclase." Proc Natl Acad Sci U S A **82**(17): 5992-6.
- Llinas, R. and Y. Yarom (1981). "Properties and distribution of ionic conductances generating electroresponsiveness of mammalian inferior olivary neurones in vitro." J Physiol **315**: 569-84.
- Lu, C. R., S. J. Hwang, et al. (2002). "Primary afferent terminals in spinal cord express presynaptic AMPA receptors." J Neurosci **22**(21): 9522-9.
- Lupashin, V. and E. Sztul (2005). "Golgi tethering factors." Biochim Biophys Acta **1744**(3): 325-39.
- Luscher, C., H. Xia, et al. (1999). "Role of AMPA receptor cycling in synaptic transmission and plasticity." Neuron **24**(3): 649-58.
- Malenka, R. C., J. A. Kauer, et al. (1988). "Postsynaptic calcium is sufficient for potentiation of hippocampal synaptic transmission." Science **242**(4875): 81-4.
- Maletic-Savatic, M., R. Malinow, et al. (1999). "Rapid dendritic morphogenesis in CA1 hippocampal dendrites induced by synaptic activity." Science **283**(5409): 1923-7.

- Markram, H., A. Gupta, et al. (1998). "Information processing with frequency-dependent synaptic connections." Neurobiol Learn Mem **70**(1-2): 101-12.
- Marrs, G. S., S. H. Green, et al. (2001). "Rapid formation and remodeling of postsynaptic densities in developing dendrites." Nat Neurosci **4**(10): 1006-13.
- Mason, J. M., J. Ransom, et al. (2004). "A deficiency screen for dominant suppressors of telomeric silencing in *Drosophila*." Genetics **168**(3): 1353-70.
- Matsuzaki, M., N. Honkura, et al. (2004). "Structural basis of long-term potentiation in single dendritic spines." Nature **429**(6993): 761-6.
- Matus, A. (2005). "Growth of dendritic spines: a continuing story." Curr Opin Neurobiol **15**(1): 67-72.
- McGee, A. W. and D. S. Bredt (2003). "Assembly and plasticity of the glutamatergic postsynaptic specialization." Curr Opin Neurobiol **13**(1): 111-8.
- Miller, K. E., J. DeProto, et al. (2005). "Direct observation demonstrates that Liprin-alpha is required for trafficking of synaptic vesicles." Curr Biol **15**(7): 684-9.
- Nagerl, U. V., G. Kostinger, et al. (2007). "Protracted synaptogenesis after activity-dependent spinogenesis in hippocampal neurons." J Neurosci **27**(30): 8149-56.
- Neher, E. (1998). "Vesicle pools and Ca²⁺ microdomains: new tools for understanding their roles in neurotransmitter release." Neuron **20**(3): 389-99.
- Neher, E. and T. Sakaba (2008). "Multiple roles of calcium ions in the regulation of neurotransmitter release." Neuron **59**(6): 861-72.
- Nicoll, R. A. and R. C. Malenka (1995). "Contrasting properties of two forms of long-term potentiation in the hippocampus." Nature **377**(6545): 115-8.
- Nikonenko, I., P. Jourdain, et al. (2002). "Activity-induced changes of spine morphology." Hippocampus **12**(5): 585-91.
- Ohtsuka, T., E. Takao-Rikitsu, et al. (2002). "Cast: a novel protein of the cytomatrix at the active zone of synapses that forms a ternary complex with RIM1 and munc13-1." J Cell Biol **158**(3): 577-90.
- Okabe, S., A. Miwa, et al. (2001a). "Spine formation and correlated assembly of presynaptic and postsynaptic molecules." J Neurosci **21**(16): 6105-14.
- Okabe, S., T. Urushido, et al. (2001b). "Rapid redistribution of the postsynaptic density protein PSD-Zip45 (Homer 1c) and its differential regulation by NMDA receptors and calcium channels." J Neurosci **21**(24): 9561-71.
- Olsen, O., K. A. Moore, et al. (2006). "Synaptic transmission regulated by a presynaptic MALS/Liprin-alpha protein complex." Curr Opin Cell Biol **18**(2): 223-7.

- Packard, M., D. Mathew, et al. (2003). "Wnts and TGF beta in synaptogenesis: old friends signalling at new places." Nat Rev Neurosci **4**(2): 113-20.
- Parks, A. L., K. R. Cook, et al. (2004). "Systematic generation of high-resolution deletion coverage of the *Drosophila melanogaster* genome." Nat Genet **36**(3): 288-92.
- Parks, S. B., B. W. Popovich, et al. (2001). "Real-time polymerase chain reaction with fluorescent hybridization probes for the detection of prevalent mutations causing common thrombophilic and iron overload phenotypes." Am J Clin Pathol **115**(3): 439-47.
- Passafaro, M., T. Nakagawa, et al. (2003). "Induction of dendritic spines by an extracellular domain of AMPA receptor subunit GluR2." Nature **424**(6949): 677-81.
- Patel, M. R., E. K. Lehrman, et al. (2006). "Hierarchical assembly of presynaptic components in defined *C. elegans* synapses." Nat Neurosci **9**(12): 1488-98.
- Pawley, J. (1997). "The development of field-emission scanning electron microscopy for imaging biological surfaces." Scanning **19**(5): 324-36.
- Petersen, S. A., R. D. Fetter, et al. (1997). "Genetic analysis of glutamate receptors in *Drosophila* reveals a retrograde signal regulating presynaptic transmitter release." Neuron **19**(6): 1237-48.
- Phillips, G. R., J. K. Huang, et al. (2001). "The presynaptic particle web: ultrastructure, composition, dissolution, and reconstitution." Neuron **32**(1): 63-77.
- Prange, O. and T. H. Murphy (2001). "Modular transport of postsynaptic density-95 clusters and association with stable spine precursors during early development of cortical neurons." J Neurosci **21**(23): 9325-33.
- Prokop, A. (1999). "Integrating bits and pieces: synapse structure and formation in *Drosophila* embryos." Cell Tissue Res **297**(2): 169-86.
- Prokop, A., M. Landgraf, et al. (1996). "Presynaptic development at the *Drosophila* neuromuscular junction: assembly and localization of presynaptic active zones." Neuron **17**(4): 617-26.
- Prokop, A. and I. A. Meinertzhagen (2006). "Development and structure of synaptic contacts in *Drosophila*." Semin Cell Dev Biol **17**(1): 20-30.
- Qin, G., T. Schwarz, et al. (2005). "Four different subunits are essential for expressing the synaptic glutamate receptor at neuromuscular junctions of *Drosophila*." J Neurosci **25**(12): 3209-18.
- Rasse, T. M., W. Fouquet, et al. (2005). "Glutamate receptor dynamics organizing synapse formation in vivo." Nat Neurosci **8**(7): 898-905.
- Renger, J. J., C. Egles, et al. (2001). "A developmental switch in neurotransmitter flux enhances synaptic efficacy by affecting AMPA receptor activation." Neuron **29**(2): 469-84.
- Renger, J. J., A. Ueda, et al. (2000). "Role of cAMP cascade in synaptic stability and plasticity: ultrastructural and physiological analyses of individual synaptic boutons in *Drosophila* memory mutants." J Neurosci **20**(11): 3980-92.

- Rheuben, M. B., M. Yoshihara, et al. (1999). "Ultrastructural correlates of neuromuscular junction development." Int Rev Neurobiol **43**: 69-92.
- Ritzenthaler, S., E. Suzuki, et al. (2000). "Postsynaptic filopodia in muscle cells interact with innervating motoneuron axons." Nat Neurosci **3**(10): 1012-7.
- Rizzoli, S. O. and W. J. Betz (2005). "Synaptic vesicle pools." Nat Rev Neurosci **6**(1): 57-69.
- Roos, J. and R. B. Kelly (2000). "Preassembly and transport of nerve terminals: a new concept of axonal transport." Nat Neurosci **3**(5): 415-7.
- Rosenmund, C., J. Rettig, et al. (2003). "Molecular mechanisms of active zone function." Curr Opin Neurobiol **13**(5): 509-19.
- Rubin, G. M. and A. C. Spradling (1982). "Genetic transformation of *Drosophila* with transposable element vectors." Science **218**(4570): 348-53.
- Saleh, M. N., R. H. Wheeler, et al. (1991). "In-111 labeled monoclonal anti-carcinoembryonic antigen antibody (ZCE025) in the immunoscintigraphic imaging of metastatic antigen-producing adenocarcinomas." Clin Nucl Med **16**(2): 110-6.
- Sambrook, J. and M. J. Gething (1989). "Protein structure. Chaperones, paperones." Nature **342**(6247): 224-5.
- Schmid, A., S. Hallermann, et al. (2008). "Activity-dependent site-specific changes of glutamate receptor composition in vivo." Nat Neurosci **11**(6): 659-66.
- Schmid, A., G. Qin, et al. (2006). "Non-NMDA-type glutamate receptors are essential for maturation but not for initial assembly of synapses at *Drosophila* neuromuscular junctions." J Neurosci **26**(44): 11267-77.
- Schmid, A. and S. J. Sigrist (2008). "Analysis of neuromuscular junctions: histology and in vivo imaging." Methods Mol Biol **420**: 239-51.
- Schneggenburger, R., T. Sakaba, et al. (2002). "Vesicle pools and short-term synaptic depression: lessons from a large synapse." Trends Neurosci **25**(4): 206-12.
- Schoch, S. and E. D. Gundelfinger (2006). "Molecular organization of the presynaptic active zone." Cell Tissue Res **326**(2): 379-91.
- Schuster, C. M., G. W. Davis, et al. (1996). "Genetic dissection of structural and functional components of synaptic plasticity. II. Fasciclin II controls presynaptic structural plasticity." Neuron **17**(4): 655-67.
- Seeburg, P. H. (1993). "The TiPS/TINS lecture: the molecular biology of mammalian glutamate receptor channels." Trends Pharmacol Sci **14**(8): 297-303.
- Setou, M., D. H. Seog, et al. (2002). "Glutamate-receptor-interacting protein GRIP1 directly steers kinesin to dendrites." Nature **417**(6884): 83-7.
- Shapira, M., R. G. Zhai, et al. (2003). "Unitary assembly of presynaptic active zones from Piccolo-Bassoon transport vesicles." Neuron **38**(2): 237-52.

- Shayan, A. J. and H. L. Atwood (2000). "Synaptic ultrastructure in nerve terminals of *Drosophila* larvae overexpressing the learning gene *dunce*." J Neurobiol **43**(1): 89-97.
- Shen, K., R. D. Fetter, et al. (2004). "Synaptic specificity is generated by the synaptic guidepost protein SYG-2 and its receptor, SYG-1." Cell **116**(6): 869-81.
- Sheng, M. and S. H. Lee (2001). "AMPA receptor trafficking and the control of synaptic transmission." Cell **105**(7): 825-8.
- Shi, S., Y. Hayashi, et al. (2001). "Subunit-specific rules governing AMPA receptor trafficking to synapses in hippocampal pyramidal neurons." Cell **105**(3): 331-43.
- Shi, S. H., Y. Hayashi, et al. (1999). "Rapid spine delivery and redistribution of AMPA receptors after synaptic NMDA receptor activation." Science **284**(5421): 1811-6.
- Shu, X., N. C. Shaner, et al. (2006). "Novel chromophores and buried charges control color in mFruits." Biochemistry **45**(32): 9639-47.
- Sigrist, S. J., D. F. Reiff, et al. (2003). "Experience-dependent strengthening of *Drosophila* neuromuscular junctions." J Neurosci **23**(16): 6546-56.
- Sigrist, S. J., P. R. Thiel, et al. (2000). "Postsynaptic translation affects the efficacy and morphology of neuromuscular junctions." Nature **405**(6790): 1062-5.
- Sigrist, S. J., P. R. Thiel, et al. (2002). "The postsynaptic glutamate receptor subunit D_{GLuR}-IIA mediates long-term plasticity in *Drosophila*." J Neurosci **22**(17): 7362-72.
- Slyter, H. S. and S. Lowey (1967). "Substructure of the myosin molecule as visualized by electron microscopy." Proc Natl Acad Sci U S A **58**(4): 1611-8.
- Sone, M., E. Suzuki, et al. (2000). "Synaptic development is controlled in the periaxial zones of *Drosophila* synapses." Development **127**(19): 4157-68.
- Stewart, B. A., H. L. Atwood, et al. (1994). "Improved stability of *Drosophila* larval neuromuscular preparations in haemolymph-like physiological solutions." J Comp Physiol [A] **175**(2): 179-91.
- Stewart, B. A., C. M. Schuster, et al. (1996). "Homeostasis of synaptic transmission in *Drosophila* with genetically altered nerve terminal morphology." J Neurosci **16**(12): 3877-86.
- Stryker, E. and K. G. Johnson (2007). "LAR, liprin alpha and the regulation of active zone morphogenesis." J Cell Sci **120**(Pt 21): 3723-8.
- Sudhof, T. C. (2004). "The synaptic vesicle cycle." Annu Rev Neurosci **27**: 509-47.
- Tada, T. and M. Sheng (2006). "Molecular mechanisms of dendritic spine morphogenesis." Curr Opin Neurobiol **16**(1): 95-101.
- Takao-Rikitsu, E., S. Mochida, et al. (2004). "Physical and functional interaction of the active zone proteins, CAST, RIM1, and Bassoon, in neurotransmitter release." J Cell Biol **164**(2): 301-11.

- Tanaka, J., Y. Horiike, et al. (2008). "Protein synthesis and neurotrophin-dependent structural plasticity of single dendritic spines." Science **319**(5870): 1683-7.
- Tao-Cheng, J. H. (2007). "Ultrastructural localization of active zone and synaptic vesicle proteins in a preassembled multi-vesicle transport aggregate." Neuroscience **150**(3): 575-84.
- Thomas, U., E. Kim, et al. (1997). "Synaptic clustering of the cell adhesion molecule fasciclin II by discs-large and its role in the regulation of presynaptic structure." Neuron **19**(4): 787-99.
- Thomson, A. M. (2000). "Facilitation, augmentation and potentiation at central synapses." Trends Neurosci **23**(7): 305-12.
- tom Dieck, S., W. D. Altmann, et al. (2005). "Molecular dissection of the photoreceptor ribbon synapse: physical interaction of Bassoon and RIBEYE is essential for the assembly of the ribbon complex." J Cell Biol **168**(5): 825-36.
- tom Dieck, S., L. Sanmarti-Vila, et al. (1998). "Bassoon, a novel zinc-finger CAG/glutamine-repeat protein selectively localized at the active zone of presynaptic nerve terminals." J Cell Biol **142**(2): 499-509.
- Trachtenberg, J. T., B. E. Chen, et al. (2002). "Long-term in vivo imaging of experience-dependent synaptic plasticity in adult cortex." Nature **420**(6917): 788-94.
- van Roessel, P., D. A. Elliott, et al. (2004). "Independent regulation of synaptic size and activity by the anaphase-promoting complex." Cell **119**(5): 707-18.
- Varoqueaux, F., A. Sigler, et al. (2002). "Total arrest of spontaneous and evoked synaptic transmission but normal synaptogenesis in the absence of Munc13-mediated vesicle priming." Proc Natl Acad Sci U S A **99**(13): 9037-42.
- Verhage, M., A. S. Maia, et al. (2000). "Synaptic assembly of the brain in the absence of neurotransmitter secretion." Science **287**(5454): 864-9.
- von Gersdorff, H. (2001). "Synaptic ribbons: versatile signal transducers." Neuron **29**(1): 7-10.
- Wagh, D. A., T. M. Rasse, et al. (2006). "Bruchpilot, a protein with homology to ELKS/CAST, is required for structural integrity and function of synaptic active zones in *Drosophila*." Neuron **49**(6): 833-44.
- Walikonis, R. S., O. N. Jensen, et al. (2000). "Identification of proteins in the postsynaptic density fraction by mass spectrometry." J Neurosci **20**(11): 4069-80.
- Wang, Y., S. Sugita, et al. (2000). "The RIM/NIM family of neuronal C2 domain proteins. Interactions with Rab3 and a new class of Src homology 3 domain proteins." J Biol Chem **275**(26): 20033-44.
- Washbourne, P., J. E. Bennett, et al. (2002). "Rapid recruitment of NMDA receptor transport packets to nascent synapses." Nat Neurosci **5**(8): 751-9.
- Westphal, V., S. O. Rizzoli, et al. (2008). "Video-rate far-field optical nanoscopy dissects synaptic vesicle movement." Science **320**(5873): 246-9.

- Willig, K. I., S. O. Rizzoli, et al. (2006). "STED microscopy reveals that synaptotagmin remains clustered after synaptic vesicle exocytosis." Nature **440**(7086): 935-9.
- Wojtowicz, J. M., L. Marin, et al. (1994). "Activity-induced changes in synaptic release sites at the crayfish neuromuscular junction." J Neurosci **14**(6): 3688-703.
- Wyszynski, M., E. Kim, et al. (2002). "Interaction between GRIP and liprin-alpha/SYD2 is required for AMPA receptor targeting." Neuron **34**(1): 39-52.
- Xia, H., M. von Zastrow, et al. (2002). "A novel anterograde trafficking signal present in the N-terminal extracellular domain of ionotropic glutamate receptors." J Biol Chem **277**(49): 47765-9.
- Yamagata, M., J. R. Sanes, et al. (2003). "Synaptic adhesion molecules." Curr Opin Cell Biol **15**(5): 621-32.
- Yamakawa, Y., H. Ochiai, et al. (1996). "Arachnoid-trabeculae tenting as a self-retaining retractor in resecting ventrally located spinal meningioma--technical note." Neurol Med Chir (Tokyo) **36**(12): 901-2.
- Yuste, R. and T. Bonhoeffer (2001). "Morphological changes in dendritic spines associated with long-term synaptic plasticity." Annu Rev Neurosci **24**: 1071-89.
- Zampighi, G. A., N. Fain, et al. (2008). "Conical electron tomography of a chemical synapse: polyhedral cages dock vesicles to the active zone." J Neurosci **28**(16): 4151-60.
- Zeng, X., M. Sun, et al. (2007). "Neurexin-1 is required for synapse formation and larvae associative learning in *Drosophila*." FEBS Lett **581**(13): 2509-16.
- Zhai, R. G. and H. J. Bellen (2004). "The architecture of the active zone in the presynaptic nerve terminal." Physiology (Bethesda) **19**: 262-70.
- Zhai, R. G., H. Vardinon-Friedman, et al. (2001). "Assembling the presynaptic active zone: a characterization of an active one precursor vesicle." Neuron **29**(1): 131-43.
- Zhong, Y., V. Budnik, et al. (1992). "Synaptic plasticity in *Drosophila* memory and hyperexcitable mutants: role of cAMP cascade." J Neurosci **12**(2): 644-51.
- Zhong, Y. and C. F. Wu (2004). "Neuronal activity and adenylyl cyclase in environment-dependent plasticity of axonal outgrowth in *Drosophila*." J Neurosci **24**(6): 1439-45.
- Zito, K., R. D. Fetter, et al. (1997). "Synaptic clustering of Fascilin II and Shaker: essential targeting sequences and role of Dlg." Neuron **19**(5): 1007-16.
- Ziv, N. E. and C. C. Garner (2001). "Principles of glutamatergic synapse formation: seeing the forest for the trees." Curr Opin Neurobiol **11**(5): 536-43.
- Ziv, N. E. and C. C. Garner (2004). "Cellular and molecular mechanisms of presynaptic assembly." Nat Rev Neurosci **5**(5): 385-99.
- Zucker, R. S. and W. G. Regehr (2002). "Short-term synaptic plasticity." Annu Rev Physiol **64**: 355-405.

6.4 Curriculum Vitae

Personal Data

Name: Wernher Fouquet
Address: Annenstr. 17
10179 Berlin
Phone: +49 176 96355627
E-Mail: wernher.fouquet@virchow.uni-wuerzburg.de
Nationality: german and brazilian
Date of birth: 16th of July 1979 in São Paulo, Brazil

Scientific education

01/1997 – 31/1998 „Colégio Visconde de Porto Seguro“ in São Paulo, Brazil. Abitur (university entrance qualification)
09/1999 – 10/2004 Undergraduate studies at the Georg-August-Universität Göttingen, Germany.
2004 Diploma in Biology at the Georg-August-Universität Göttingen, Germany and subsequent diploma thesis at the European Neuroscience Institute (ENI-G) entitled “Konfokalmikroskopische Analyse der Ausbildung individueller synaptischer Kontakte an neuromuskulären Terminalen lebender Larven der Fruchtfliege *Drosophila melanogaster*”
01/2005 – 31/2006 PhD student in the Neuroplasticity group, ENI, Göttingen, Germany. PhD thesis: “Analysis of synapse assembly at *Drosophila melanogaster*”
since 01/2007 Change of the graduate school to the “Graduate School of Life Science” at the Julius Maximilians-Universität Würzburg, Germany.

Scientific work

- 2004** **The *Drosophila* Bruchpilot protein is required for presynaptic active zone assembly and calcium channel clustering to ensure high vesicle release probability**
R. Kittel, C. Wichmann, T. Rasse, W. Fouquet, M. Schmidt, A. Schmid, D. Wagh, E. Buchner, M. Heckmann, S. J. Sigrist
ENI Network meeting, Prague
- 2005** **Towards in vivo observation of synaptic plasticity in the *Drosophila* olfactory system**
W. Fouquet, R. Kittel, C. Wichmann, and S. J. Sigrist
Neuronal circuits, CSHL, NY, USA
- 2007** ***Drosophila* „live-imaging“ course**, Cold Spring Harbor Laboratories (NY, USA) in line with the „Neurobiology of *Drosophila*“ course.
- 2008** **“Dynamic microscopy” workshop** in the Rudolf-Virchow Zentrum, Würzburg, Germany
- 2008** **Using STED microscopy to probe synapse architecture**
W. Fouquet, D. Oswald, S. Mertel, C. Wichmann, M. Dyba, S. J. Sigrist¹
Neurofly 2008, Würzburg, Germany

6.5 Publications

Glutamate receptor dynamics organizing synapse formation in vivo.

Nature Neuroscience, 2005

Rasse TM, Fouquet W, Schmid A, Kittel RJ, Mertel S, Sigrist CB, Schmidt M, Guzman A, Merino C, Qin G, Quentin C, Madeo FF, Heckmann M, Sigrist SJ.

Bruchpilot promotes active zone assembly, Ca²⁺ channel clustering, and vesicle release.

Science, 2006

Kittel RJ, Wichmann C, Rasse TM, Fouquet W, Schmidt M, Schmid A, Wagh DA, Pawlu C, Kellner RR, Willig KI, Hell SW, Buchner E, Heckmann M, Sigrist SJ.

Non-NMDA-type glutamate receptors are essential for maturation but not for initial assembly of synapses at *Drosophila* neuromuscular junctions.

Journal of Neuroscience, 2006

Schmid A, Qin G, Wichmann C, Kittel RJ, Mertel S, Fouquet W, Schmidt M, Heckmann M, Sigrist SJ.

Rapid activity-dependent modifications in synaptic structure and function require bidirectional Wnt signaling.

Neuron, 2008

Ataman B, Ashley J, Gorczyca M, Ramachandran P, Fouquet W, Sigrist SJ, Budnik V.

Orchestration of Synaptic Active Zone Assembly.

Submitted, PloS Biology

Fouquet W*, Oswald D*, Wichmann C, Schmidt M, Mertel S, Christiansen F, Depner H, Hallermann S, Kittel RJ, Eimer S, Heckmann M, Sigrist SJ